Review of SBIR Phase II Ferrite-Backed Patch Antennas

October 22, 1998

L. Andersen, A. Brown, Z. Li and J. Volakis (University of Michigan)
K. Trott (Mission Research Corp.)
C. Vittoria and H. How (EMA)

AGENDA

MRC Visit
Thursday, October 22, 1998

9:00-9:10 a.m.	Welcome Remarks
9:10-9:40 a.m.	Project Overview Dr. Keith Trott
9:40-10:10 a.m.	Overview of U of M Work in Progress Prof. John Volakis
10:10-10:30 a.m.	Status of Ferrite-Tetra Simulator Arik Brown
10:30-10:50 a.m.	Frequency Extrapolation and Ferrite Antenna Design Zhifang Li
10:50-11:15 a.m.	Higher Order Elements for Ferrite Patch Antennas Lars Andersen
11:15 a.m. - 12:00 p.m.	Discussion

Presentation
by
Keith Trott

Presentation
by
John Volakis

Ferrite Patch Antennas- Phase II

October 1998 Update

Students: Arik Brown, Zhifang Li, Lars Andersen, Y. Erdemli

PI: John Volakis

Radiation Laboratory
University of Michigan
Ann Arbor, MI 48109-2122
volakis@umich.edu

Phone: 313-764-0500 Fax:-313-647-2106
HomePage: http://www-personal.engin.umich.edu/~volakis/

Phase II Tasks/Project Goals

- Enhance capabilities of Ferrite-Brick
  - solver upgrades (Y1)
  - optimization/design studies (Y1)

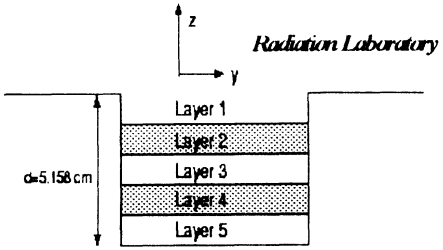

Layer 1: d=0.726 cm, ε_r=2.2, μ_r=1.0
Layer 2: d=1.790 cm, ε_r=13.9, $4\pi M_s$=800G, ΔH=50e
Layer 3: d=0.737 cm, ε_r=2.2, μ_r=1.0
Layer 4: d=0.762 cm, ε_r=13.9, $4\pi M_s$=800G, ΔH=50e
Layer 5: d=1.143 cm, ε_r=1.0, μ_r=1.0

Improved Convergence for Biased Substrates Using GMRES

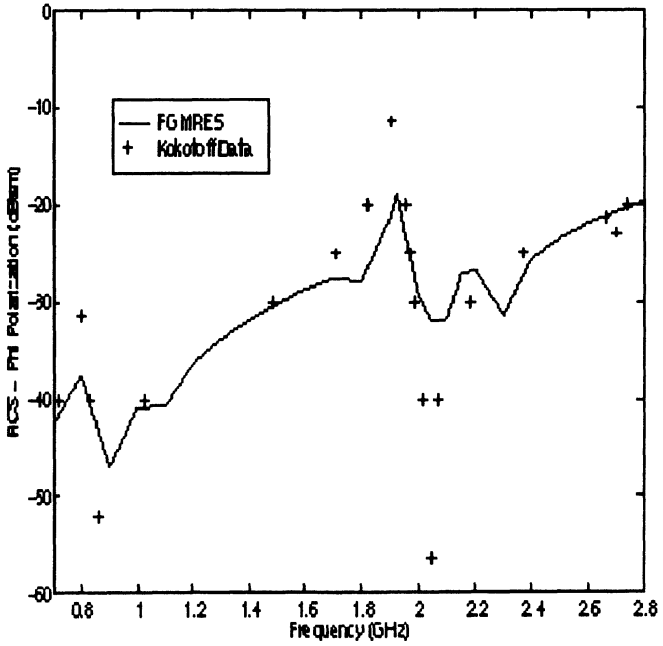

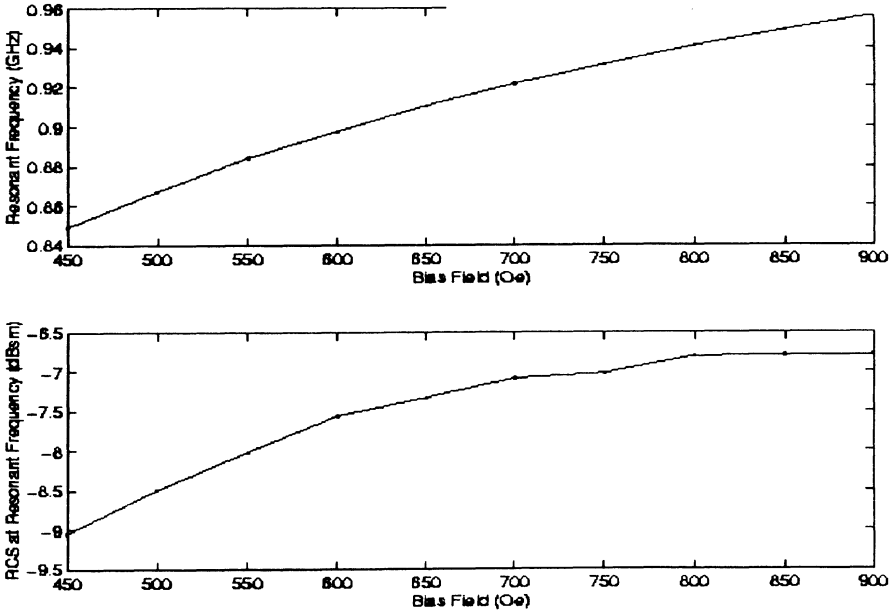

Resonance Tracking

Phase II Tasks - Year 1 (cont'd)

- Develop a FE-BI Tetrahedral Ferrite Antenna Simulator
  - **handle non-uniform biasing (Y1)**
  - **has automatic meshing (prisms to tetras) Y1**
  - **incorpates best solvers for non-symmetric systems (Y1/Y2)**
    - **eigenvalue study, H-field vs E-field formulation**
  - **curved antenna modeling using PML truncation (Y1/Y2)**
  - **validation and exploration of ferrite capabilities (Y1/Y2)**
    - **arrays, beam control/steering, frequency control with bias, polarization diversity, RCS control**
  - **fast algorithms for BI evaluation (Y2)**
  - **frequency extrapolation (Y2)**
  - **design/frequ tracking capability using SQP (Y1/Y2)**

Phase II: Tasks (cont)

– **Hierarchical higher order elements for efficient modeling of antennas in high contrast dielectrics/ferrites (Y1/Y2)**

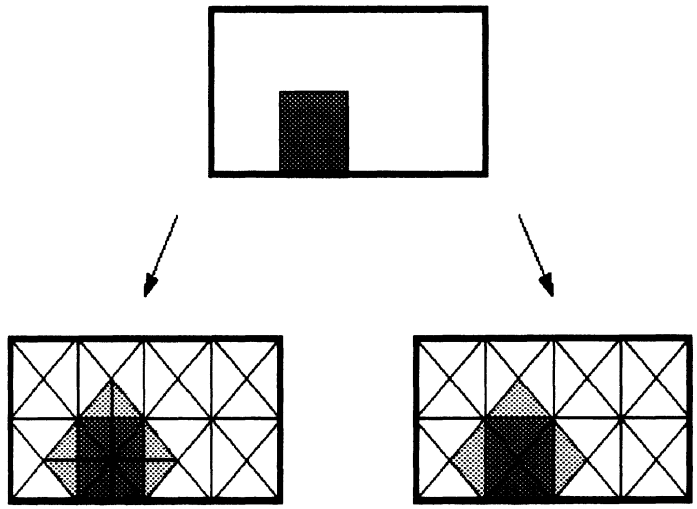

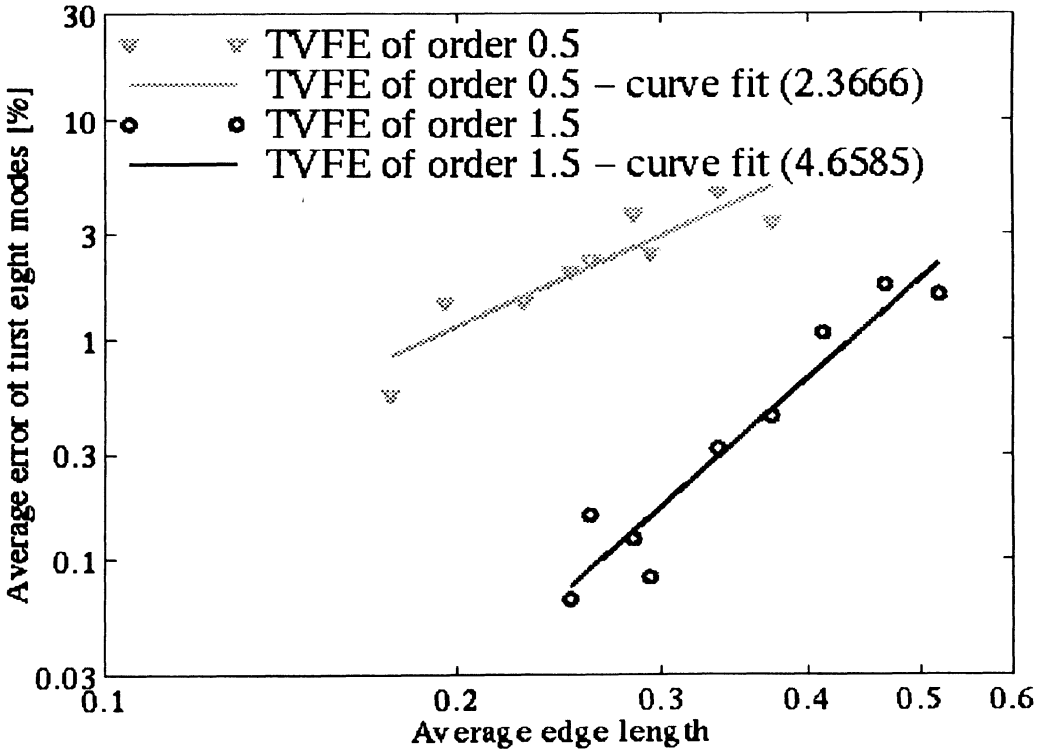

Summary of Actual Progress to Date-1

- Ferrite-Tetra Code and Solver
  - developed and validated
  - ported and validated AIM implementation
  - automatic structured meshing complete
    - (manual and code to MRC---see UM report)
  - PC/Windows mesh/fields display tool also available
  - Array and non-uniform biasing studies in progress

Summary of Actual Progress to Date-2

Radiation Laboratory

- Design/Frequency Tracking capability
  - many design examples carried out using SQP in Ferrite_Brick
  - ported SQP in FEMA-PRISM
  - ported AWE/Frequ. Extrapolation in PRISM
  - currently porting SQP and AWE in Ferrite-Tetra

Summary of Actual Progress to Date-3

Radiation Laboratory

- Hierarchical Elements TVFEs for efficient ferrite modeling
  - New TVFEs developed in Y1
  - 2nd order TVFEs implemented in new Ferrite-Tetra
  - Recent tests show dramatic speed-ups and accuracy improvements by selective placement of 2nd order TVFE

Status Summary of Codes

Code/ Capability	Ferrite-Tetra Linear Elements	Ferrite-Tetra 2nd order TVFEs	Fema Prism	Ferrite-Brick
Ferrite	√	√	-----	√
AIM	√	------	√	FFT (no need)
Auto meshing	√	√	√	√
Higher Order TVFE	----	√	------	------
PML (Curved)	√ (note tested)	-----	------	-------
Frequ. Extrapolation	---	------	√	partial
SQP	-----	------	----	√
Geometry/ Currents Viewing	√	------	√	

AIM in **Ferrite-Tetra**

Radiation Laboratory

AIM sped-up BI by factor of 2 for 400 Unk.

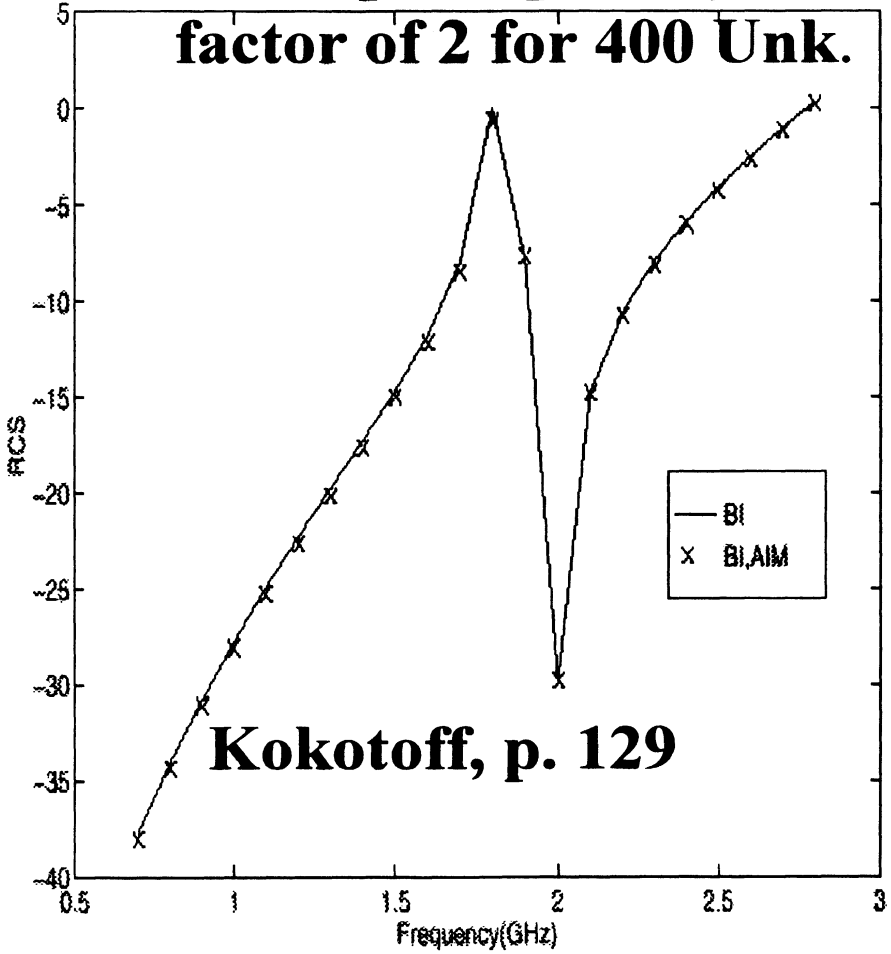

Kokotoff, p. 129

Yang patch, X-bias

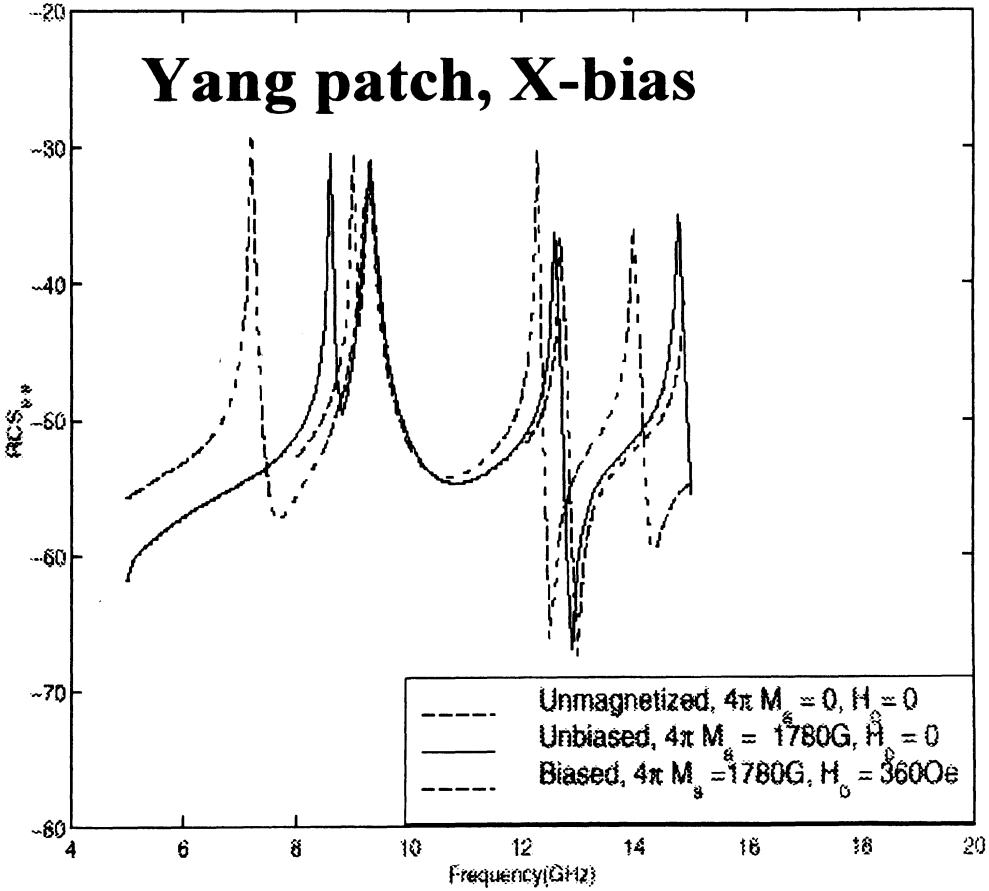

Automatic Mesher and Prism-Viewer

Radiation Laboratory

Prismatic Mesher

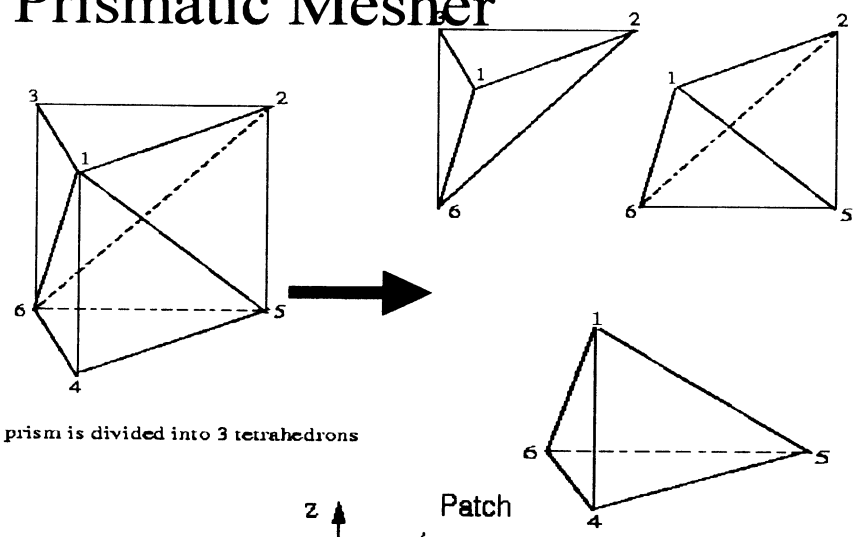

A single prism is divided into 3 tetrahedrons

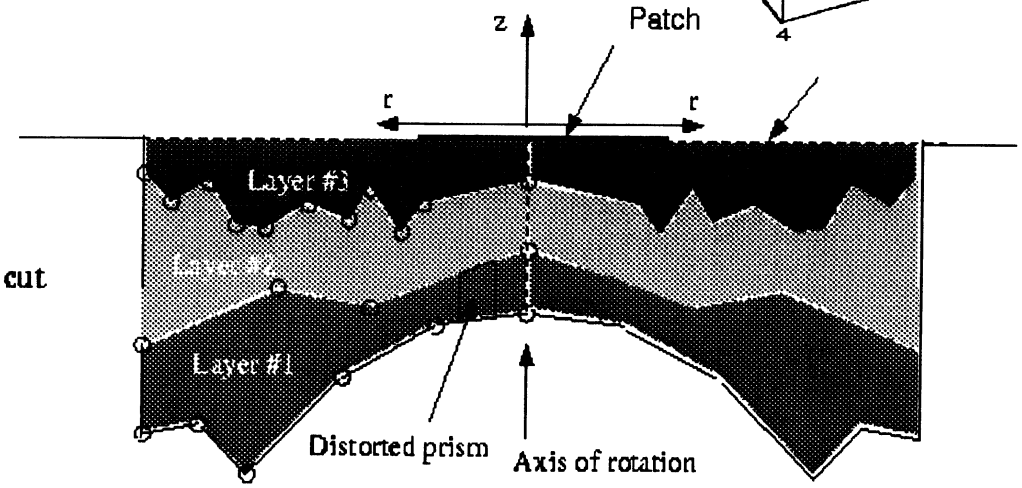

ϕ - cut

Vertical growth in non-planar layers

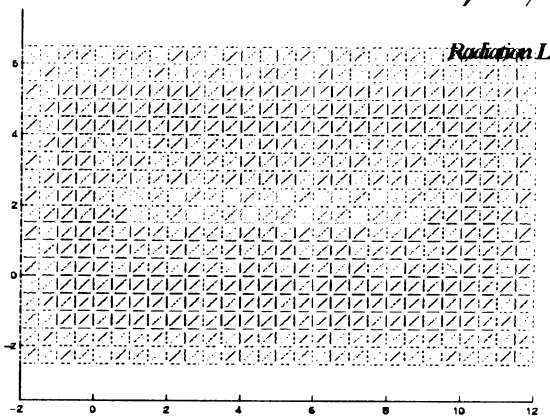

Rectangular Patch

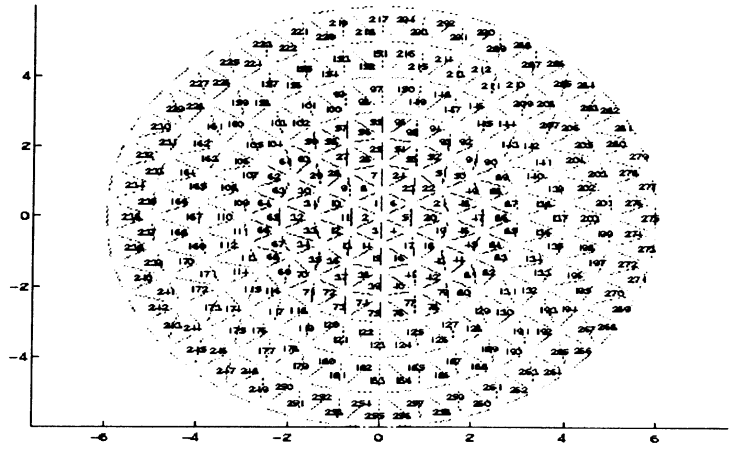

Circular Patch

Starting Point:

Radiation Laboratory

Slot Fed Dual Patch Design

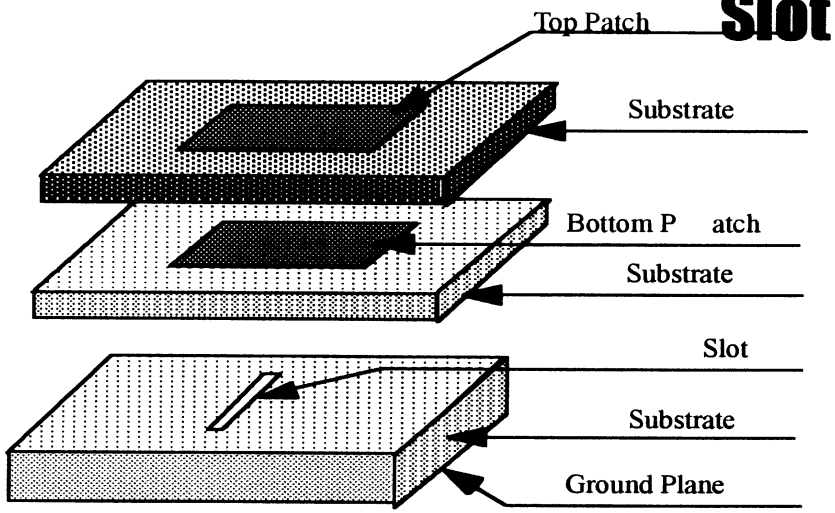

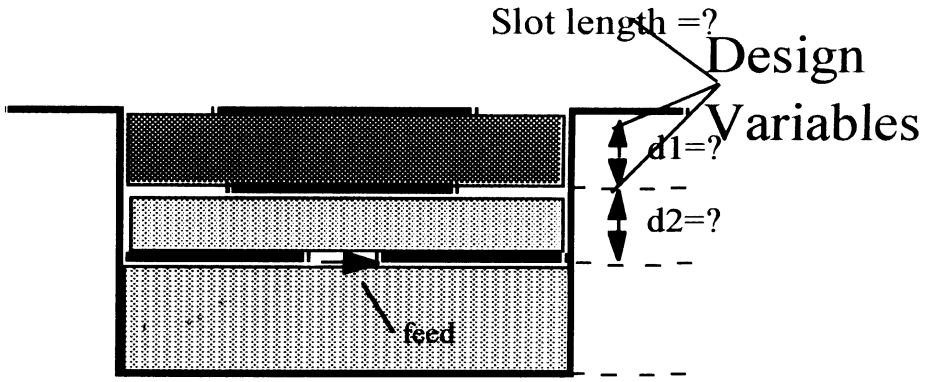

Performance at d1=0.85 mm, d2=0.55mm, slot length=4.0 mm

FINAL DESIGN:

VSWR = 1.414

BW = 18%

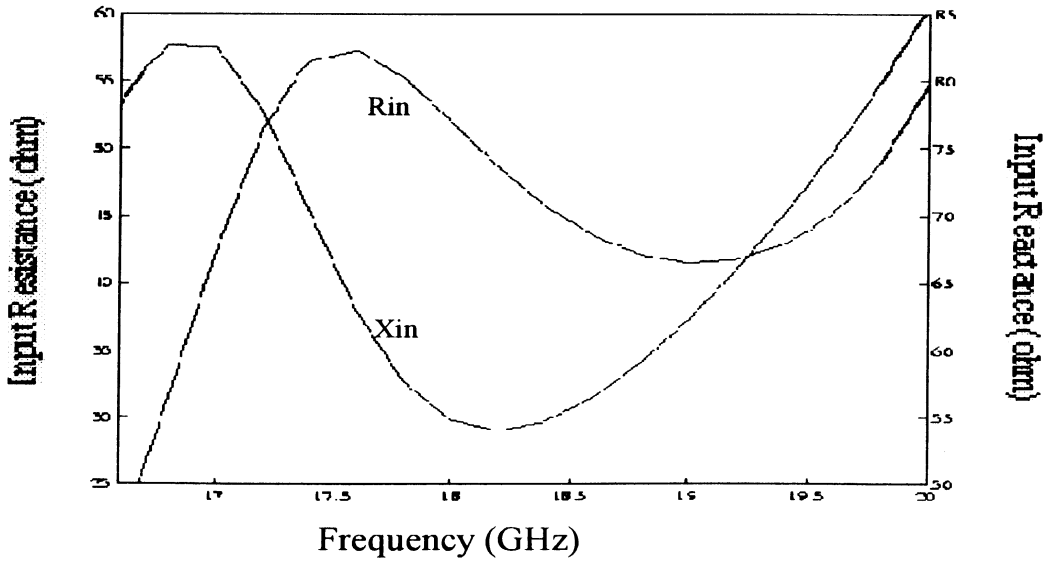

Frequency Tracking

Prediction of Analytical Formula for Ferrite Patches Using SQP Optimizer

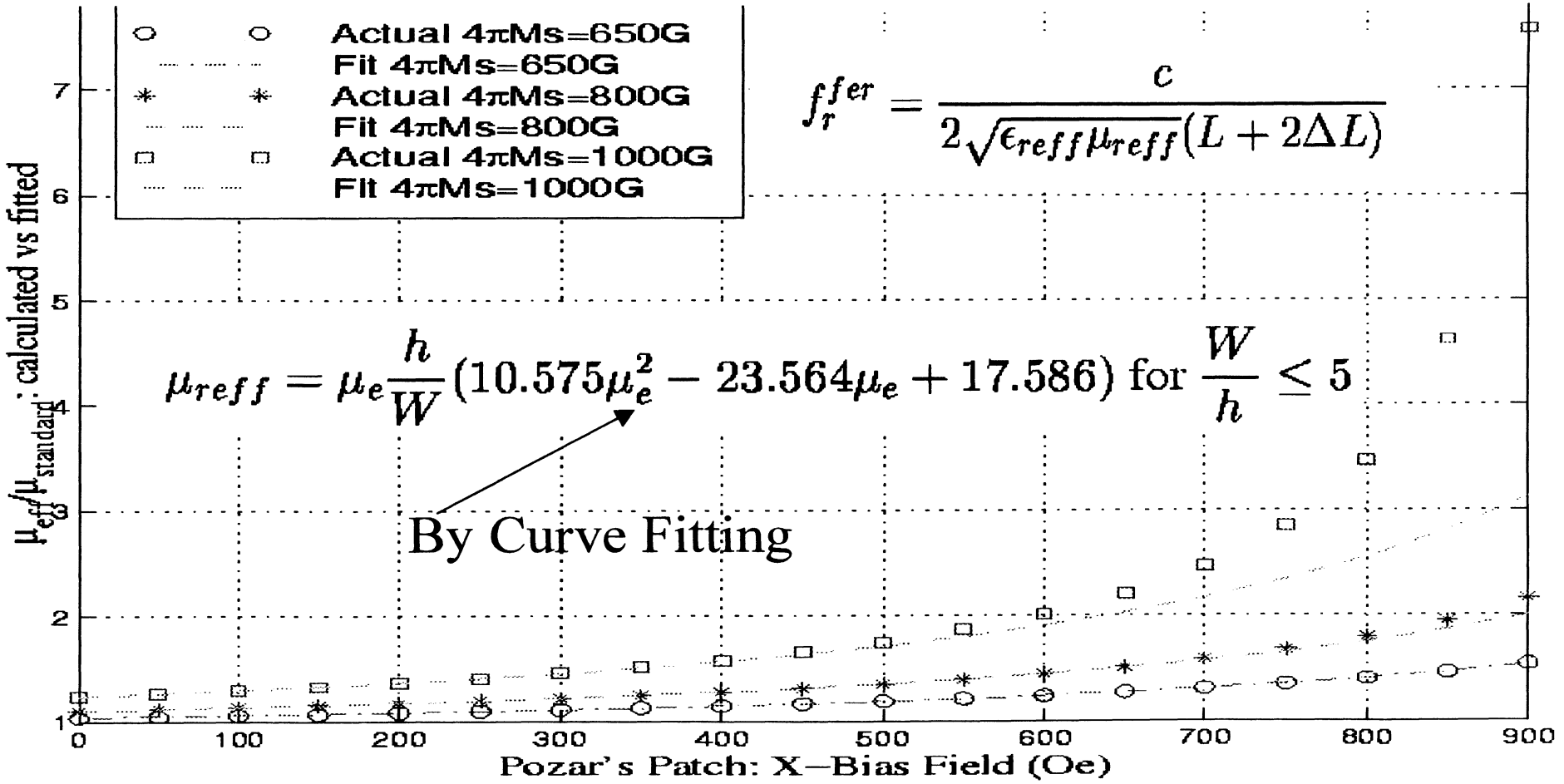

Example: AWE with FE-BI

Comparison of FE-BI and AWE Solutions

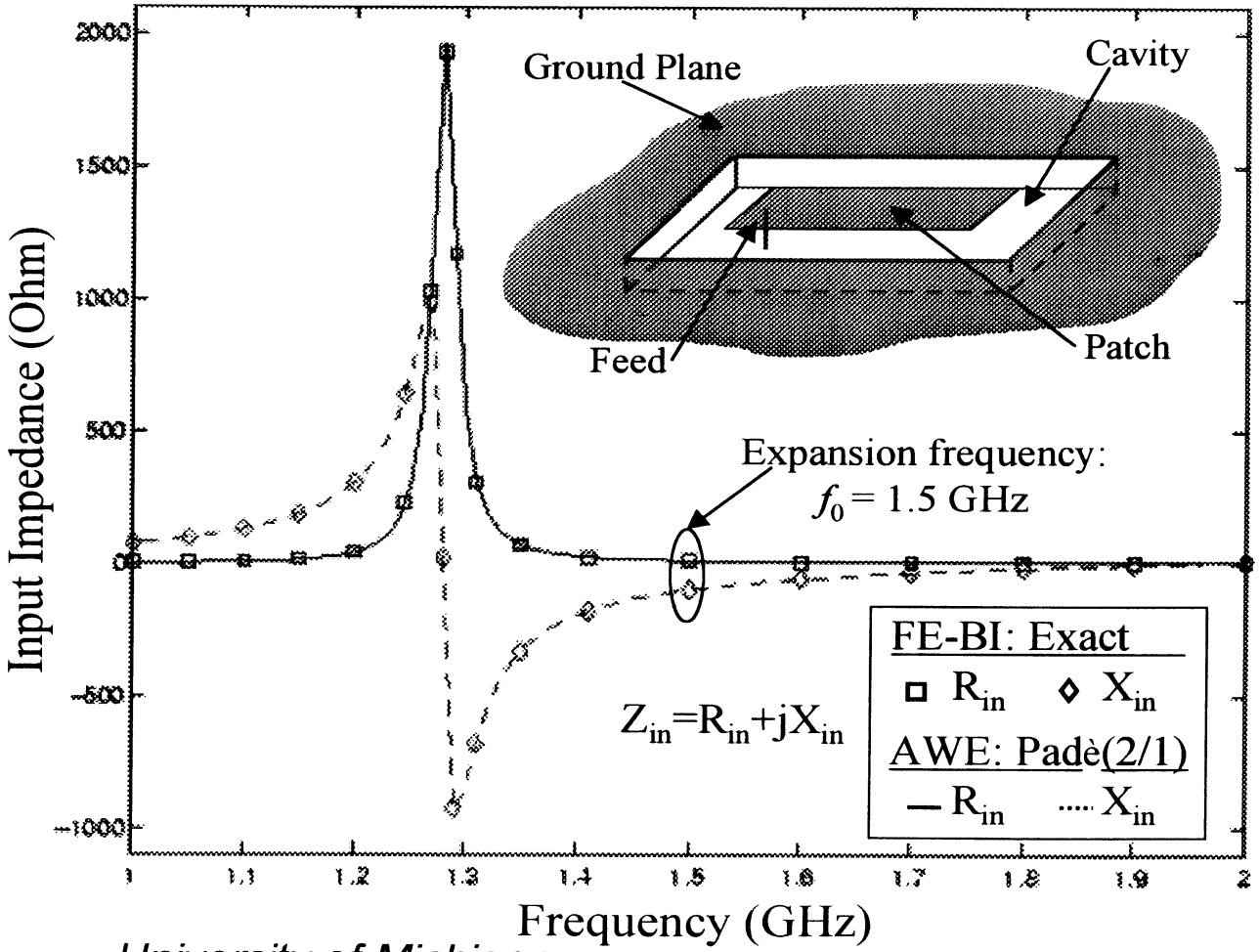

Rectangular Patch Antenna

CPU Time Comparison	
FE-BI (18 freq.)	117 secs.
AWE (101 freq.)	24 secs. (80% reduction)

Cavity Filling: Air ($\varepsilon_r=\mu_r=1.0$)
Cavity Size: 14cmx6cmx1cm
No. of FE unknowns = 649
No. of BI unknowns = 160
Feed: Vertical current probe

Speed-Ups From Higher Order TVFEs

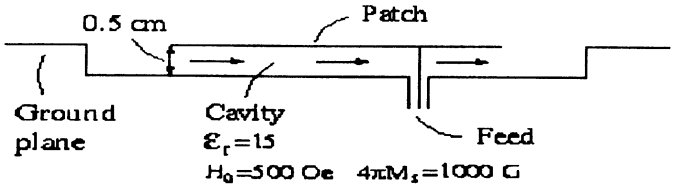

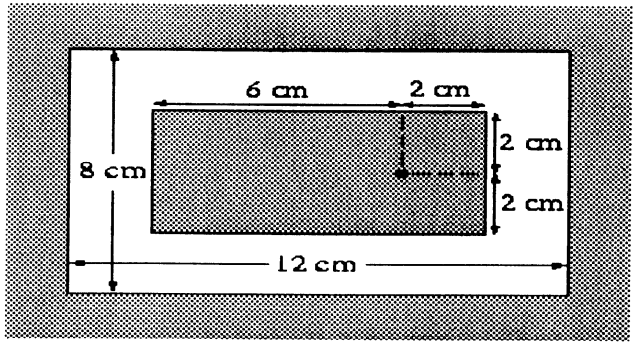

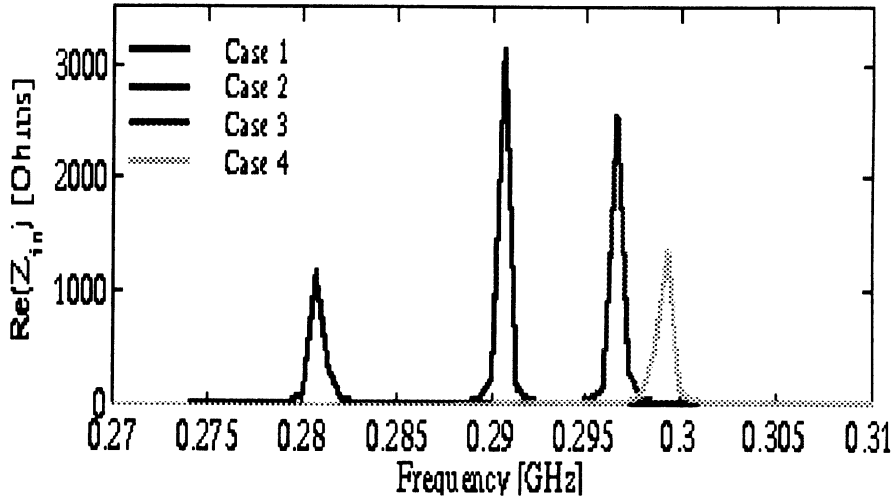

Case	TVFE order(s)	Average edge length	# of unknowns	# of BI unknowns	# of matrix entries	Time per frequency point
1	0.5	1.09 cm	505	160	29607	12 sec
2	0.5	0.77 cm	1189	384	157291	107 sec
3	0.5	0.62 cm	2161	704	**513807**	**501 sec**
4	0.5/1.5	1.09 cm	1263	160	50989	32 sec

Presentation
by
Arik Brown

FE-BI Formulation

Radiation Laboratory

Reference: A.D. Brown, J. Volakis, L. C. Kempel, Y.Botros,"Patch Antennas on Ferromagnetic Substrates", Accepted for Publication in *IEEE Antenn. Prop.*

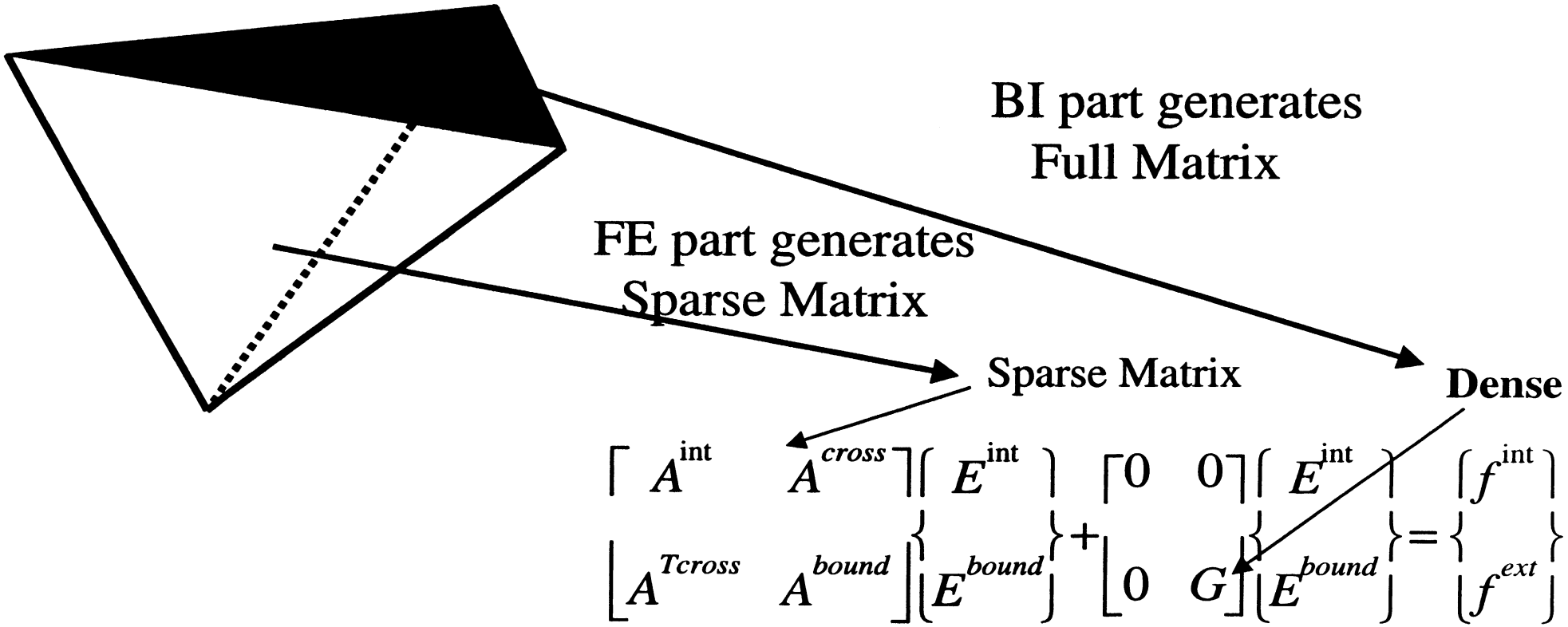

FEM Element Matrices Formulation

Radiation Laboratory

edge i	i_1	i_2
1	1	2
2	1	3
3	4	1
4	2	3
5	4	2
6	4	3

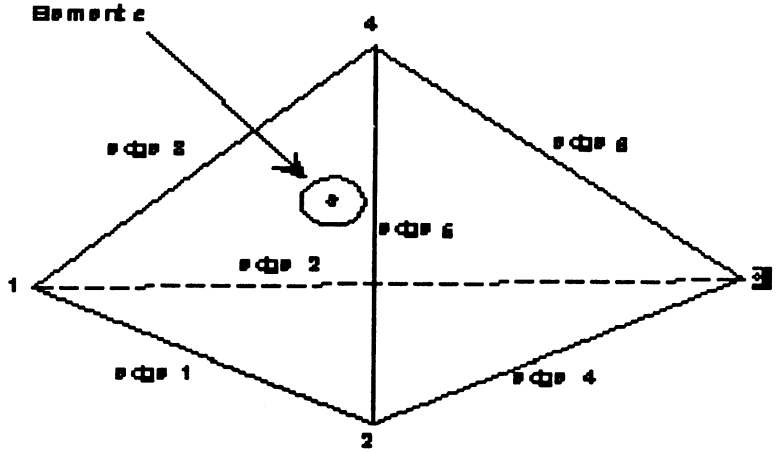

In each tetrahedral element the electric field is represented by

$$\vec{E}^e = \sum_{i=1}^{6} E_i^e \vec{W}_i^e \qquad \text{and} \qquad \vec{W}_i^e = L_{i_1} \nabla L_{i2} - L_{i_2} \nabla L_{i_1}$$

Using several identities the element matrices can be represented by the following equations

$$A_{ij}^e = \frac{1}{9V^{e^2}} \left(\vec{b}_{7-i} \cdot \bar{\bar{\mu}}_r^{-1} \cdot \vec{b}_{7-i} \right), i = 1,..,6; j = 1,..,6$$

$$B_{ij}^e = \iiint_V \frac{1}{9V^{e^2}} \left[L_{i_1} L_{j_1} \left(\bar{\bar{\varepsilon}}_r \cdot \vec{A}_{i_2} \right) \cdot \vec{A}_{j_2} - L_{i_1} L_{j_2} \left(\bar{\bar{\varepsilon}}_r \cdot \vec{A}_{i_2} \right) \cdot \vec{A}_{j_1} - L_{i_2} L_{j_1} \left(\bar{\bar{\varepsilon}}_r \cdot \vec{A}_{i_1} \right) \cdot \vec{A}_{j_2} - L_{i_2} L_{j_2} \left(\bar{\bar{\varepsilon}}_r \cdot \vec{A}_{i_1} \right) \cdot \vec{A}_{j_1} \right] dV$$

FE-BI Formulation

$$\langle \mathbf{E}, \mathbf{T} \rangle = \iiint_V \left[(\nabla \times \mathbf{T}) \cdot \bar{\bar{\mu}}_r^{-1} \cdot (\nabla \times \mathbf{E}) - k_o^2 \mathbf{T} \cdot (\bar{\bar{\varepsilon}}_r \cdot \mathbf{E}) + jkZ_0 \mathbf{T} \cdot \mathbf{J}^{\text{int}} \right] dv + jkZ_0 \iint_S \mathbf{T} \cdot (\mathbf{H} \times \hat{n}) ds$$

$$\mathbf{H} = -2j \frac{k}{Z_0} \left[\iint_S g(\mathbf{r}, \mathbf{r}') (\mathbf{E} \times \hat{n}) ds - \frac{1}{k^2} \nabla \iint_S g(\mathbf{r}, \mathbf{r}') \nabla' \cdot (\mathbf{E} \times \hat{n}) ds \right] + \mathbf{H}^{inc}$$

$$B_{ij} = -2j \frac{k}{Z_0} \iint_S ds\, \mathbf{b_i}(\mathbf{r}) \cdot \iint_{S'} ds' \left[\mathbf{b_j}(\mathbf{r}') - \frac{1}{k^2} \nabla' \cdot \mathbf{b_j}(\mathbf{r}') \nabla \right] \frac{e^{-jkR}}{R}$$

Basic Principles of the Adaptive Integral Method (AIM)

Radiation Laboratory

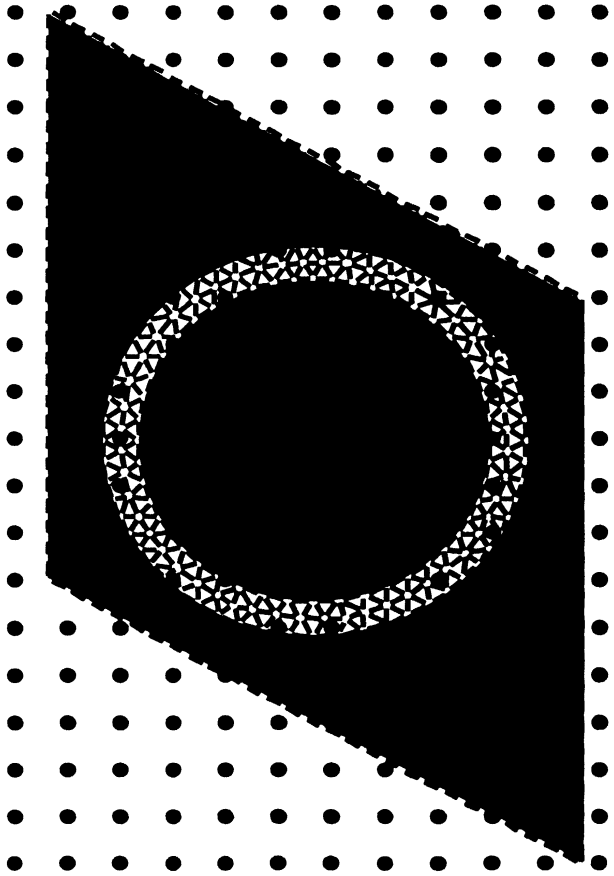

- overlay uniform mesh on original mesh
- relate the meshes via moments of basis functions
- utilize convolutional properties of Green's function for uniform mesh
- calculate matrix-vector products (convolutions) in DFT domain and employ FFT algorithm (iterative solver assumed)
- correct for near-coupling terms of original mesh

→ $O(n \log n)$ for matrix-vector product (planar BI surface assumed)

$O(n)$ memory requirement

Some Details of the AIM Algorithm

Radiation Laboratory

Decompose BI matrix in near-zone and far-zone contributions

$$[Z]=[Z]^{near}+[Z]^{far}$$

$[Z]^{near}$ is calculated in a conventional way (MPIE formulation in this work).

For the calculation of $[Z]^{far}$ lets consider the scalar coupling integral

$$Z_{mn}=\iint_{S_m} q_m(\vec{r}) \iint_{S_n} G_p(\vec{r}\,|\,\vec{r}\,') q_n(\vec{r}\,')\; dS'dS$$

Goal: Calculate the coupling integral in the DFT domain employing the auxiliary uniform mesh.

Therefore, the basis functions must be replaced by equivalent basis functions on the uniform mesh.

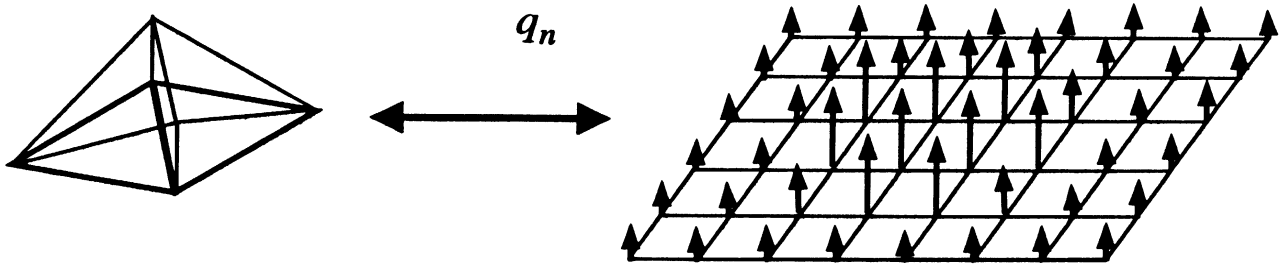

$$q_n(\vec{r}) \quad \Leftrightarrow \quad \sum_{i=1}^{I}\sum_{j=1}^{J} \Lambda_{ij}^{n}\; \delta(x-i\Delta x)\,\delta(y-j\Delta y)$$

Some Details of the AIM Algorithm: Continuation 1

Radiation Laboratory

Consider $Z_{mn} = \iint_{S_m} q_m(\vec{r}) \underbrace{\iint_{S_n} G_p(\vec{r} \mid \vec{r}\,') q_n(\vec{r}\,')\, dS'}\, dS$

$$\boxed{Z_{mn} = \iint_{S_m} q_m(\vec{r})\, g(\vec{r})\, dS}$$

Introducing the Taylor series expansion $g(\vec{r}) = \sum_{q=q_1+q_2=0}^{\infty} a_q (x-x_1)^{q_1} (y-y_1)^{q_2}$

$$\rightarrow \quad Z_{mn} = \sum_{q=q_1+q_2=0}^{\infty} a_q \underbrace{\iint_{S_m} q_m(\vec{r}) (x-x_1)^{q_1} (y-y_1)^{q_2} dS}$$

summation of moments of test function multiplied by Taylor coefficients a_q

moments of test function

Enforcing

$$\boxed{\iint_{S_m} q_m(\vec{r}) (x-x_1)^{q_1} (y-y_1)^{q_2} dS = \sum_{i=1}^{I} \sum_{j=1}^{J} \Lambda_{ij}^{m} (i\Delta x - x_1)^{q_1} (j\Delta y - y_1)^{q_2} \qquad q = q_1 + q_2 = 0,\ldots,\infty}$$

gives the required relation between the original and uniform meshes and allows the calculation of Λ_{ij}^{m}

Some Details of the AIM Algorithm: Continuation 2

Radiation Laboratory

In numerical implementation:
Only finite number of moments possible to relate each test or basis function to a finite number of δ-functions on the uniform grid (accurate for far interactions)

Each test and basis function can now be replaced by the related δ-functions on the uniform grid.

$$Z_{mn} \approx \sum_{i=(i_m-1)}^{(i_m+1)} \sum_{j=(j_m-1)}^{(j_m+1)} \sum_{k=(k_n-1)}^{(k_n+1)} \sum_{l=(l_n-1)}^{(l_n+1)} \Lambda_{kl}^{n}\, G_p((i\Delta x, j\Delta y)\,|\,(k\Delta x, l\Delta y))\; \Lambda_{ij}^{m}$$

Important advantage of this concept:

Mapping procedure independent of Green's function

AIM in **Ferrite-Tetra**

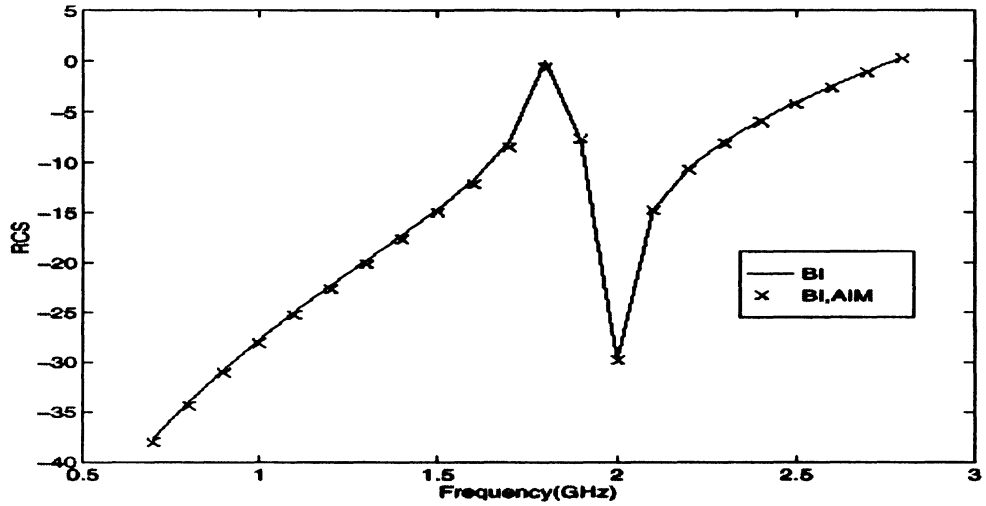

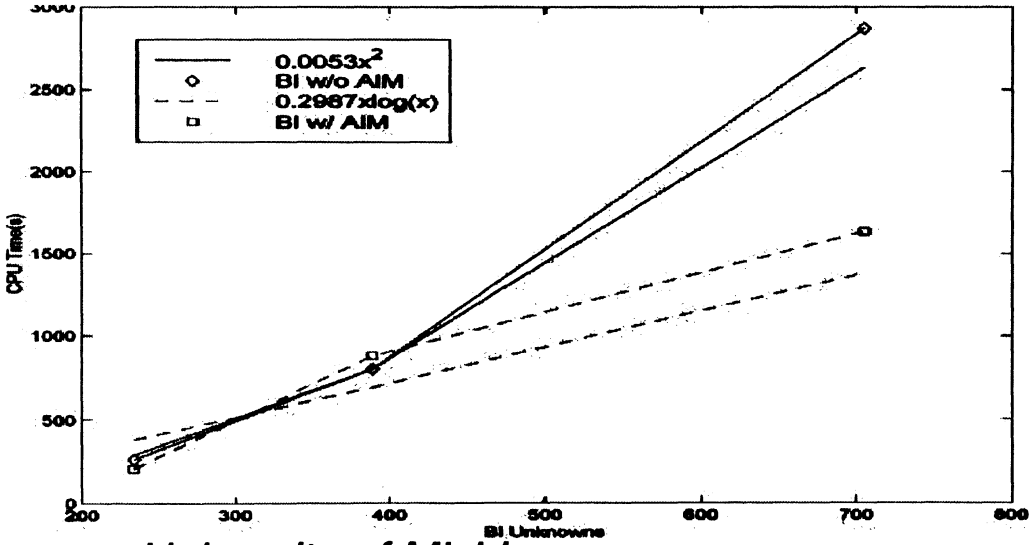

-Validation of Kokotoff Data Using AIM

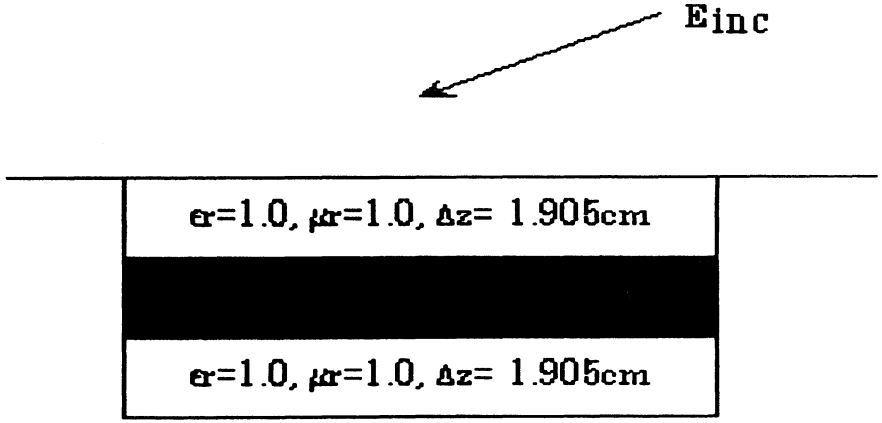

-AIM Outperforms Regular BI As Expected as the Number of BI Unknowns Increases

Validation Results

Radiation Laboratory

Tetra Code Validation, Kokotoff p.162

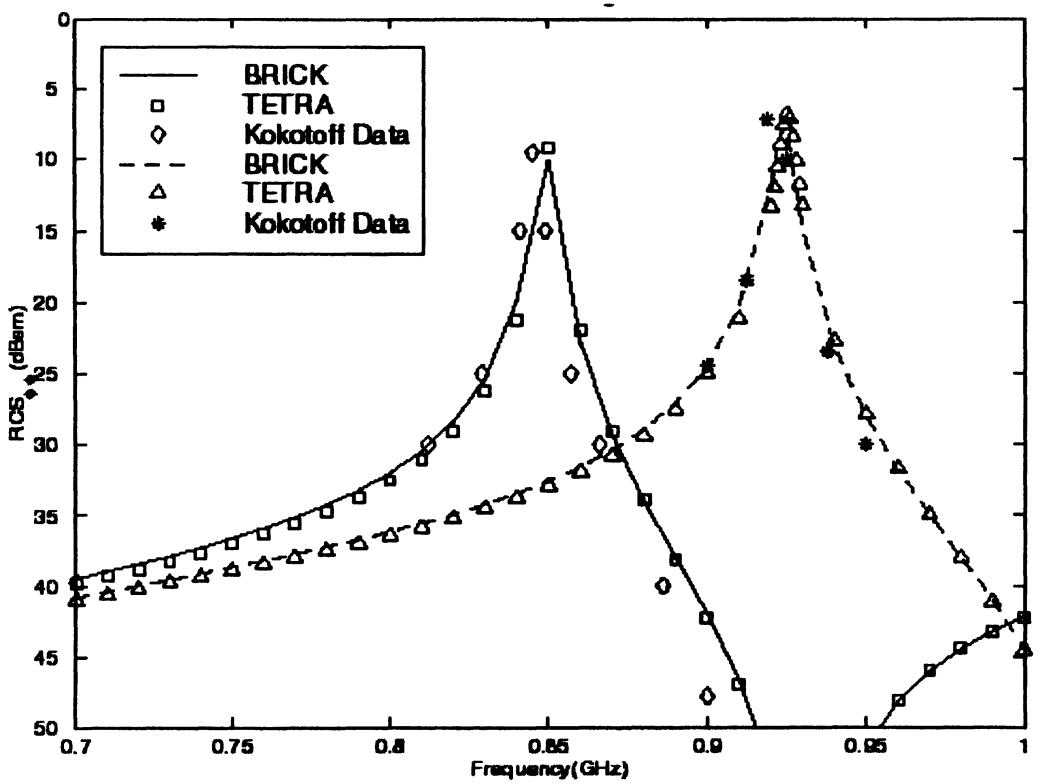

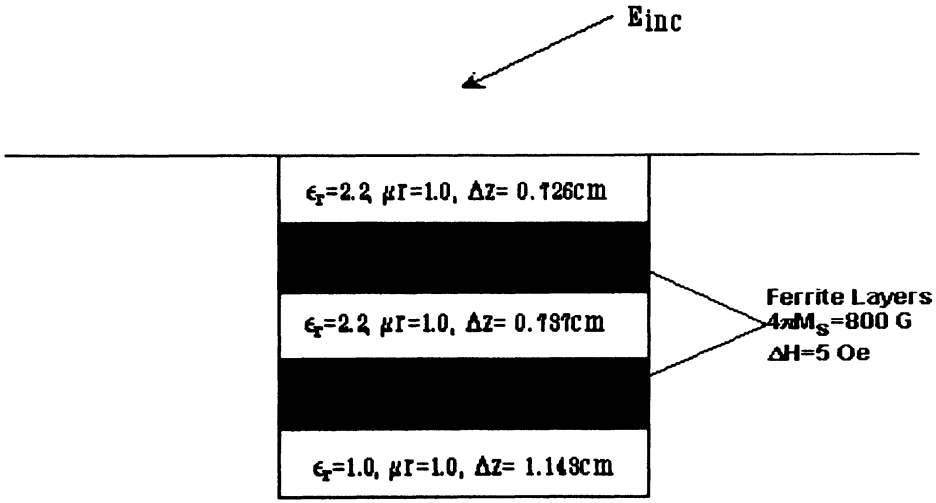

- Excellent agreement with both ferrite brick code, and actual data

Presentation
by
Zhifang Li

Outline

- Prism/Tetra Geometry Drive (completed Year1)
- Ferrite Antenna Optimization (started Year1)
  - Sequential Quadratic Programming
  - Design Formulae
- Fast Simulation Algorithm - Asymptotic Waveform Evaluation (AWE)
  - Introduction
  - Procedures
  - Results
- Future Plan

Basic Optimization Concepts

- Design Optimization Problem

  Minimize $f(x, p)$ - Objective function

  Subject to: $\bar{g}(\bar{x}, \bar{p}) \leq \bar{0}$ - Inequality constraints

  $\bar{h}(\bar{x}, \bar{p}) = \bar{0}$ - Equality constraints

  $\bar{x} \in \chi \subseteq R^n$ - Design variables

  $\bar{p} \in R^m$ - Parameters with fixed values

- Numerical Gradient-based Optimization Methods

  1. Initialize: set $\bar{x}_0$.
  2. Iteratively find the next best point $x_{k+1} = x_k + \alpha_k s_k$ by:

     Direction-finding to determine $\bar{s}_k$

     Line search along $\bar{s}_k$ to determine α_k

     such that $f(x_{k+1}) < f(x_k)$.
  3. Repeat step 2 until convergence criteria are satisfied.

Antenna Design Optimization: Sequential Quadratic Programming (SQP) methods

- A gradient-based algorithm to find local optima
- Great for continuous objective function
- Fast to converge and robust
- Find the search direction $\bar{s}_k$ by solving a QP problem (hence the name)
- Determine the step size α_k by minimizing a one-dimensional function along the search direction

Design Formulae for Ferrite Patch

- Step 1: use SQP to find resonant frequencies of the ferrite patch with various values of bias field and magnetization

  i.e. find frequency f which minimizes $\left|Imag(Z_{in})\right|$

- Step 2: obtain an empirical formula from large amount of data, using curve-fitting and physical insight.

New formula: $$f_r^{fer} = \frac{c}{2\sqrt{\varepsilon_{reff}}(L+2\Delta L)\sqrt{\mu_{reff}}}$$

where $$\mu_{reff} = \mu_e \cdot f\left(\mu_e, \frac{W}{h}\right) \quad , \quad \mu_e = \frac{1}{\mu_0}\frac{\mu^2-\kappa^2}{\mu} \quad \text{(in-plane bias)}$$

$$\mu = \mu_0\left[1+\frac{\omega_0\omega_m}{\omega_0^2-\omega^2}\right], \kappa = \mu_0\frac{\omega\omega_m}{\omega_0^2-\omega^2}$$

$$\omega_0 = \mu_0\gamma H_0, \omega_m = \mu_0\gamma M_s, \gamma = 1.76\times 10^7 rad/(\sec \cdot oe)$$

Resonant Frequency Tracking

Antenna geometry: L = W = 0.61 cm, h = 0.127 cm,
cavity size = 1.22 by 1.22 cm, relative permittivity = 13.9.

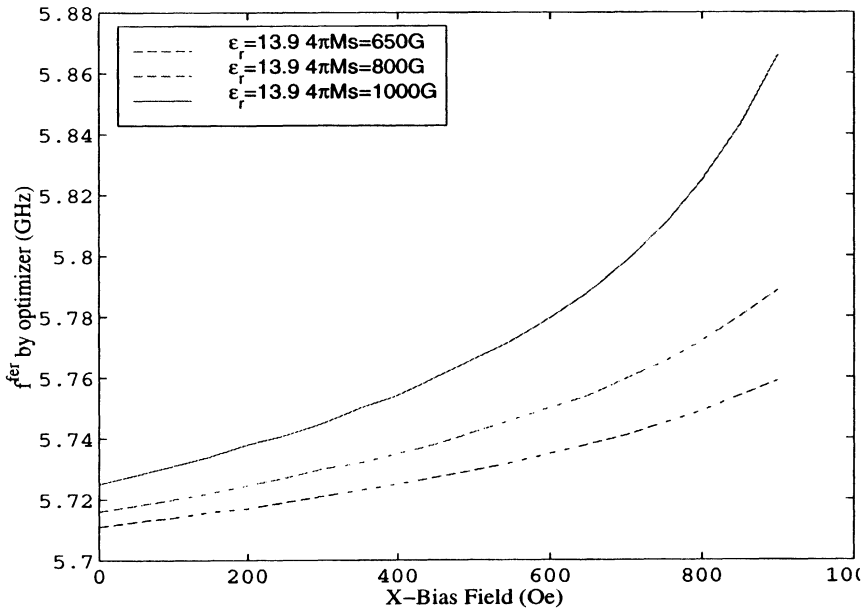

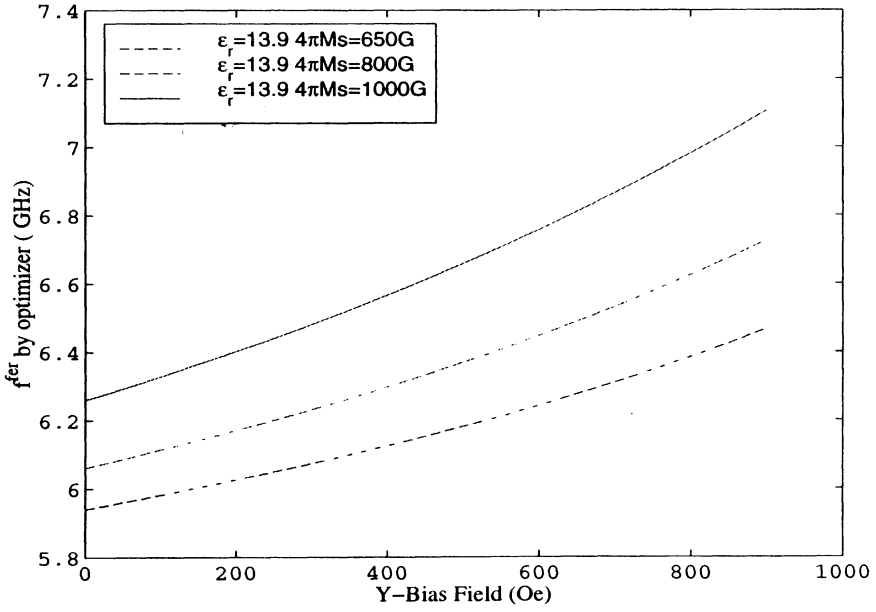

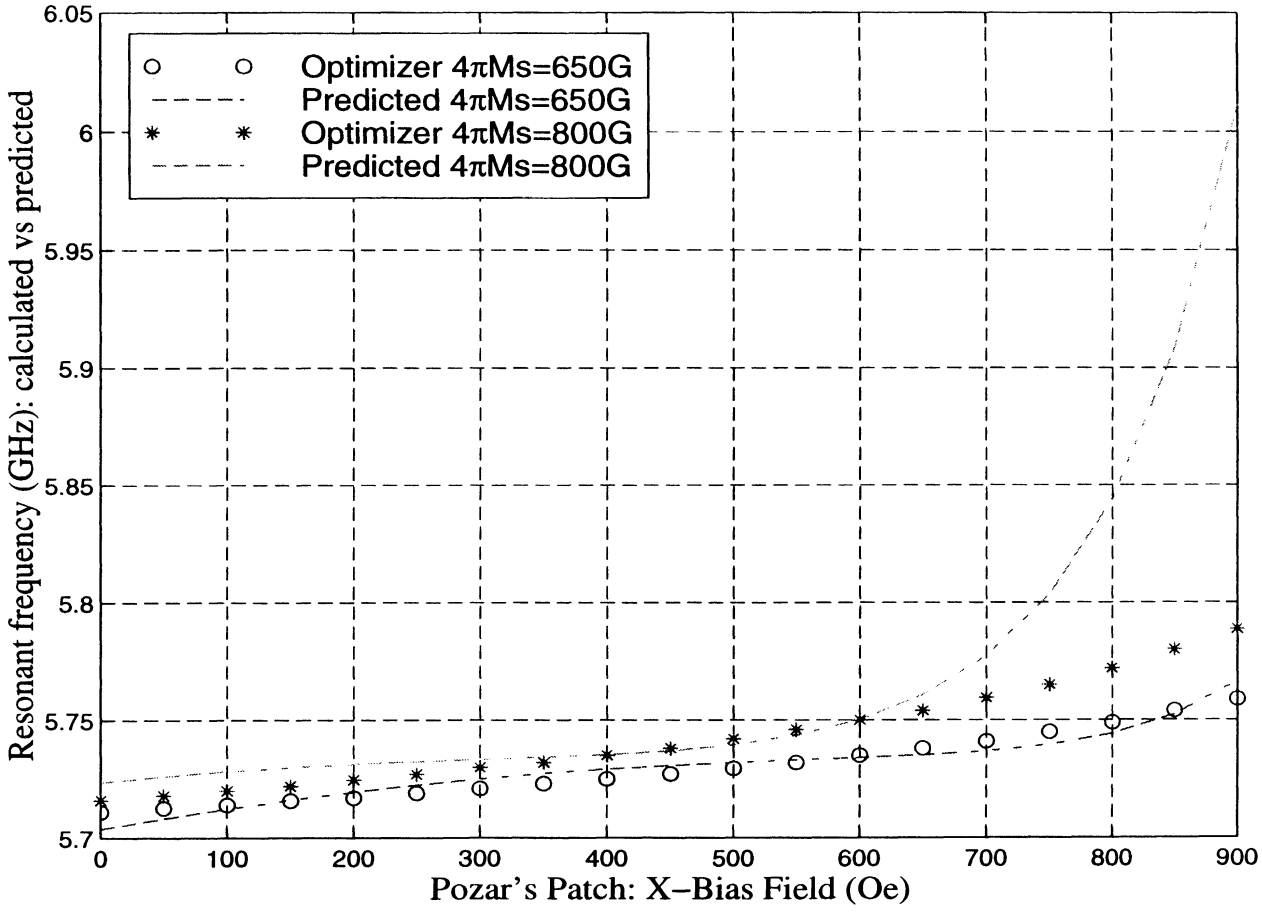

$$\mu_{reff} = \mu_e \frac{h}{W}(10.575\mu_e^2 - 23.564\mu_e + 17.586) \text{ for } \frac{W}{h} \leq 5$$

AWE Technique

- Constructs a reduced-order model of a linear system.
- Employs Taylor series expansion of the matrix system at a specific value of the system parameter (freqn., angle).
- Utilizes power series "moments" to extract the poles and residues of the system, yielding a rational function of two polynomials in the system parameter (Padè approximant).
- Padè representation provides an extension of the region of convergence (RoC) of the power series, thus the accuracy of the analysis is increased to a larger band.

AWE Formulation

Radiation Laboratory

TAYLOR

$$f(z) = \sum_{n=0}^{\infty} c_n (z - z_0)^n$$

$$c_0 = f(z_o),\ c_n = f^{(n)}(z_o) \,/ n!$$

$$f(z) = \sum_{n=0}^{N} c_n (z - z_0)^n + O(z^{N+1})$$

example expansion for each matrix element

$c_n,\ n = 0, \ldots, N$

$N \geq L + M + 1$

casting of Taylor expansion to a more convergent Padè representation

PADÈ

$$f(z) = P(L/M) + O(z^{L+M+1})$$

$$P(L/M) = \sum_{l=0}^{L} a_l (z - z_0)^l \Big/ 1 + \sum_{m=1}^{M} b_m (z - z_0)^m$$

$$\sum_{j=1}^{l} c_{l-j} b_j = -c_l\ ,\ L+1 \leq l \leq L+M\ ,\ b_j = 0 \text{ for } l > M$$

$$a_0 = c_0\ ,\ a_l = c_l + \sum_{j=1}^{\min(l,M)} c_{l-j} b_j\ ,\ 1 \leq l \leq L$$

Frequency Extrapolation-1

Radiation Laboratory

Original Matrix System

MoM

unknown current

$$[Z_{mn}(k)]\{I_n(k;\phi,\theta)\} = \{V_m(k;\phi,\theta)\}$$

excitation

incident electric field

$$V_m(k;\theta,\phi) = \iint \mathbf{T}_m(\vec{r}) \cdot \mathbf{E}_{inc}(k;\phi,\theta)\, ds$$

$$\mathbf{E}_{inc}(k;\theta,\phi) = \hat{p}_i(\theta,\phi)\, e^{jk\hat{k}(\theta,\phi)\cdot\vec{r}}$$

$$Z_{mn}(k) = F(ke^{jk}, e^{jk}/k)$$

dependence on frequency

$$k = 2\pi f\sqrt{\varepsilon_0\mu_0}$$

matrix element

$\phi = \phi_0, \theta = \theta_0$

AWE

Taylor expansion of unknown current

$$\{I_n(k)\} = \{I_n(k_0)\} + \sum_{s=1}^{\infty} \{M_n\}^s (k-k_0)^s$$

s^{th} moment

recursive relation to get moments

$$\{M_n\}^s = [Z_{mn}(k_0)]^{-1}\left[\frac{\{V_m^{(s)}(k_0)\}}{s!} - \sum_{q=1}^{s} \frac{[Z_{mn}^{(q)}(k_0)]\{M_n\}^{s-q}}{q!}\right]$$

q^{th} derivative of matrix element

$(s\text{-}q)^{th}$ moment

final Padè representation of the current

$$I_n(k) = P_n(L/M) + O(k^{L+M+1}), \quad P_n(L/M) = \frac{\sum_{l=0}^{L} a_n^l (k-k_0)^l}{1+\sum_{m=1}^{M} b_n^m (k-k_0)^m}$$

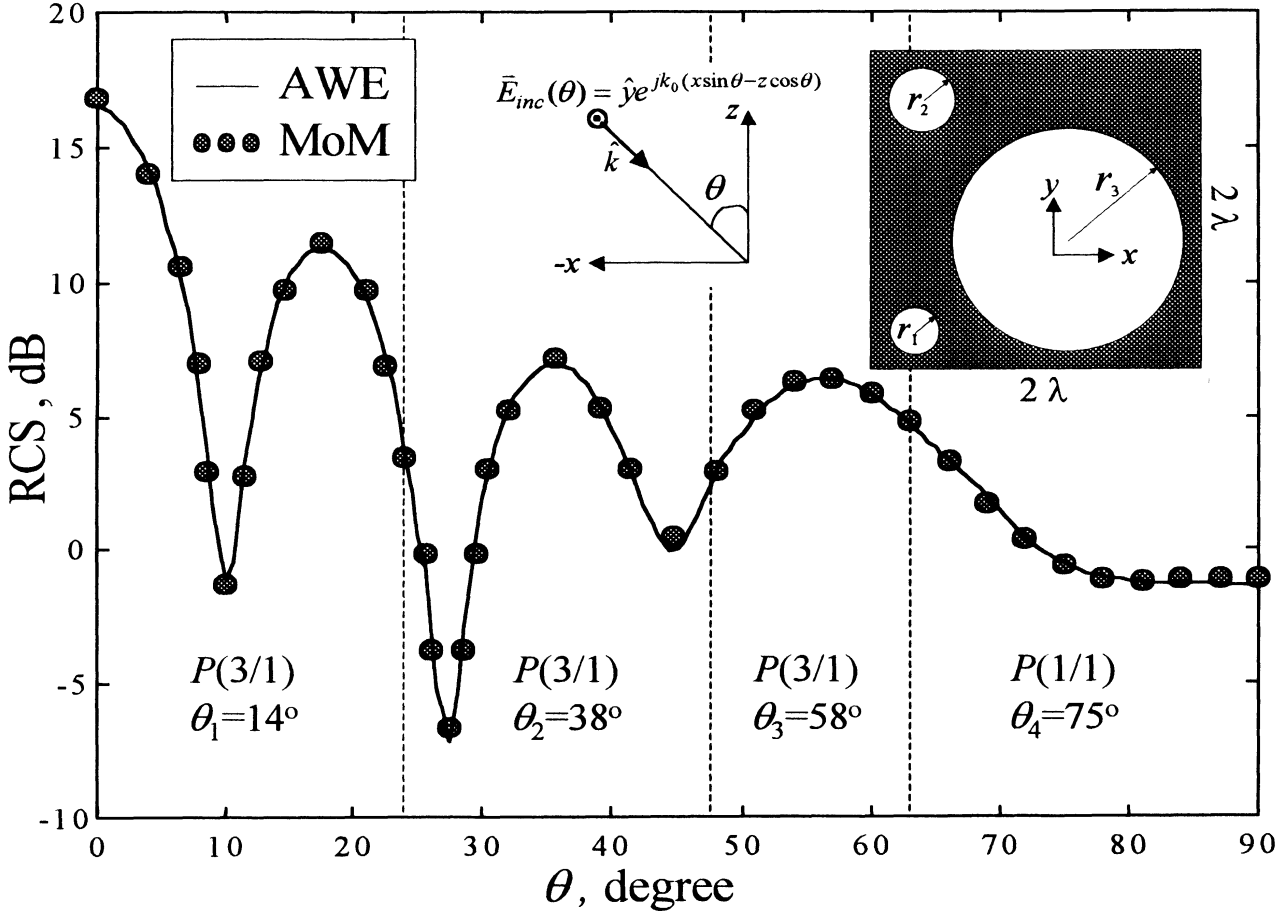

PEC Plate w/ Circular Holes

CPU Time Comparison	
MoM (91 ang.)	97 min.
AWE (181 ang.)	25 min. (74% reduction)

No. of unknowns = 649
Extrapolation region: 0°-90°
Expansion @ θ_1 = 14°, θ_2 = 38°, θ_3 = 58°, θ_4 = 75°

Reference: *IEEE Transactions on Antennas and Propagation*, to be published.

Frequency Extrapolation

FE-BI

Dense+Sparse system: $[A_{mn}(k)]\{e_n(k)\}=\{g_m(k)\}$

Dependence on frequency: $A_{mn}(k)=F(k^2,e^{-jk},k^2e^{-jk})$

$g_m(k)=k\,g_{m0}\,,\ k=2\pi f/c$

AWE

Taylor expansion of unknown electric field:

$$\{e_n(k)\}=\{e_n(k_0)\}+\sum_{s=1}^{\infty}\{M_n\}^s(k-k_0)^s$$

($\{M_n\}^s$: s^{th} moment)

Recursive computation of moments:

$$\{M_n\}^s=[A_{mn}(k_0)]^{-1}\left[\frac{\{g_m^{(s)}(k_0)\}}{s!}-\sum_{q=1}^{s}\frac{[A_{mn}^{(q)}(k_0)]\{M_n\}^{s-q}}{q!}\right]$$

($A_{mn}^{(q)}(k_0)$: q^{th} derivative of matrix element)

Equivalent Padè representation:

$$e_n(k)=P_n(L/M)+O(k^{L+M+1})\ ,\ P_n(L/M)=\frac{\sum_{l=0}^{L}a_n^l(k-k_0)^l}{1+\sum_{m=1}^{M}b_n^m(k-k_0)^m}$$

Example: AWE with FE-BI

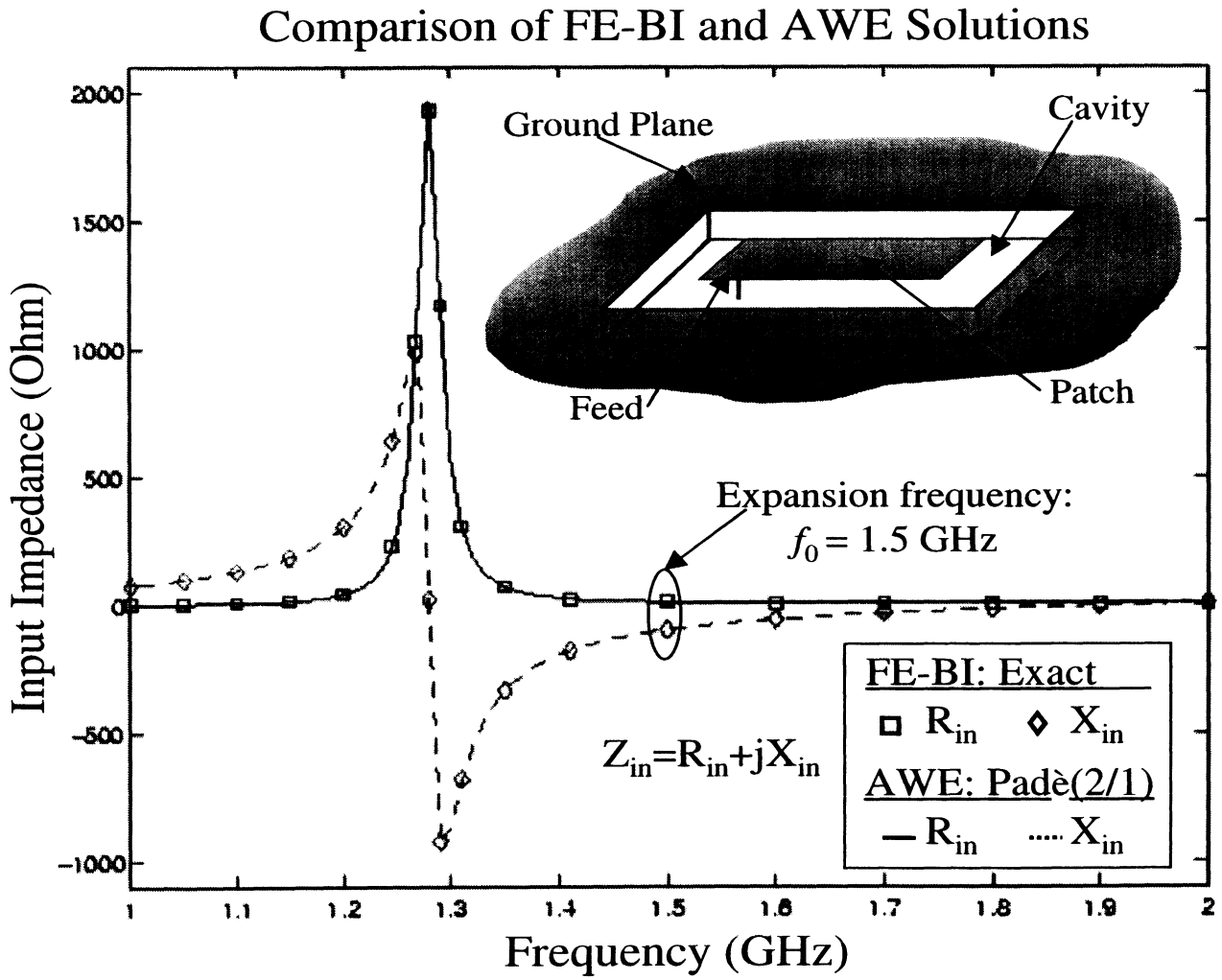

Rectangular Patch Antenna

CPU Time Comparison	
FE-BI (18 freq.)	117 secs.
AWE (101 freq.)	24 secs. (80% reduction)

Cavity Filling: Air ($\varepsilon_r=\mu_r=1.0$)

Cavity Size: 14cmx6cmx1cm

No. of FE unknowns = 649

No. of BI unknowns = 160

Feed: Vertical current probe

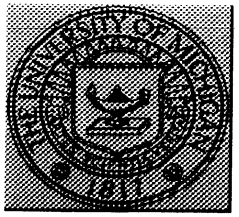

Conclusions

- Implementation of AWE technique in connection with frequency domain EM methods (MoM and hybrid FE-BI) was demonstrated for three-dimensional scattering and radiation problems.

- AWE was employed as an extrapolator, and it was shown that AWE can generate broadband frequency or angular responses using only a few exact solutions.

- Also, AWE results in considerable CPU time savings, e.g. it is at least twice faster than the conventional methods.

Presentation
by
Lars Andersen

Hierarchical Methods for Simulation and Design of Antennas

MRC/UM review meeting

October 22, 1998

Outline

- Motivation
- Basic definitions
- Proposed approach
- Accomplishments
  - ◇ Overview
  - ◇ Specifics
- Proposed future work
  - ◇ Overview
  - ◇ Specifics
- Summary

Motivation

- Consider a ferrite-loaded antenna

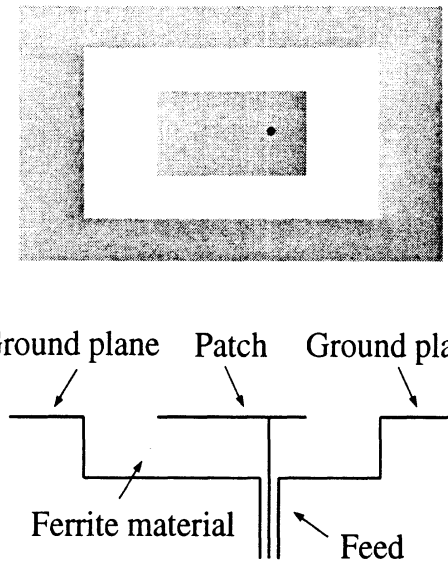

- Accurate simulation of importance :
  - ◇ Antenna miniaturization
  - ◇ Pattern synthesis
- Characteristic for these and numerous other applications : Disjoint regions with high and low field / field variation
- Many existing numerical techniques have difficulties simulating such field behaviors
- Motivation to look into alternative methods to this end

Basic definitions

- Finite element method (FEM) expansion :
  - ◇ Node based finite elements : Unknowns associated with nodes in the mesh
  - ◇ Tangential vector finite elements (TVFEs) : Unknowns associated with edges, faces and cells in the mesh

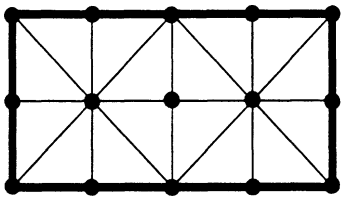

- Polynomial-complete TVFE of order n :
  - ◇ Polynomial variations up to and including order n captured within element and on element boundary
- Nédélec : Polynomial-complete expansion may not be advantageous for representation of electromagnetic fields
- Mixed-order TVFE of order $n - 0.5$:
  - ◇ Polynomial variations up to and including order $n - 1$ captured for tangential component along edges
  - ◇ Polynomial variations up to and including order n captured within element
- Hierarchical mixed-order TVFEs : Vector basis functions of order $n - 0.5$ subset of vector basis functions of order $n + 0.5$
- 'Hierarchical mixed-order TVFE of order $n - 0.5$' has now been defined

Proposed approach

- Principle of 'Selective field expansion'

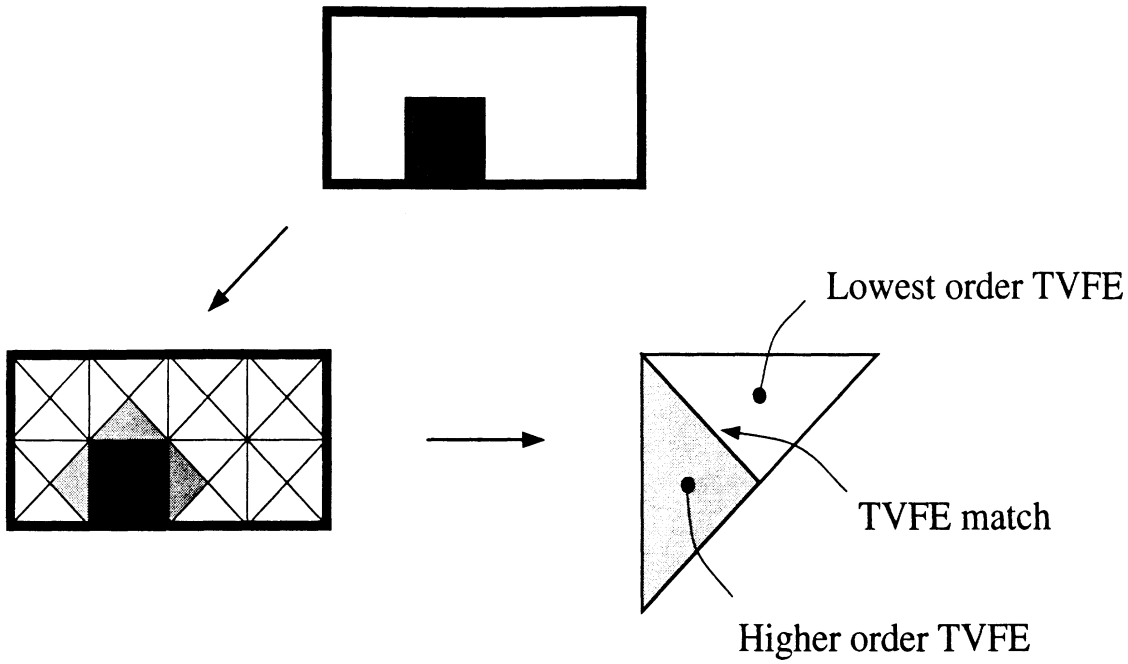

- Selective field expansion using hierarchical mixed-order TVFEs for triangles and tetrahedra seems very attractive

$\Downarrow$

- Proposed approach :
  - ◇ Development and test of hierarchical mixed-order TVFEs for triangular elements (2D problems)
  - ◇ Development and test of hierarchical mixed-order TVFEs for tetrahedral elements (3D problems)
  - ◇ More complex issues and realistic applications

Accomplishments - Overview

- Development of hierarchical mixed-order TVFEs of order 0.5, 1.5 and 2.5 for triangular (2D problems) and tetrahedral (3D problems) elements
- Test of these TVFEs for closed-domain (eigenvalue) as well as open-domain (scattering and radiation) problems

$\Downarrow$

- In terms of accuracy / memory / time requirements, selective field expansion is effective for solution of certain classes of 2D and 3D electromagnetic problems

Hierarchical TVFEs for tetrahedra

- Consider a tetrahedral element with simplex / volume coordinates defined in the usual manner

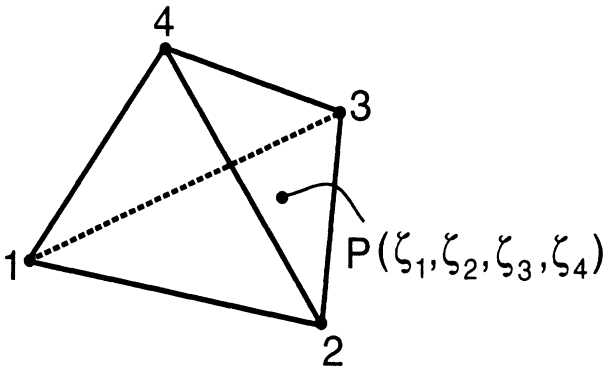

- The number of vector basis functions for a mixed-order TVFE of order $n - 0.5$

$$N_n^{tet} = \frac{n(n+2)(n+3)}{2}$$

- TVFE of order 0.5 ($n = 1 \Longrightarrow N_1^{tet} = 6$)

$$\zeta_i \nabla \zeta_j - \zeta_j \nabla \zeta_i \quad , \; i < j$$

- TVFE of order 1.5 ($n = 2 \Longrightarrow N_2^{tet} = 20 = 6 + 6 + 4 + 4$)

$$\zeta_i \nabla \zeta_j - \zeta_j \nabla \zeta_i \quad , \; i < j$$

$$(\zeta_i - \zeta_j)(\zeta_i \nabla \zeta_j - \zeta_j \nabla \zeta_i) \quad , \; i < j$$

$$\zeta_k(\zeta_i \nabla \zeta_j - \zeta_j \nabla \zeta_i) \quad , \; i < j < k$$

$$\zeta_j(\zeta_k \nabla \zeta_i - \zeta_i \nabla \zeta_k) \quad , \; i < j < k$$

Convergence rate for different order TVFEs

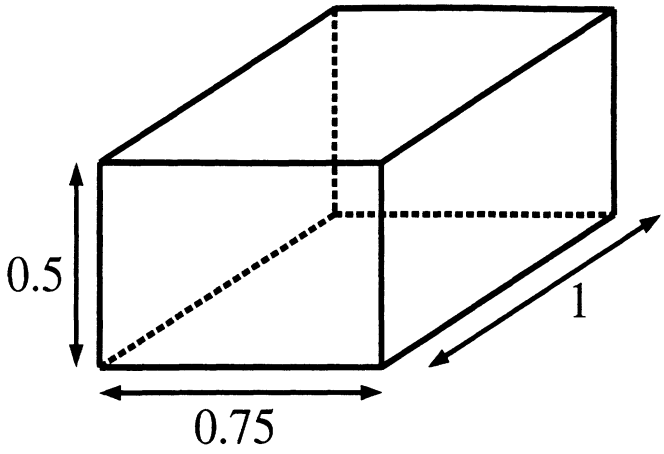

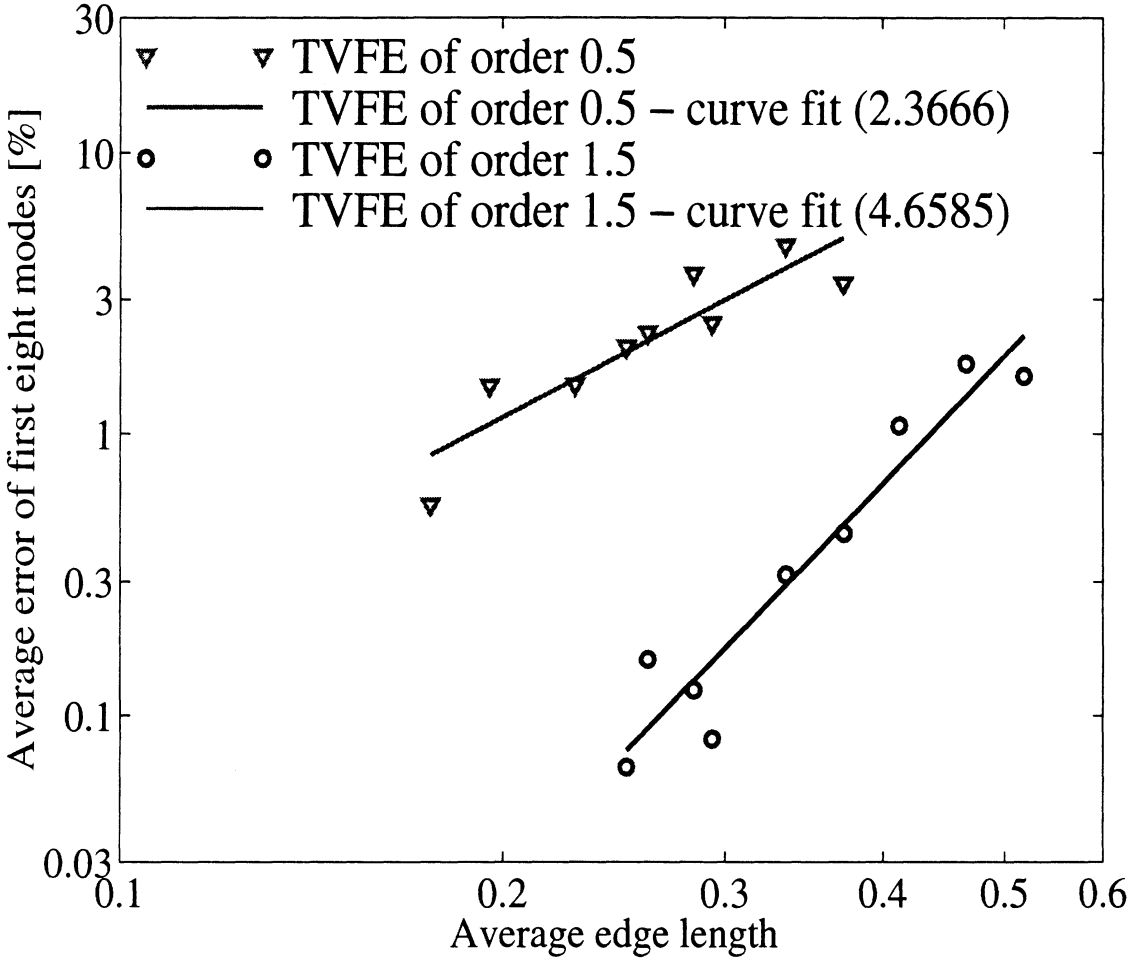

Resonant frequency of patch antenna I

- Geometry (side and top view)

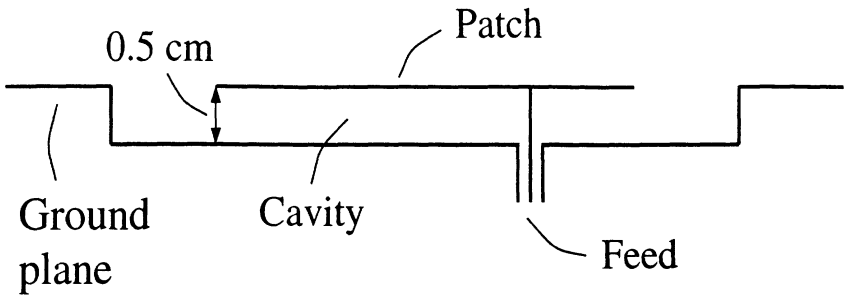

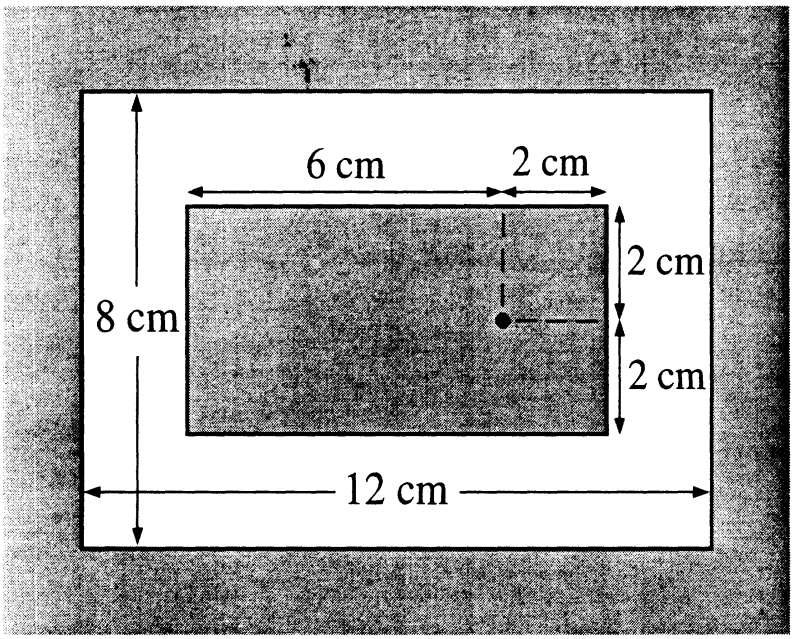

- Standard FEM - Boundary Integral (BI) approach
- Four different cases

Case	TVFE order(s)	Average edge length
1	0.5	1.09 cm
2	0.5	0.77 cm
3	0.5	0.62 cm
4	0.5/1.5	1.09 cm

Resonant frequency of patch antenna II

- Input impedance as a function of frequency

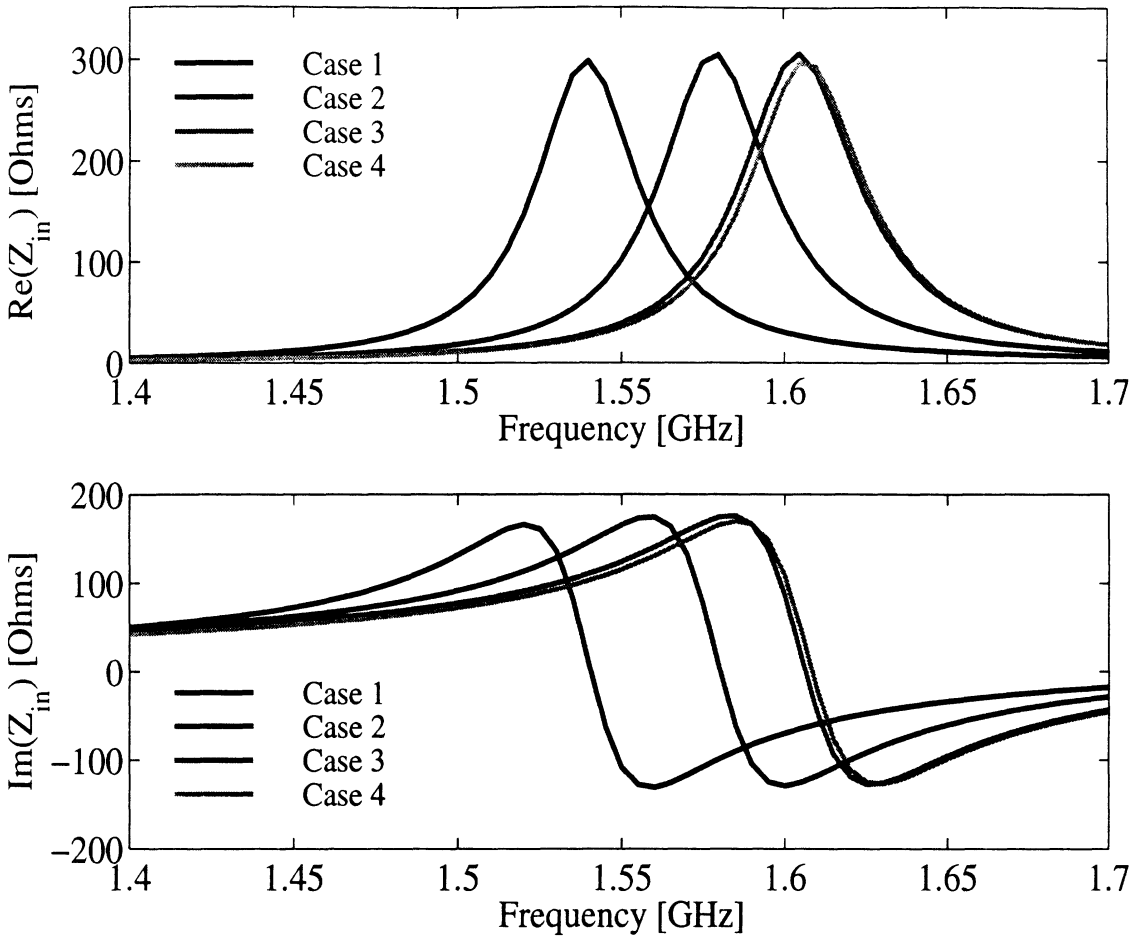

- Some numbers quantifying computational effort

Case	TVFE order(s)	Average edge length	# of unknowns	# of BI unknowns	# of matrix entries	Time per frequency point
1	0.5	1.09 cm	505	160	29607	12 sec
2	0.5	0.77 cm	1189	384	157291	107 sec
3	0.5	0.62 cm	2161	704	**513807**	**501 sec**
4	0.5/1.5	1.09 cm	1263	160	50989	32 sec

Resonant frequency of patch antenna III

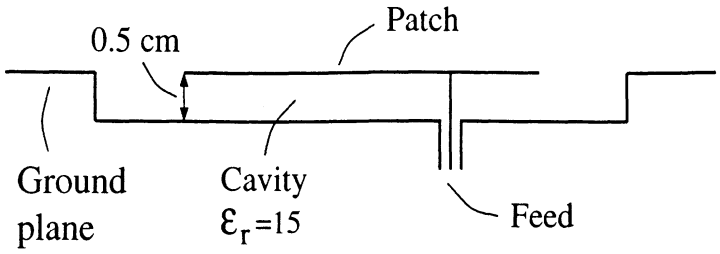

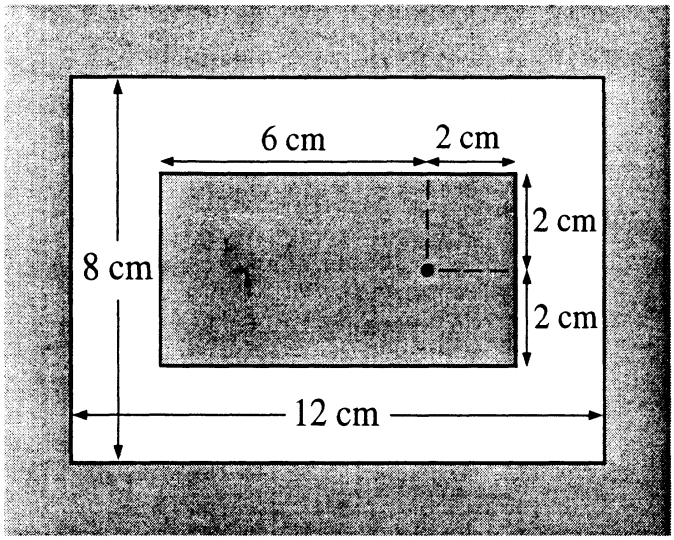

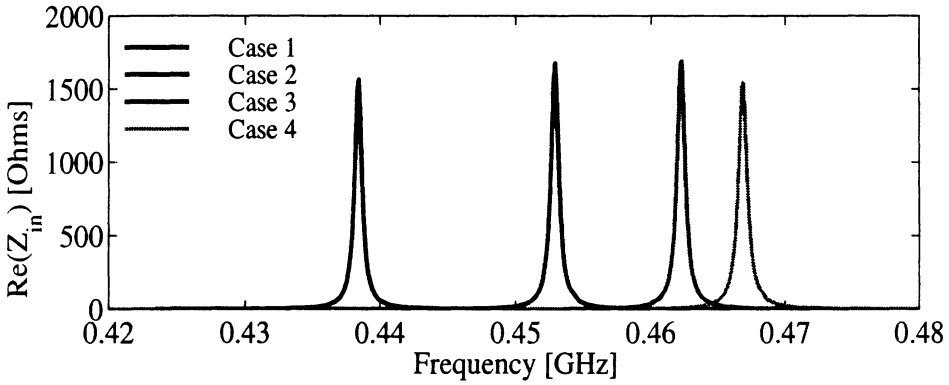

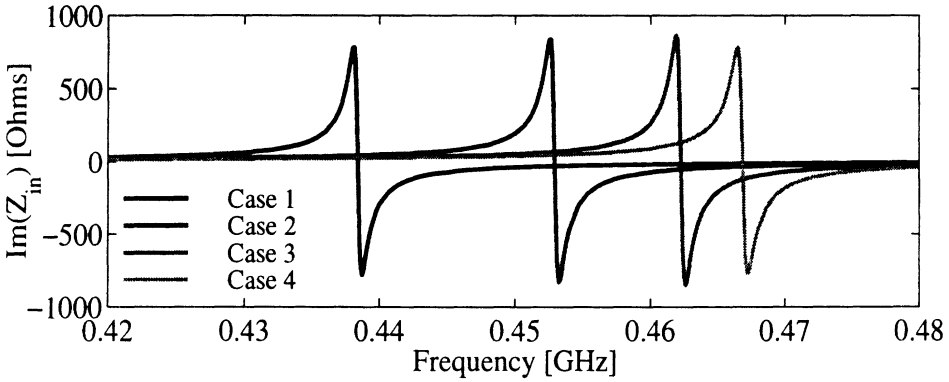

Resonant frequency of patch antenna IV

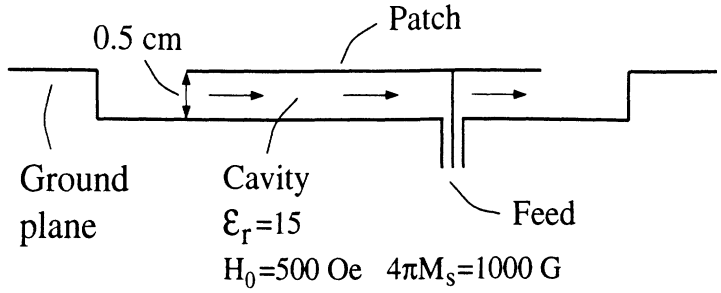

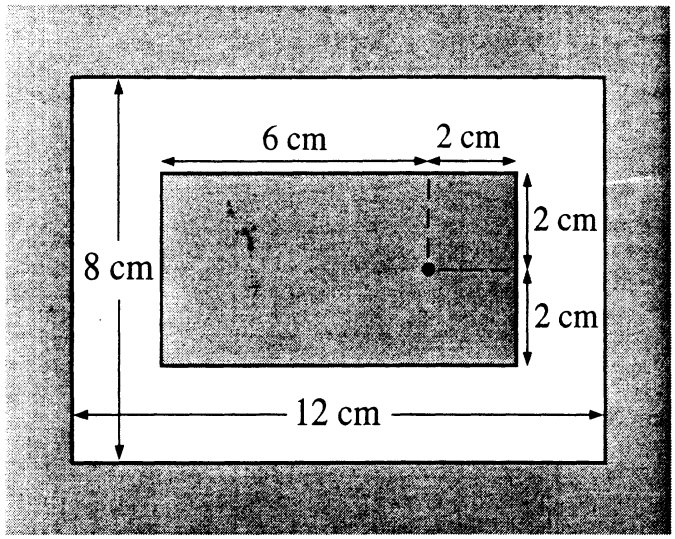

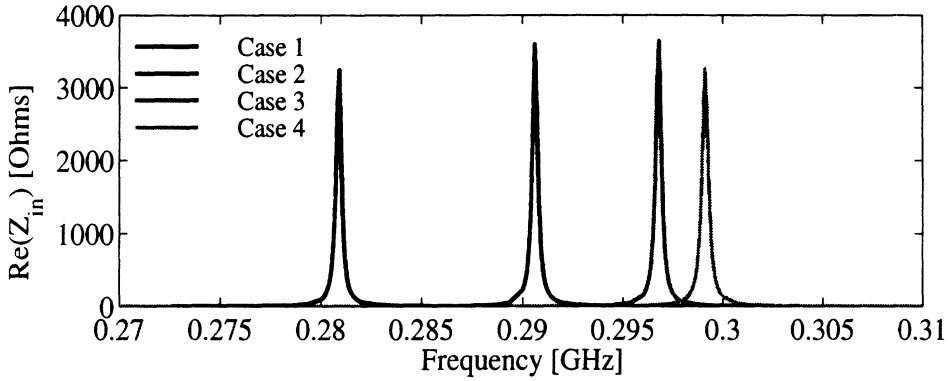

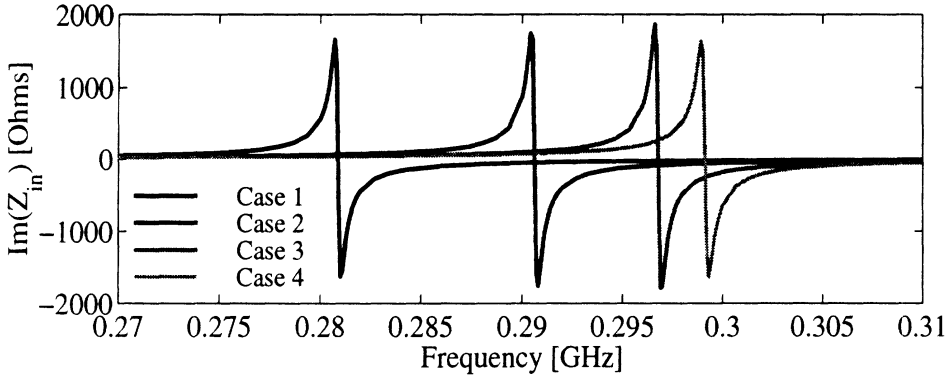

Proposed future work - Overview

- Simple patch antennas
  - ◇ Aim : Understanding of pros and cons of method for simple radiation problems
- Matrix condition numbers
  - ◇ Aim : Investigate possibility of improved matrix conditioning
- Development of adaptive methods for TVFE refinement
  - ◇ Aim : Implementation and test of robust adaptive method for TVFE refinement
- Application of adaptive methods for TVFE refinement
  - ◇ Aim : Use adaptive methods for TVFE refinement to establish design tools for certain classes of ferrite-loaded antennas
- Formulation based on magnetic field
  - ◇ Aim : Carry out a magnetic or a combined electric / magnetic field formulation and investigate its effectiveness
- (Partly) higher order BI formulation
  - ◇ Aim : Carry out such a formulation and investigate its effectiveness

Eigenvalues of inhomogeneous cavity

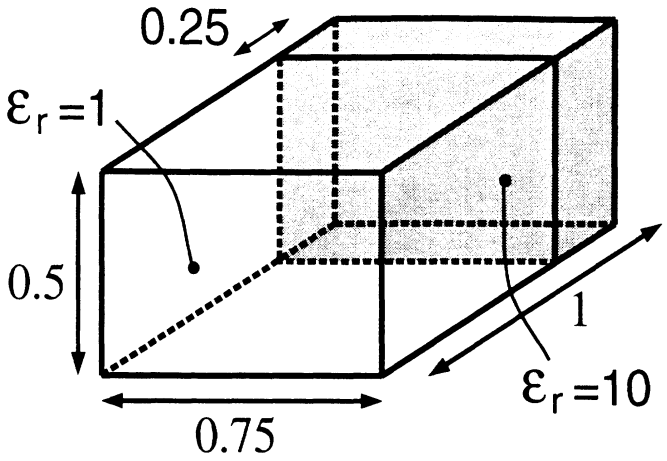

1 : TVFE of order 0.5 (fine mesh)

2 : TVFE of order 1.5 (coarse mesh)

3 : TVFEs of order 0.5 and 1.5 (coarse mesh)

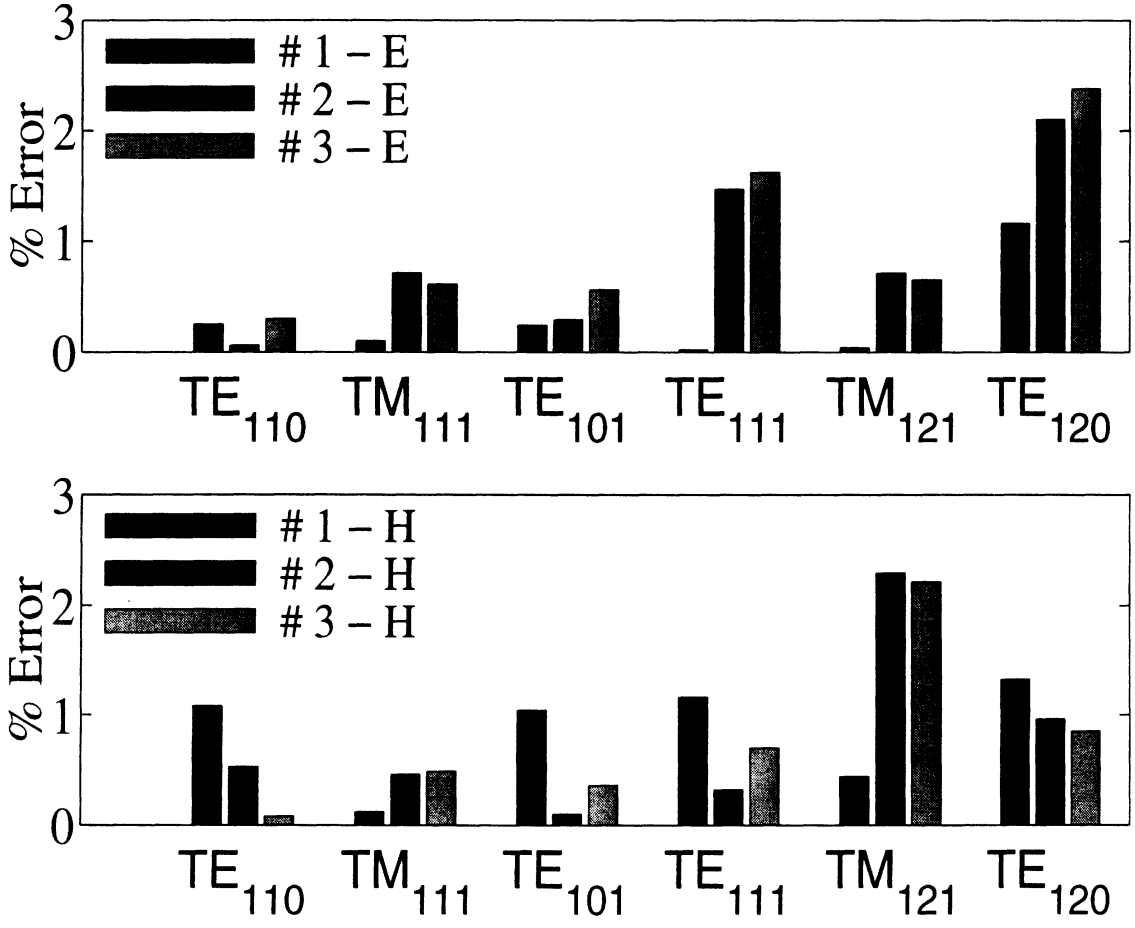

Eigenmode of inhomogeneous cavity

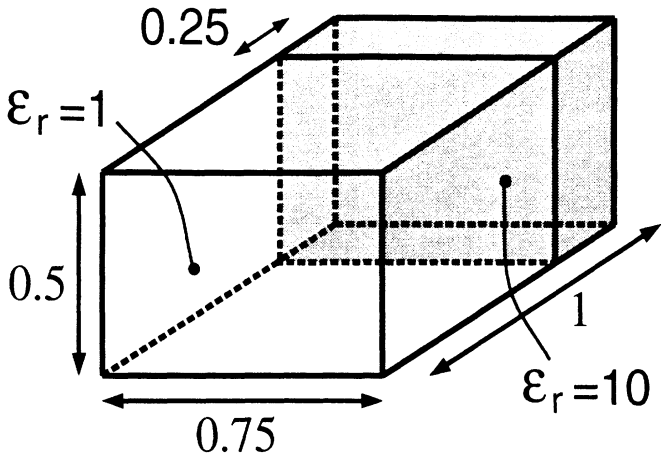

H on back wall for TM_{111} mode (H-formulation)

TVFE of order 0.5

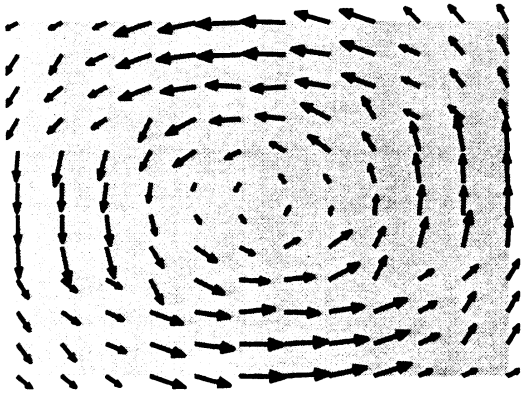

TVFE of order 0.5

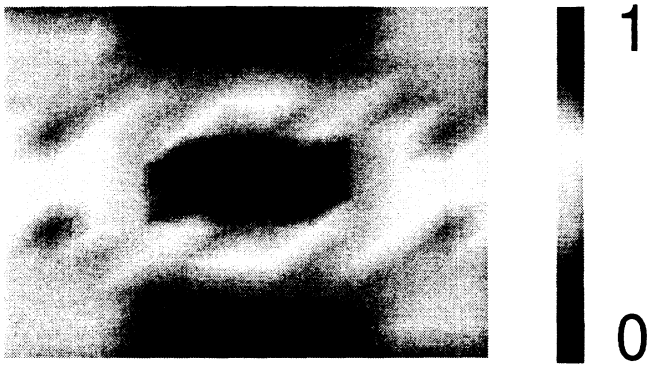

TVFEs of order 0.5/1.5

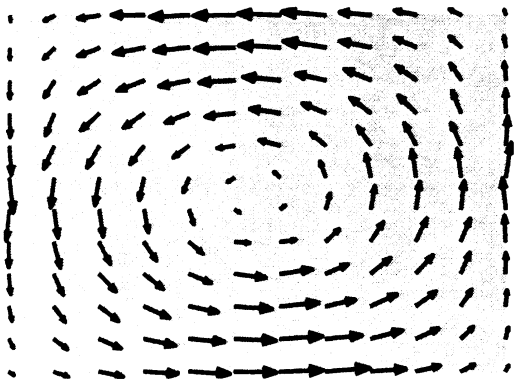

TVFEs of order 0.5/1.5

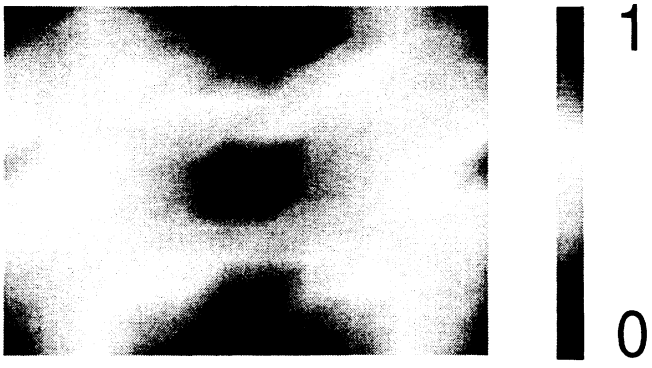

Attached Documents

1. Tetrahedral FE-BI Progress Report
   Arik Brown
2. Formula for Resonant Frequency of Ferrite Patch Antennas
   Zhifang Li
3. FE-BI Analysis of Cavity-Backed Patch Antennas Using Hierarchical Mixed-Order TVFEs
   Lars Andersen
4. Eigenvalue Analysis of 3D Cavities Filled with Complex Materials
   Lars Andersen
5. Review of Microstrip Patch Antennas on Ferrite Substrates
   Zhifang Li

Tetrahedral Finite Element - Boundary Integral(FE-BI) Progress Report

Arik Darnell Brown

October 6, 1998

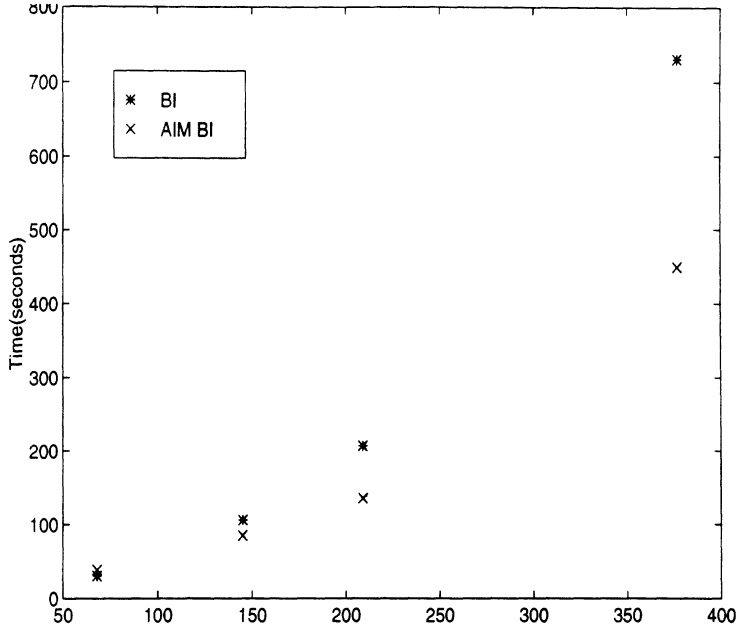

Figure 1: AIM Performance

1 FE-BI Code Enhancement

UofM has successfully implemented the Adaptive Integral Method(AIM) within their tetrahedral FEM-BI code. Figure 1 shows the improvement in speed. Because the ferrite substrates require high sampling, it was imperative to add AIM, in order to combat the increasing number of BI unknowns, which was becoming a bottleneck in relation to cpu time. Figure 2 shows a simple RCS validation of the AIM implementation.

Currently UofM's efforts are being focused on producing a careful analysis of the effects of nonuniform biasing on ferrite patch antennas. In order to proceed with this study, it was necessary to find a result in the literature to validate, and then use this example as a benchmark for nonuniform biasing results. Using Dr. Kempel's FE-BI brick code UofM has validated the paper by Yang [2] for x and y biasing. Figures 3 and 4 show validation results. These results do not pick up the minimum peak levels where the RCS is below -80 dBsm, but tracks the resonance and overall RCS shape.

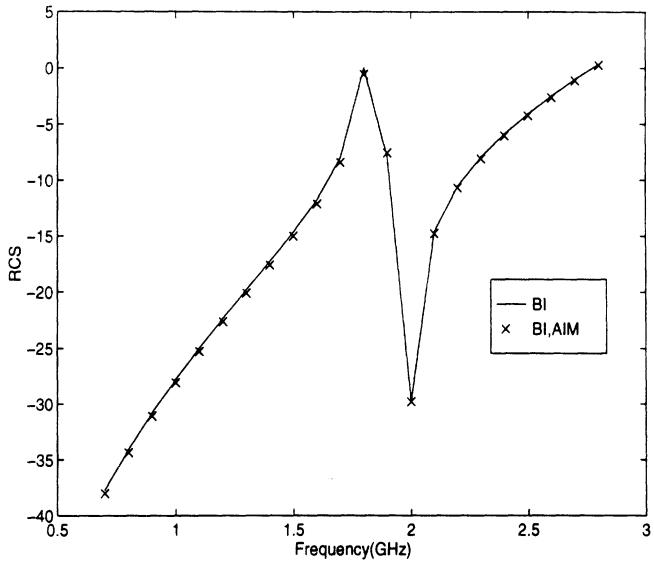

Figure 2: AIM Validation, Kokotoff Thesis p.129 [1]

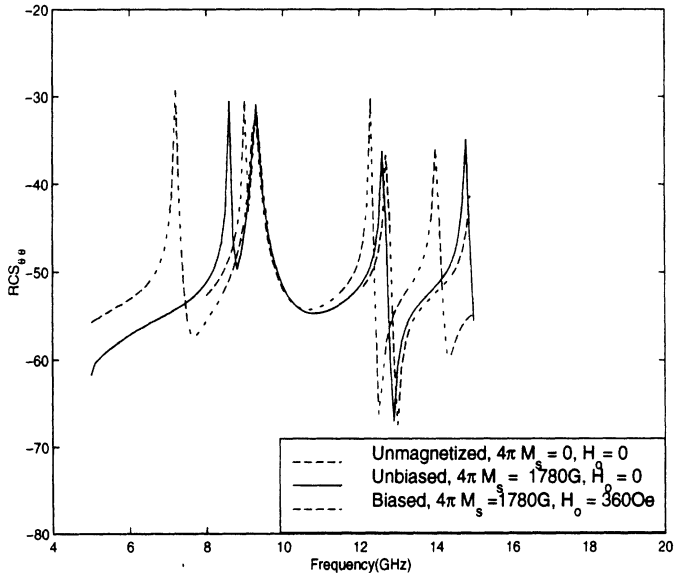

Figure 3: Yang Validation, *x-bias*[2]

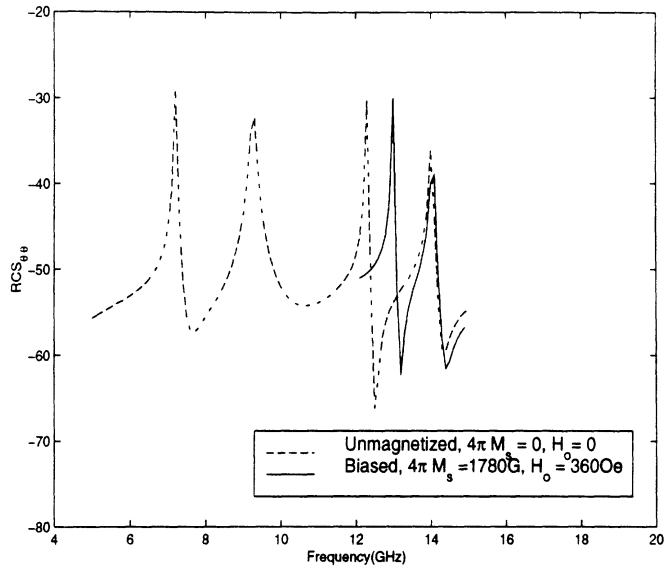

Figure 4: Yang Validation, *y-bias*[2]

The unbiased result was run using the tetrahedral code also. Figure 5 shows the results. From the graph it is recognizable that this validation is similar to the result produced by the brick code, but the RCS resonances are shifted. This is due to the fact that the sampling for the tetrahedral example was not as high as that for the brick. With the addition of AIM it is now possible to sample higher, with reasonable computation time.

Future work will involve:

1. Changing the storage scheme for the BI matrix. This is necessary to facilitate using a higher number of BI unknowns.

2. Producing the Yang results using the tetrahedral code, and then using the tetrahedral code to finish the nonuniform biasing study.

3. Producing circular patch results for ferrite substrates.

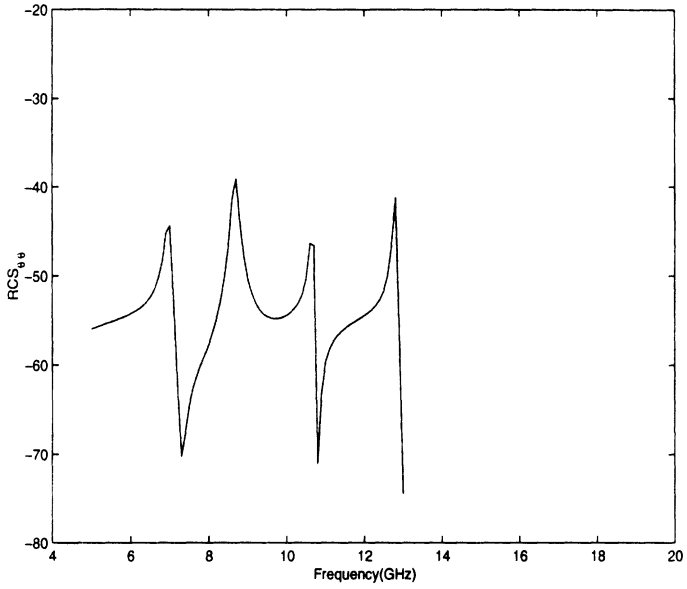

Figure 5: Yang Validation(Tetra Code) [2]

References

[1] D. M. Kokotoff,*Full wave analysis of a ferrite-tuned cavity-backed slot antenna.* PhD thesis, Arizona State University, 1995.

[2] H.Y. Yang, J.A. Castaneda, and N.G. Alexopoulos,"The RCS of a microstrip patch on an arbitrarily biased ferrite substrate,"*IEEE Trans. Antennas Propagat.*, vol. AP-41, no. 12, pp. 1610-1614, 1993.

1 Introduction

In this small report our purpose is to find an empirical formula for the resonant frequency of patch antennas with ferrite substrates and biasing.

It is well known that the resonant frequency for pure dielectric patch antennas can be predicted from

$$f_r^{diel} = \frac{c}{2\sqrt{\epsilon_{reff}}(L+2\Delta L)} \tag{1}$$

where [1]

$$\epsilon_{reff} = \frac{\epsilon_r+1}{2} + \frac{\epsilon_r-1}{2}\frac{1}{(1+12h/W)^{-1/2}} \quad (W/h \geq 1) \tag{2}$$

$$\Delta L = 0.412h\frac{(\epsilon_{reff}+0.3)}{(\epsilon_{reff}-0.258)}\frac{(W/h+0.264)}{(W/h+0.8)} \tag{3}$$

or []

$$\epsilon_{reff} = \frac{\epsilon_r+1}{2} + \frac{\epsilon_r-1}{2}\frac{1}{(1+10h/W)^{-1/2}} \quad (W/h \geq 1) \tag{4}$$

$$\Delta L = \frac{h}{\pi}\frac{(W/h+0.336)}{(W/h+0.556)}\{0.28+\frac{\epsilon_r+1}{\epsilon_r}[0.274+\ln(\frac{W}{h}+2.518)]\} \tag{5}$$

here c is the speed of light, ϵ_{reff} is the effective relative permittivity of the dielectric substrate, L and W are the length and width of the rectangular patch, respectively, and h is the thickness of the dielectric substrate.

Analogous to (1), and taking into consideration of the effective permeability, we would have the same formula for the resonant frequency of ferrite patch antennas:

$$f_r^{fer} = \frac{c}{2\sqrt{\epsilon_{reff}\mu_{reff}}(L+2\Delta L)} \tag{6}$$

However, we do not know the relationship of μ_{reff} with bias field and saturation magnetization. Although we have a standard formula for μ_{reff} (which can be found in next section), that formula does not work very well. Thus, we need to find a practical formula for μ_{reff}.

2 Ferrite Antenna Properties and Relations [3]

Saturation magnetization is a physical property of the ferrite material, and its typical range is from $4\pi M_s = 300$ to 5000 Gauss. Ferrites are usually operated in the saturated state to avoid more loss.

The relationship between *internal bias field* H_0 and *external applied field* H_e is

$$H_0 = H_e - N(4\pi M_s) \tag{7}$$

where N is *demagnetizing factor*, a scalar number between 0 and 1 (in CGS units).

Linewidth ΔH is related to the magnetic loss of ferrites. Its range is typically from 100 Oe to 500 Oe.

Ferrite is a gyrotropic material with *tensor permeability:*

$$[\mu] = \begin{bmatrix} \mu_0 & 0 & 0 \\ 0 & \mu & j\kappa \\ 0 & -j\kappa & \mu \end{bmatrix} (\hat{x} - bias) \tag{8}$$

$$[\mu] = \begin{bmatrix} \mu & 0 & -j\kappa \\ 0 & \mu_0 & 0 \\ j\kappa & 0 & \mu \end{bmatrix} (\hat{y} - bias) \tag{9}$$

where

$$\mu = \mu_0[1 + \frac{\omega_0\omega_m}{\omega_0^2 - \omega^2}] \tag{10}$$

$$\kappa = \mu_0\frac{\omega\omega_m}{\omega_0^2 - \omega^2} \tag{11}$$

with $\omega_0 = \mu_0\gamma H_0$ (Larmor/precession frequency), $\omega_m = \mu_0\gamma M_s$, and γ is the gyromagnetic ratio ($\gamma = 1.76 \times 10^7 radians/sec \cdot oersted$ in CGS units). In unmagnetized state, $M_s = H_0 = 0$. Then $\mu = \mu_0$ and $\kappa = 0$, as expected for nonmagnetic material.

The CGS units are used in ferrite materials traditionally. Here 1 Gauss = 10^{-4} Weber/m^2, and $4\pi \times 10^{-3}$ Oersteds = 1 A/m. Also, with CGS units, the Larmor frequency can be expressed as $f_0 = \omega_0/2\pi$ = (2.8 MHz/Oersted) (H_0 Oersted), and $f_m = \omega_m/2\pi$ = (2.8 MHz/Oersted) ($4\pi M_s$ Gauss)

For a plane wave propagating in a ferrite medium, the field is determined not only by the wave propagation direction, but also by its orientation of the magnetic bias field. Thus, there are two cases to determine the effective permeability μ_e. In the case that both wave propagation and the bias field are in the z direction

$$\mu_e = \frac{1}{\mu_0}(\mu \pm \kappa) \tag{12}$$

whereas in the case that the magnetic field is in-plane biased, transverse to the direction of wave propagation

$$\mu_e = \frac{1}{\mu_0}\frac{\mu^2 - \kappa^2}{\mu} \tag{13}$$

3 Empirical Formula for Patch Antennas with Ferrite Substrate

In this section, we will study a ferrite patch antenna and try to find out the empirical formula of the resonant frequency for ferrite patch. The antenna geometry under investigation is the same as in [4], with $L = W = 0.61$ cm, $h = 0.127$ cm, and $\epsilon_r = 13.9$. We placed the antenna in a 1.22×1.22 cm cavity and a probe feed is located at (0, -0.3) cm relative to the center of the patch. For the isotropic case, the resonance should occur around 5.5 GHz using formulae (1), (4) and (5).

We will concentrate on the in-plane bias case which is more practical, and we only study the $\hat{x}$-bias case in this report. First, we fix the values of saturation magnetization as $4\pi M_s = 650$ G, 800 G, and 1000 G, respectively, when varying the strength of the bias field H_0 for each value of the $4\pi M_s$. To find the resonant frequency which is defined as $f_r = f_{Imag(Z_{in})=0}$, we use constrained optimization methods in combination with the finite element analysis [5]. Figure 1 plots the curves of resonant frequency for the three values of magnetization and for bias field from 0 to 900 Oe.

If we use the standard formula (13) given in last section along with the resonant frequency formula (6), the results are not consistent with Figure 1. Thus, we try to find a modified formula for μ_{reff}.

From (6), we have

$$\mu_{reff} = [\frac{c}{2(L+2\Delta L)f_r^{fer}}]^2 \frac{1}{\epsilon_{reff}} \tag{14}$$

This computed μ_{reff} using f_r^{fer} from optimizer is plotted in Figure 2. It is a function of the standard μ_e and the antenna width-to-thickness ratio $\frac{W}{h}$. Using an order-two polynomial fit, we get an approximate formula for μ_{reff}:

$$\mu_{reff} = \mu_e \frac{h}{W}(10.575\mu_e^2 - 23.564\mu_e + 17.586) \text{ for } \frac{W}{h} \leq 5 \tag{15}$$

where μ_e is from (13). The actual and fitted $\frac{\mu_{reff}}{\mu_e}$ are plotted in Figure 3.

Use this empirical formula, we plot the predicted resonant frequency in Figure 4. It is seen that the predicted ones are quite close to those computed by the optimizer, with errors within 3%.

The above is only the first step to obtain the empirical formula for ferrite patch antennas. We are continuing working on this to get a general formula which can be used for other patches.

References

[1] I.J. Bahl and P. Bhatia, *Microstrip Antennas*, Norwood, MA: Artech House 1980, Ch.2.

[2] C.W. Garvin *et.al.*, "Missile base mounted microstrip antennas,", *IEEE Trans. Antennas Propagat.*, vol. AP-25, pp.604-610, Sept. 1977.

[3] D.M. Pozar, Chap. 10, *Microwave Engineering*, Addison-Wesley, MA 1990.

[4] D.M. Pozar, "Radiation and scattering characteristics of microstrip antennas on normally biased ferrite substrates", *IEEE Trans. Antennas Propagat.*, vol. 40, no. 9, pp. 1084-1092, Sept. 1992.

[5] Zhifang Li, Panos Y. Papalambros, and John L. Volakis, "Designing broadband patch antennas using the sequential quadratic programming method", *IEEE Transactions on Antennas and Propagation*, v.45, n.11, November 1997.

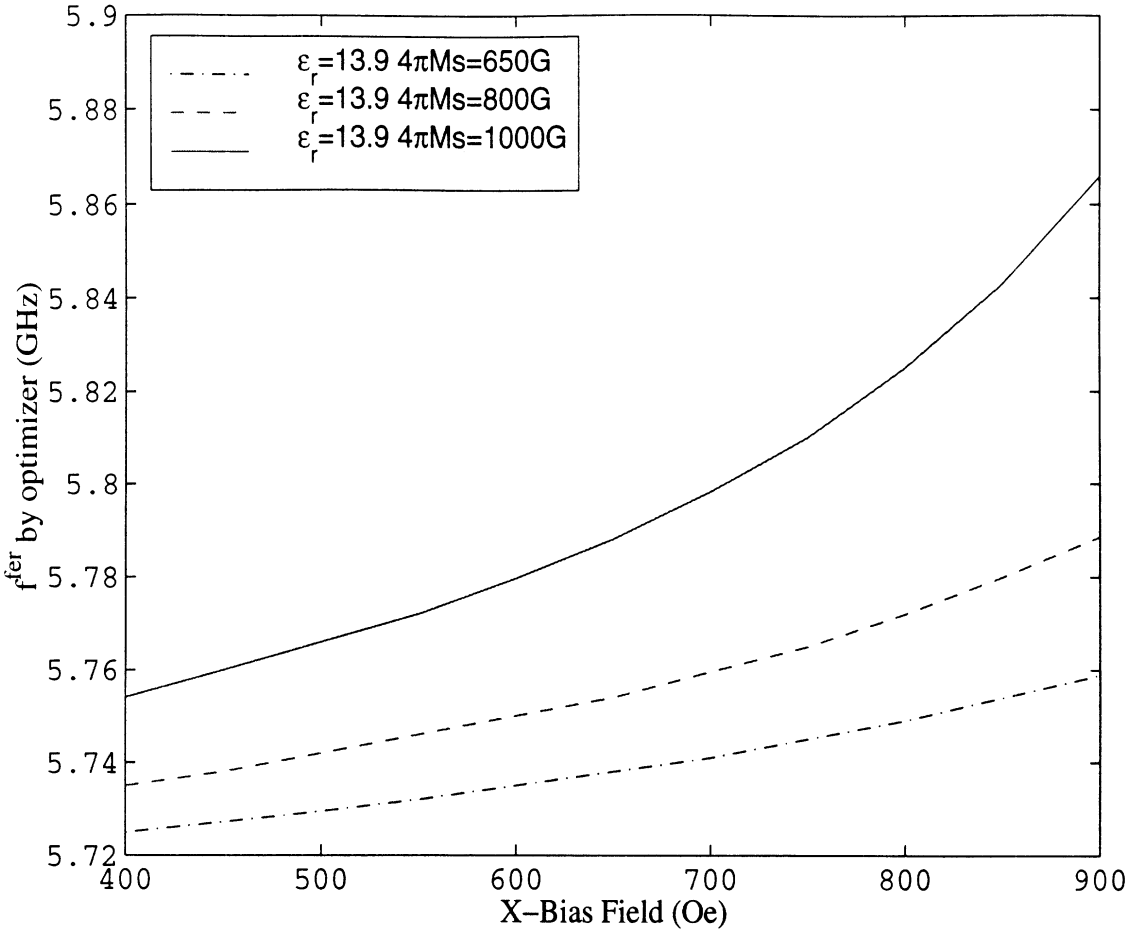

Figure 1: Resonant frequency as a function of X-bias field and saturation magnetization.

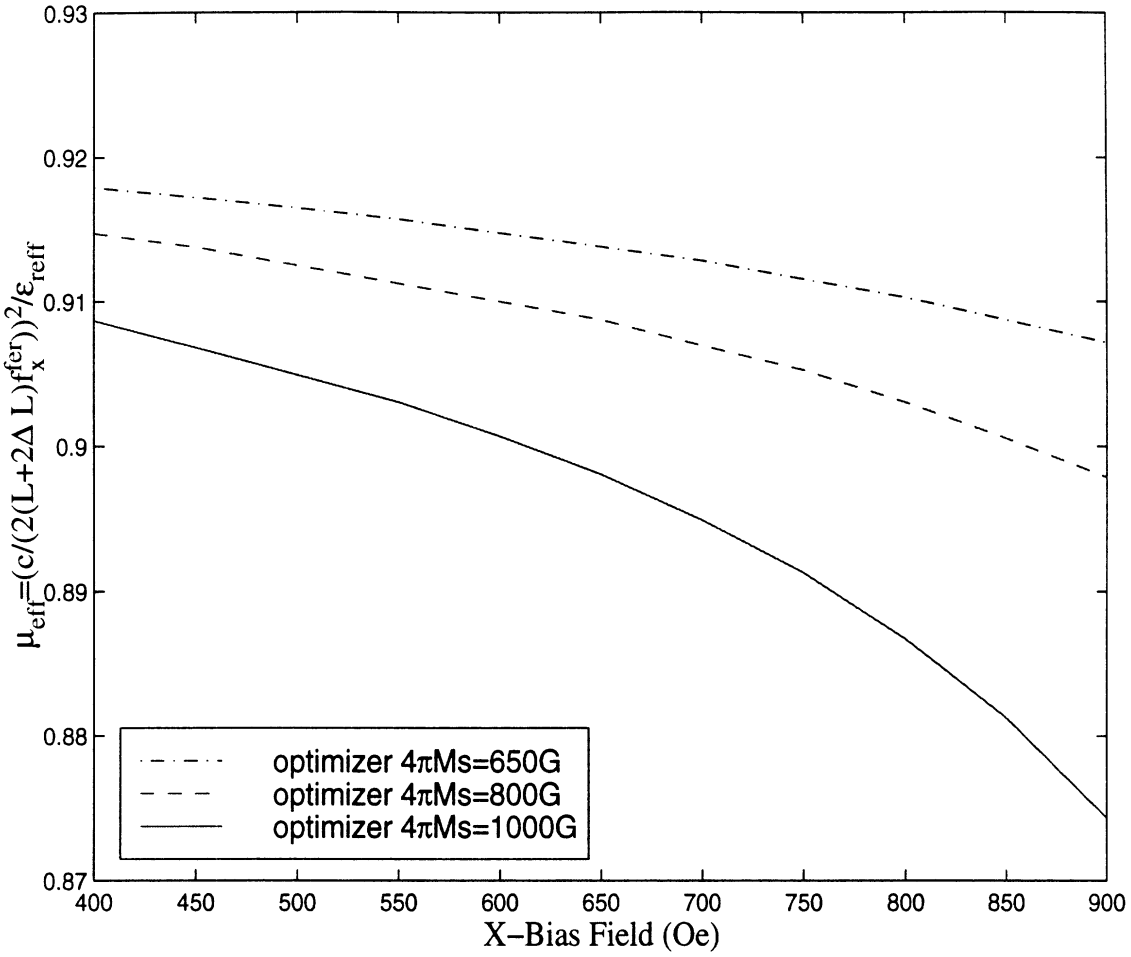

Figure 2: Actual effective permeability from optimizer that needs to be fit.

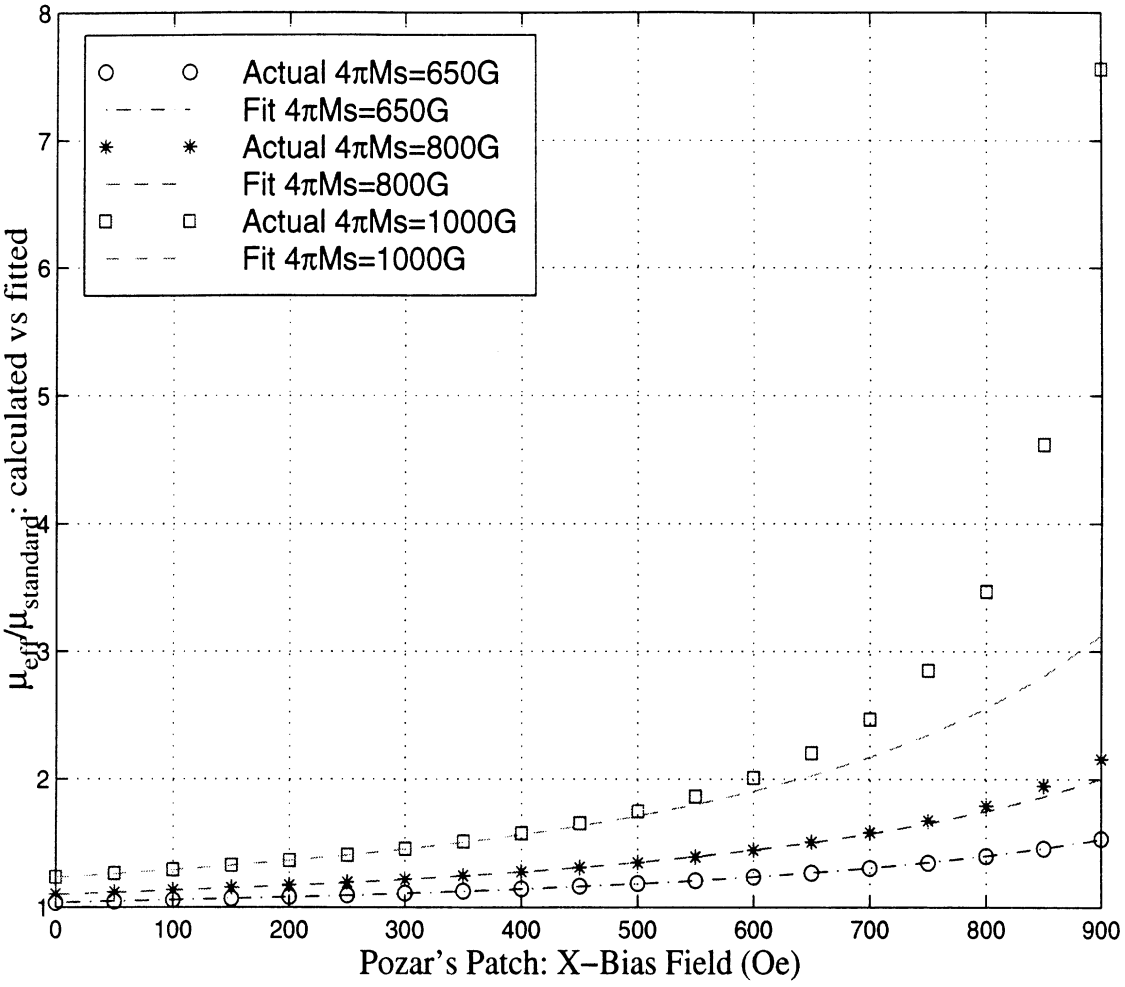

Figure 3: Effective permeability : actual vs fitted.

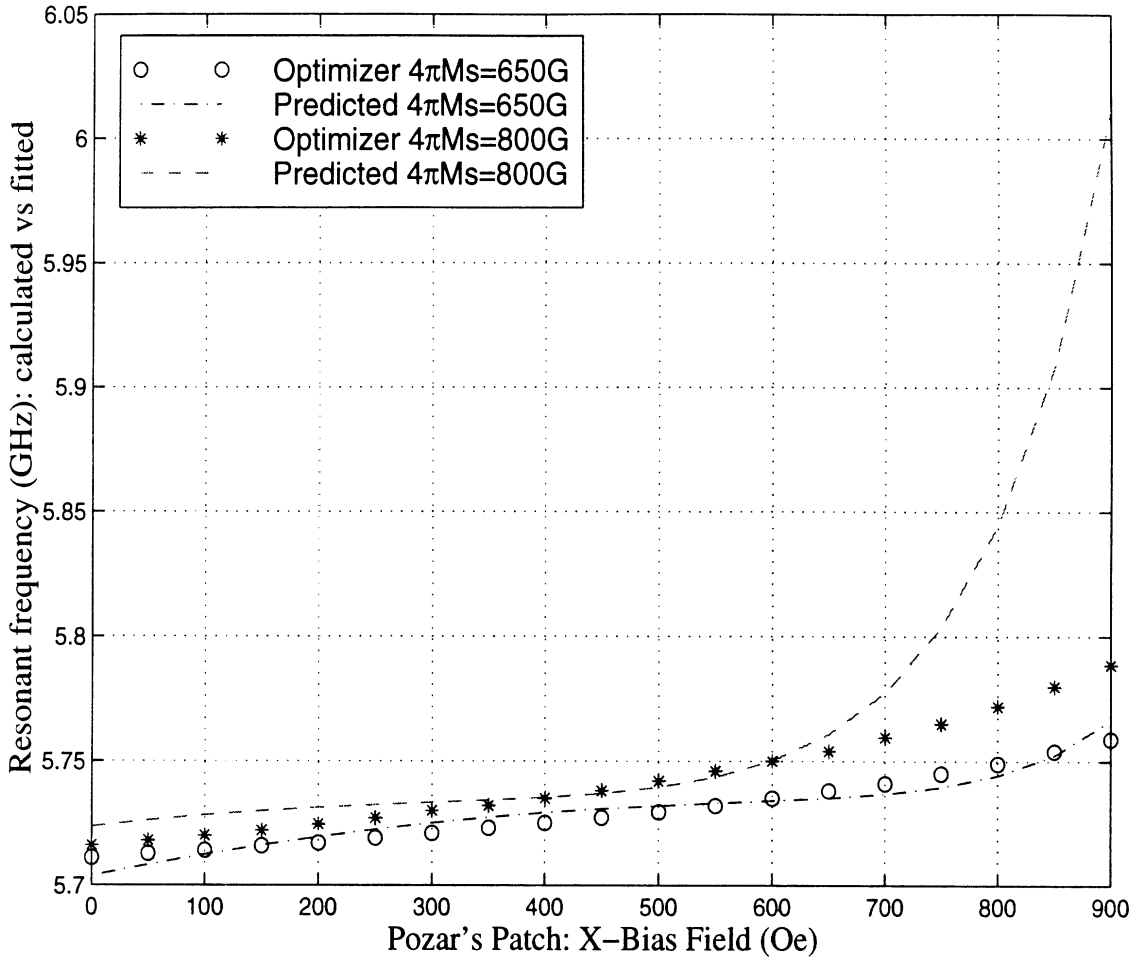

Figure 4: Resonant frequency: actual vs predicted.

Finite Element – Boundary Integral Analysis of Cavity-Backed Patch Antennas using Hierarchical Mixed–Order Tangential Vector Finite Elements for Tetrahedral Elements

Lars S. Andersen

Radiation Laboratory,
Department of Electrical Engineering and Computer Science,
University of Michigan,
Ann Arbor, MI 48109-2122, USA

Abstract

An electric field formulation is presented for finite element - boundary integral analysis of cavity-backed patch antennas recessed in an infinite ground plane using hierarchical mixed-order tangential vector finite elements for tetrahedral elements. Numerical results are included to show the validity of the formulation and to demonstrate that selective field expansion using hierarchical mixed-order tangential vector finite elements for tetrahedral elements is a promising approach for a certain class of antenna radiation problems.

1 Introduction

Ferro- and ferri-magnetic materials are attractive for antenna miniaturization and pattern synthesis. Accurate simulation of such complex materials is therefore of increasing practical importance. However, brute force application of existing numerical methods often fails to efficiently model antennas containing such materials. Proper discretization in a certain region of the computational domain can lead to excess discretization elsewhere resulting in an unmanageable computational problem. Further, ferro- and ferri-magnetic materials can result in poor system matrix conditioning and consequently lead to convergence difficulties for an iterative linear system solver. Hence, computational engines based on existing numerical methods have serious difficulties in simulating and designing antennas involving complex materials.

Robust and efficient modeling of material-loaded antennas calls for a numerical discretization scheme permitting a combination of higher and lower order field or current expansions

within a computational domain. The finite element method (FEM) has been demonstrated to be attractive for modeling complex material compositions and in the context of the FEM, a discretization scheme is referred to as hierarchical if the expansion of order, say, n is a subset of the expansion of order $n+1$. Hierarchical discretization schemes permit robust combination of different order expansions within a computational domain for an effective discretization of the unknown quantity. The concept of hierarchality is widely known but the applications hereof in electromagnetics seem few and far between. Nevertheless, FEM discretization exploiting hierarchality appears to be a nearly ideal candidate for simulating and designing material-loaded antennas of high geometric complexity.

For FEM discretization of a computational domain, the so-called mixed-order tangential vector finite elements (TVFEs) are attractive because they guarantee tangential field continuity across element boundaries and suppress spurious modes. Based on an existing expansion of surface currents over a generalized quadrilateral, a set of hierarchical mixed-order TVFEs for a triangular element has been developed [1, 2]. These TVFEs have been thoroughly tested for electromagnetic scattering computations involving two-dimensional cylinders of complicated shape and material composition. Because of the promising results when different order TVFEs are combined within a computational domain (as compared to cases where the same TVFE is used throughout the computational domain, more accurate results are obtained using less CPU time and less memory when different order TVFEs are combined within the computational domain), a set of hierarchical mixed-order TVFEs for a tetrahedral element has also been developed [3, 4] and tested for eigenvalue analysis of cavities filled with complex materials [5].

This report describes the testing of the set of hierarchical mixed-order TVFEs for a tetrahedral element [3, 4] for finite element (FE) - boundary integral (BI) analysis of cavity-backed patch antennas recessed in an infinite ground plane. In section 2, an electric field formulation is presented for FE-BI analysis of cavity-backed patch antennas recessed in an infinite ground plane using TVFEs. Numerical results are given in section 3 to show the validity of the formulation and to demonstrate that selective field expansion using hierarchical mixed-order TVFEs for tetrahedral elements is a promising approach for a certain class of antenna radiation problems.

2 Formulation

Consider a perfectly electrically conducting (PEC) patch antenna backed by a cavity and recessed in an infinite PEC ground plane. The cavity-backed patch antenna is situated in free space characterized by the permittivity ε_0 and the permeability μ_0 as illustrated in Fig. 1 (side view) and Fig. 2 (top view) for the case of a triangular patch backed by a finite circular cylindrical cavity. The volume of the possibly inhomogeneous and anisotropic cavity is denoted by V and characterized by the permittivity tensor $\overline{\overline{\varepsilon}}$ and the permeability tensor $\overline{\overline{\mu}}$. The boundary of the cavity V is denoted by Γ_V. The non-PEC part of Γ_V (i.e. the surface between the ground plane and the patch) is denoted by S while the PEC part of Γ_V (i.e. the patch and the bottom and side walls of the cavity) is denoted by $\Gamma_V \setminus S$.

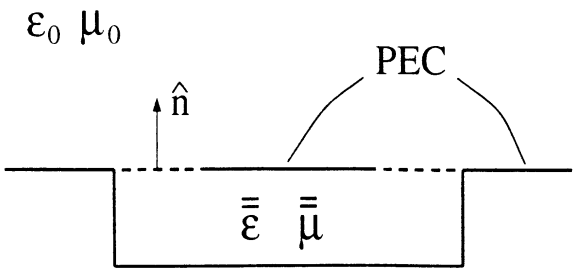

Figure 1: Side view of cavity-backed patch antenna recessed in an infinite PEC ground plane.

Figure 2: Top view of cavity-backed patch antenna recessed in an infinite PEC ground plane for the case of a triangular patch and a circular cylindrical cavity.

Assuming the antenna feed is described by an electric volume current density $\mathbf{J}$ within V, the electric and magnetic field intensities $\mathbf{E}$ and $\mathbf{H}$, respectively, fulfill Maxwell's two curl equations [1]

$$\nabla \times \mathbf{E} = -j\omega \bar{\bar{\mu}} \cdot \mathbf{H} \tag{1}$$

$$\nabla \times \mathbf{H} = j\omega \bar{\bar{\varepsilon}} \cdot \mathbf{E} + \mathbf{J} \tag{2}$$

Combination of Maxwell's equations (1) and (2) leads to the vector wave equation

$$\nabla \times (\bar{\bar{\mu}}^{-1} \cdot \nabla \times \mathbf{E}) - \omega^2 \bar{\bar{\varepsilon}} \cdot \mathbf{E} = -j\omega \mathbf{J} \tag{3}$$

for $\mathbf{E}$. By applying Galerkin's method with the vector weighting function $\mathbf{T}$ onto (3), we derive the weak form

$$\int_V [(\nabla \times \mathbf{T}) \cdot (\bar{\bar{\mu}}^{-1} \cdot \nabla \times \mathbf{E}) - \omega^2 \mathbf{T} \cdot (\bar{\bar{\varepsilon}} \cdot \mathbf{E})]\, dV = -j\omega \int_V \mathbf{T} \cdot \mathbf{J}\, dV + j\omega \int_S \mathbf{T} \cdot (\hat{n} \times \mathbf{H})\, dS \tag{4}$$

where $\hat{n}$ denotes the unit normal vector to S directed out of V and where a surface integral over the PEC part $\Gamma_V \setminus S$ of Γ_V has been eliminated since it vanishes. Introducing now the relative permittivity and permeability tensors $\bar{\bar{\varepsilon}}_r$ and $\bar{\bar{\mu}}_r$ by

$$\bar{\bar{\varepsilon}} = \bar{\bar{\varepsilon}}_r \varepsilon_0 \tag{5}$$

$$\bar{\bar{\mu}} = \bar{\bar{\mu}}_r \mu_0 \tag{6}$$

we obtain

$$\int_V [(\nabla \times \mathbf{T}) \cdot (\bar{\bar{\mu}}_r^{-1} \cdot \nabla \times \mathbf{E}) - k_0^2 \mathbf{T} \cdot (\bar{\bar{\varepsilon}}_r \cdot \mathbf{E})]\, dV = -j\omega\mu_0 \int_V \mathbf{T} \cdot \mathbf{J}\, dV + j\omega\mu_0 \int_S \mathbf{T} \cdot (\hat{n} \times \mathbf{H})\, dS \tag{7}$$

[1] Throughout the report, a time factor $e^{j\omega t}$ is assumed and suppressed.

with $k_0 = \omega\sqrt{\varepsilon_0\mu_0}$ being the free space wavenumber.

We now proceed to discretize (7) using the FE-BI method. We initially neglect the surface integral in (7) and discretize

$$\int_V [(\nabla \times \mathbf{T}) \cdot (\bar{\bar{\mu}}_r^{-1} \cdot \nabla \times \mathbf{E}) - k_0^2\, \mathbf{T} \cdot (\bar{\bar{\varepsilon}}_r \cdot \mathbf{E})]\, dV = -j\omega\mu_0 \int_V \mathbf{T} \cdot \mathbf{J}\, dV \tag{8}$$

to obtain a FE system of linear equations. Upon discretization of the surface integral

$$j\omega\mu_0 \int_S \mathbf{T} \cdot (\hat{n} \times \mathbf{H})\, dS \tag{9}$$

of (7) using a BI (an expression of $\mathbf{H}$ in terms of $\mathbf{E}$) and subsequent correction of the FE system of equations according to (7), the final FE-BI system of linear equations is obtained.

We consider (8). Let us discretize V via

$$V = \sum_{e=1}^{N_V} V^e \tag{10}$$

where N_V denotes the number of tetrahedral elements and enforce (8) in each element V^e. Next, we expand the electric field $\mathbf{E}^e$ in V^e via

$$\mathbf{E}^e = \sum_{j=1}^{N} E_j^e \mathbf{W}_j^e \tag{11}$$

where E_j^e and $\mathbf{W}_j^e$ are unknown expansion coefficients and vector basis functions, respectively, for the eth element. Choosing the vector weighting functions $\mathbf{T} = \mathbf{W}_i^e$, $i = 1, \cdots, N$, leads to

$$\sum_{j=1}^{N} \int_{V^e} [(\nabla \times \mathbf{W}_i^e) \cdot (\bar{\bar{\mu}}_r^{-1} \cdot \nabla \times \mathbf{W}_j^e) - k_0^2\, \mathbf{W}_i^e \cdot (\bar{\bar{\varepsilon}}_r \cdot \mathbf{W}_j^e)]\, dV\, E_j^e = -j\omega\mu_0 \int_{V^e} \mathbf{W}_i^e \cdot \mathbf{J}\, dV \tag{12}$$

The N element equations (12) for the eth element can be formulated in the matrix form

$$A^e E^e = g^e \tag{13}$$

where E^e is a vector containing the unknown expansion coefficients E_j^e, A^e is the element matrix with entries

$$A_{ij}^e = \int_{V^e} [(\nabla \times \mathbf{W}_i^e) \cdot (\bar{\bar{\mu}}_r^{-1} \cdot \nabla \times \mathbf{W}_j^e) - k_0^2\, \mathbf{W}_i^e \cdot (\bar{\bar{\varepsilon}}_r \cdot \mathbf{W}_j^e)]\, dV \tag{14}$$

and g^e is the excitation vector with entries

$$g_i^e = -j\omega\mu_0 \int_{V^e} \mathbf{W}_i^e \cdot \mathbf{J}\, dV \tag{15}$$

Assembly of the element equations (13) and elimination of unknowns along $\Gamma_V \setminus S$ then leads to a global matrix equation system that can be formulated

$$\begin{bmatrix} A^{II} & A^{IS} \\ A^{SI} & A^{SS} \end{bmatrix} \begin{bmatrix} E^I \\ E^S \end{bmatrix} = \begin{bmatrix} g^I \\ g^S \end{bmatrix} \tag{16}$$

In (16), A^{II}, A^{IS}, A^{SI} and A^{SS} are known matrices, g^I and g^S are known vectors and E^I and E^S are vectors containing the unknown expansion coefficients associated with the interior of V (superscript I) and the boundary S of V (superscript S). This is the desired FE system of linear equations resulting from discretization of (8).

We now consider the surface integral (9) which is in terms of the magnetic field $\mathbf{H}$. As mentioned earlier, we seek an expression in terms of the electric field $\mathbf{E}$. This is obtained by using the surface equivalence principle [6] to relate $\mathbf{H}$ to $\mathbf{E}$ just outside S via

$$\mathbf{H} = -2j\omega\varepsilon_0 \int_S \overline{\overline{\mathrm{G}}}_0(\mathbf{r},\mathbf{r}') \cdot (\mathbf{E}' \times \hat{n}')\, dS' \tag{17}$$

where $\overline{\overline{\mathrm{G}}}_0$ is the dyadic free space Green's function given by

$$\overline{\overline{\mathrm{G}}}_0(\mathbf{r},\mathbf{r}') = (\,\bar{\bar{\mathrm{I}}} + \frac{1}{k_0^2}\nabla\nabla\,)\, G_0(\mathbf{r},\mathbf{r}') \tag{18}$$

with $\bar{\bar{\mathrm{I}}}$ being the unit dyad and G_0 denoting the scalar free space Green's function given by

$$G_0(\mathbf{r},\mathbf{r}') = \frac{e^{-jk_0|\mathbf{r}-\mathbf{r}'|}}{4\pi|\mathbf{r}-\mathbf{r}'|} \tag{19}$$

Substitution of (17) for $\mathbf{H}$ into the surface integral (9) yields

$$j\omega\mu_0 \int_S \mathbf{T} \cdot (\hat{n} \times \mathbf{H})\, dS = 2\, k_0^2 \int_S \mathbf{T} \cdot (\hat{n} \times \int_S \overline{\overline{\mathrm{G}}}_0(\mathbf{r},\mathbf{r}') \cdot (\mathbf{E}' \times \hat{n}')\, dS'\,)\, dS \tag{20}$$

which is in terms of $\mathbf{E}$ and can be directly discretized. Before doing so, it is advantageous to substitute $\overline{\overline{\mathrm{G}}}_0$ from (18) and use elementary vector identities to obtain

$$\begin{aligned} j\omega\mu_0 \int_S \mathbf{T} \cdot (\hat{n} \times \mathbf{H})\, dS =& 2\, k_0^2 \int_S \int_{S'} G_0(\mathbf{r},\mathbf{r}')\, (\mathbf{E}' \times \hat{n}') \cdot (\mathbf{T} \times \hat{n})\, dS'\, dS \\ & -2 \int_S \int_{S'} G_0(\mathbf{r},\mathbf{r}')\, \nabla' \cdot (\mathbf{E}' \times \hat{n}')\, \nabla \cdot (\mathbf{T} \times \hat{n})\, dS'\, dS \end{aligned} \tag{21}$$

Consistent with the discretization of V into elements via (10), we now discretize S into segments via

$$S = \sum_{e=1}^{N_S} S^e \tag{22}$$

Next, we expand the tangential electric field $\mathbf{E}^e_{tang}$ linearly in S^e via

$$\mathbf{E}^e_{tang} = \sum_{j=1}^{M} E^e_{t,j} \mathbf{V}^e_j \tag{23}$$

where $E^e_{t,j}$ and $\mathbf{V}^e_j$ are unknown expansion coefficients and vector basis functions, respectively, for the eth segment. We obtain for $\mathbf{T} = \mathbf{V}^e_i$, $i = 1, \cdots, M$, the equations

$$j\omega\mu_0 \int_S \mathbf{T} \cdot (\hat{n} \times \mathbf{H})\, dS = \sum_{e'=1}^{N_S} \sum_{j=1}^{M} \int_{S^e} \int_{S^{e'}} G_0(\mathbf{r}, \mathbf{r}') \Big[2\, k_0^2\, \mathbf{V}^{e'}_j \cdot \mathbf{V}^e_i - 2\, \nabla' \cdot (\mathbf{V}^{e'}_j \times \hat{n}')\, \nabla \cdot (\mathbf{V}^e_i \times \hat{n}) \Big]\, dS'\, dS\, E^{e'}_{t,j} \tag{24}$$

Upon assembly of these equations, we end up with

$$j\omega\mu_0 \int_S \mathbf{T} \cdot (\hat{n} \times \mathbf{H})\, dS = \begin{bmatrix} 0 & 0 \\ 0 & B^{SS} \end{bmatrix} \begin{bmatrix} E^I \\ E^S \end{bmatrix} \tag{25}$$

which it the desired discretization of (9).

The FE-BI discretization of (7) now follows from the FE discretization (16) of (8) representing the FE part of (7) by combining it with the BI discretization (25) of (9) representing the BI part of (7). We obtain the final FE-BI system

$$\begin{bmatrix} A^{II} & A^{IS} \\ A^{SI} & A^{SS} - B^{SS} \end{bmatrix} \begin{bmatrix} E^I \\ E^S \end{bmatrix} = \begin{bmatrix} g^I \\ g^S \end{bmatrix} \tag{26}$$

3 Numerical results

To test the developed hierarchical mixed-order TVFEs for tetrahedral elements and investigate the effectiveness of selective field expansion where different mixed-order TVFEs are combined within a computational domain, we consider in this section a simple antenna radiation problem.

Consider a PEC rectangular patch antenna backed by a rectangular cavity and recessed in an infinite PEC ground plane. The cavity-backed patch antenna is situated in free space as illustrated in Fig. 3 (side view) and Fig. 4 (top view). The possibly inhomogeneous and anisotropic cavity is of height h, width w and depth d. The patch is centered above the cavity and of width w_p and depth d_p. It is fed by a vertical coaxial line whose outer conductor is attached to the ground plane and whose inner conductor is attached to the patch at distances w_f (width) and d_f (depth) from the lower left corner of the cavity. In our simulation, the coaxial feed will be modeled as a vertical probe of constant current. We choose the parameters $h = 0.5$ cm, $w = 12$ cm, $d = 8$ cm, $w_p = 8$ cm, $d_p = 4$ cm, $w_f = 8$ cm and $d_f = 4$ cm.

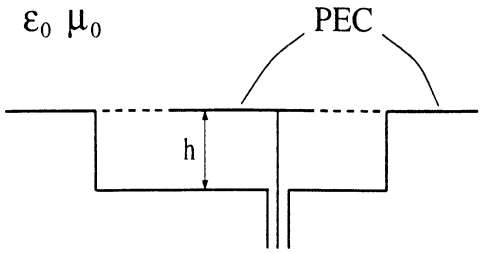

Figure 3: Side view of a rectangular patch antenna backed by a rectangular cavity recessed in an infinite PEC ground plane.

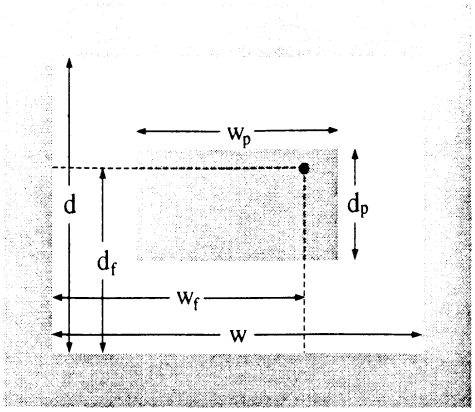

Figure 4: Top view of a rectangular patch antenna backed by a rectangular cavity recessed in an infinite PEC ground plane.

The antenna can be analyzed using the FE-BI method presented in section 2. We discretize V into tetrahedral elements and consequently discretize S into triangular segments. Two different TVFE options will be applied. Whitney [7] proposed a mixed-order TVFE of order 0.5 for a tetrahedral element and we will use this TVFE as our first option. For a mesh of average edge length 1.09 cm (Case 1), the input impedance will be determined as a function of frequency and the resonant frequency of the patch will be estimated. The coarse discretization means that this resonant frequency is most likely not accurate. For meshes of average edge lengths of 0.77 cm (Case 2) and 0.62 cm (Case 3), more accurate resonant frequencies but also more computational effort can be expected. Andersen and Volakis [3, 4] proposed hierarchical mixed-order TVFEs of order 0.5 (identical to the Whitney TVFE), 1.5 and 2.5 for a tetrahedral element. The property of hierarchality permits a combination of different order TVFEs within the computational domain. As our second option, we will use the mixed-order TVFE of order 1.5 within part of the cavity (close to the radiating edges where we expect high field variation) and the mixed-order TVFE of order 0.5 elsewhere (where we expect little field variation). For the mesh of average edge length 1.09 cm (Case 4), the resonant frequency will again be estimated. The effectiveness of this approach in terms of accuracy and time / memory requirements will be compared to the previous approach of refining the mesh density. The four cases are summarized in Tab. 1.

3.1 Empty cavity

Consider an empty cavity, i.e. $\bar{\bar{\varepsilon}}_r = \bar{\bar{I}}$ and $\bar{\bar{\mu}}_r = \bar{\bar{I}}$. Real and imaginary parts of the input impedance as a function of frequency is given in Fig. 5 for Case 1-4 [2]. As expected, each of the Cases 1-3 gives a different resonant frequency. More importantly, this change is picked up very well when we partly change the TVFE order to 1.5 instead of changing the mesh density (Case 4). Case 4 matches Case 3 exactly which validates the selective field expansion approach. Tab. 2 shows the computational effort (number of unknowns, number

[2]The resonant frequency for the patch was confirmed by a previously validated FE-BI code based on TVFEs of order 0.5 for prismatic elements [8].

Case	TVFE order(s)	Average edge length
1	0.5	1.09 cm
2	0.5	0.77 cm
3	0.5	0.62 cm
4	0.5/1.5	1.09 cm

Table 1: Definition of Case 1-4.

of BI unknowns, number of non-zero matrix entries (proportional to memory) and time per frequency point) for the four cases. We see that the improvement in accuracy from Case 1 to Case 3 comes at a much higher cost than the improvement from Case 1 to Case 4 (about a factor of 10 in memory and 15 in time). Thus, without compromising accuracy, selective field expansion can offer significant computational savings as compared to the more traditional approach of refining the mesh density.

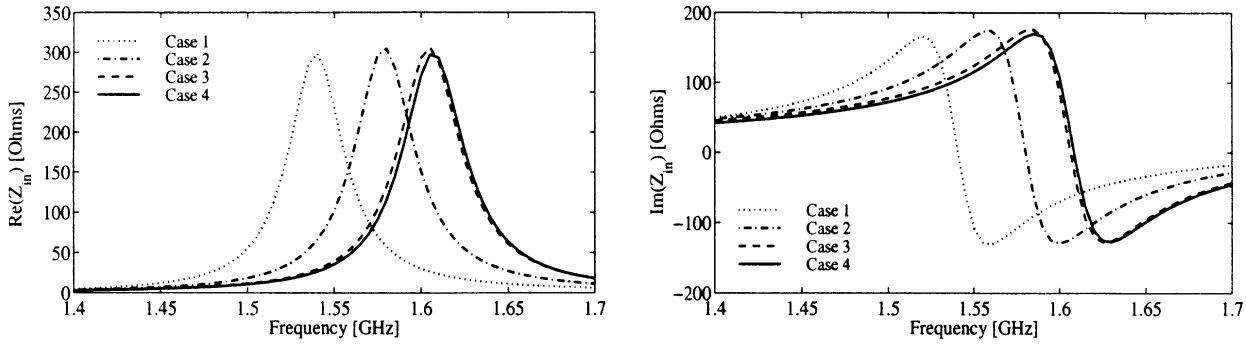

Figure 5: Real and imaginary part of the input impedance of a cavity-backed patch antenna recessed in an infinite ground plane for an empty cavity.

Case	TVFE order(s)	Average edge length	# of unknowns	# of BI unknowns	# of matrix entries	Time per frequency point
1	0.5	1.09 cm	505	160	29607	12 sec
2	0.5	0.77 cm	1189	384	157291	107 sec
3	0.5	0.62 cm	2161	704	513807	501 sec
4	0.5/1.5	1.09 cm	1263	160	50989	32 sec

Table 2: Computational effort for Case 1-4 for empty cavity.

3.2 Cavity containing a dielectric material

Consider a cavity containing a dielectric material for which $\bar{\bar{\varepsilon}}_r = 15\ \bar{\bar{I}}$ and $\bar{\bar{\mu}}_r = \bar{\bar{I}}$. Real and imaginary parts of the input impedance as a function of frequency is given in Fig. 6 for Case 1-4. Although the agreement between Case 3 and Case 4 is not as good as for the empty cavity, the same trends can be observed. In fact, the differences between the

Cases 1-3 suggest that use of a TVFE of order 0.5 for a mesh of average edge length less than 0.62 cm would result in a slightly larger resonant frequency and very possibly an even better agreement with Case 4. Differences in the level of input impedances at resonance are probably due to a too low frequency sampling rate.

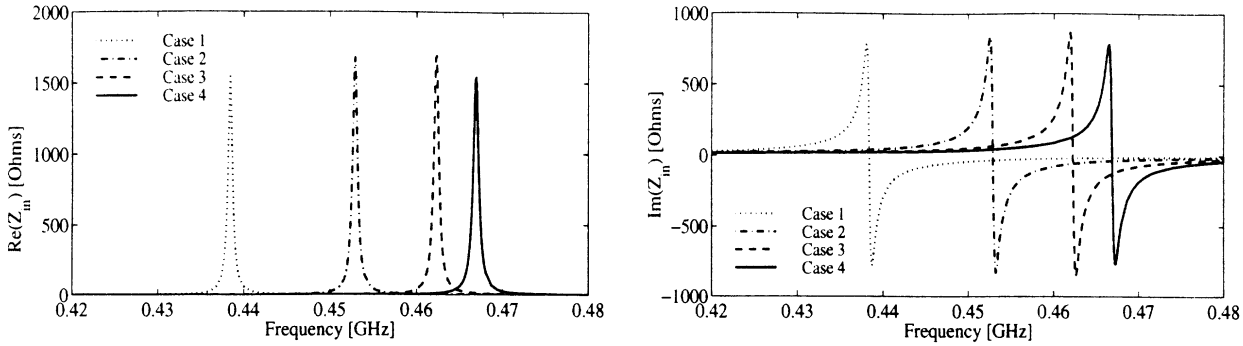

Figure 6: Real and imaginary part of the input impedance of a cavity-backed patch antenna recessed in an infinite ground plane for a cavity containing a dielectric material.

3.3 Cavity containing a gyrotropic material

Consider a cavity containing a gyrotropic material for which $\overline{\overline{\varepsilon}}_r = 15\ \overline{\overline{I}}$ and $\overline{\overline{\mu}}_r$ is given by

$$\overline{\overline{\mu}}_r = \begin{bmatrix} 1 & 0 & 0 \\ 0 & \mu & j\kappa \\ 0 & -j\kappa & \mu \end{bmatrix} \tag{27}$$

in a coordinate system with $\hat{x}$, $\hat{y}$ and $\hat{z}$ directed left to right, front to back and bottom to top, respectively. In the dyad (27)

$$\mu = 1 + \frac{\omega_0 \omega_m}{\omega_0^2 - \omega^2} \tag{28}$$

$$\kappa = \frac{\omega \omega_m}{\omega_0^2 - \omega^2} \tag{29}$$

with ω_0 and ω_m being parameters characterizing the gyrotropic material. The material is biased in the $\hat{x}$-direction, i.e. left to right. We choose the parameters $\omega_0 = 8.80\,10^9$ rad and $\omega_0 = 1.76\,10^{10}$ rad corresponding to a bias field of H_0=500 Oersted and a saturation magnetization of $4\pi M_s$=1000 Gauss. Real and imaginary parts of the input impedance as a function of frequency is given in Fig. 7 for Case 1-4. Remarks similar to those for a cavity containing a dielectric material hold in this case.

4 Summary and conclusions

An electric field formulation was presented for FE-BI analysis of cavity-backed patch antennas recessed in an infinite ground plane using TVFEs. Numerical results were given to show

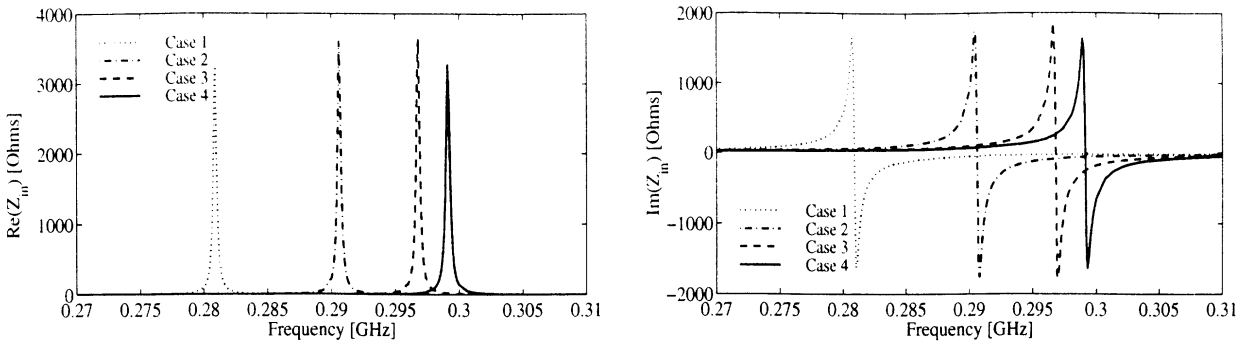

Figure 7: Real and imaginary part of the input impedance of a cavity-backed patch antenna recessed in an infinite ground plane for a cavity containing a gyrotropic material.

the validity of the formulation and to demonstrate that selective field expansion using hierarchical mixed-order TVFEs for tetrahedral elements is a promising approach for a certain class of antenna radiation problems.

References

[1] L.S. Andersen and J.L. Volakis, 'A novel class of hierarchical higher order tangential vector finite elements for electromagnetics', *Proceedings of the IEEE Antennas and Propagation Society International Symposium 1997*, Montréal, Québec, Canada, vol. 2, pp. 648-651, July 1997.

[2] L.S. Andersen and J.L. Volakis, 'Development and application of a novel class of hierarchical tangential vector finite elements for electromagnetics', Submitted to *IEEE Trans. Antennas Propagat.*, September 1997.

[3] L.S. Andersen and J.L. Volakis, 'Hierarchical tangential vector finite elements for tetrahedra', *IEEE Microwave and Guided Wave Letters*, vol. 8, pp. 127-129, March 1998.

[4] L.S. Andersen and J.L. Volakis, 'Hierarchical tangential vector finite elements for tetrahedra', *Proceedings of the IEEE Antennas and Propagation Society International Symposium 1998*, Atlanta, Georgia, USA, vol. 1, pp. 240-243, June 1998.

[5] L.S. Andersen, 'Eigenvalue analysis of three-dimensional cavities filled with complex materials', Internal report, Radiation Laboratory, Department of Electrical Engineering and Computer Science, University of Michigan, Ann Arbor, MI 48109-2122, Spring 1998.

[6] J.-M. Jin and J.L. Volakis, 'A finite element - boundary integral formulation for scattering by three-dimensional cavity-backed apertures', *IEEE Trans. Antennas Propagat.*, vol. AP-39, pp. 97-104, January 1991.

[7] H. Whitney, *Geometric integration theory*, Princeton University Press, 1957.

[8] T. Özdemir, *Finite element analysis of conformal antennas*, Ph.D. dissertation, Radiation Laboratory, University of Michigan, 1998.

Eigenvalue Analysis of Three-Dimensional Cavities Filled with Complex Materials

Lars S. Andersen

Radiation Laboratory,
Department of Electrical Engineering and Computer Science,
University of Michigan,
Ann Arbor, MI 48109-2122, USA

Abstract

Electric and magnetic field formulations are presented for finite element method solution of three-dimensional eigenvalue problems in the case of inhomogeneous and anisotropic volumes enclosed by perfectly electrically conducting surfaces. Issues related to efficient and robust numerical eigenvalue computation are discussed. Numerical results are included to show the validity of the formulations and the computer code and to demonstrate that selective field expansion using hierarchical mixed-order tangential vector finite elements for tetrahedral elements is a promising approach for a certain class of eigenvalue problems.

1 Introduction

Complex materials such as ferro- and ferri-magnetic materials are attractive for antenna miniaturization and pattern synthesis and accurate simulation of complex materials is therefore of increasing practical importance. However, brute force application of existing numerical methods typically fails to efficiently model antennas containing such materials. Proper discretization in a certain region of the computational domain often leads to excess discretization elsewhere resulting in an unmanageable computational problem. Further, material complexity can result in convergence problems for a linear system solver. Hence, computational engines based on existing numerical methods have serious difficulties in simulating and designing antennas involving complex materials.

Robust and efficient modeling of material-loaded antennas calls for a numerical discretization scheme which allows for combination of higher and lower order field or current expansions within a computational domain. The finite element method (FEM) has been demonstrated to be attractive for modeling complex material compositions and in the context of the FEM, a discretization scheme is referred to as hierarchical if the expansion of order, say, n is a

subset of the expansion of order $n+1$. Hierarchical discretization schemes allow for robust combination of expansions of different orders within a computational domain for effective discretization of the unknown quantity. The concept of hierarchality is widely known but the applications hereof in electromagnetics seem few and far between. Nevertheless, FEM discretization exploiting hierarchality appears to be a nearly ideal candidate for simulating and designing material-loaded antennas of high geometric complexity.

For FEM discretization of a computational domain, the so-called mixed-order tangential vector finite elements (TVFEs) are attractive because they guarantee tangential field continuity across element boundaries and suppress spurious modes. Based on an existing expansion of surface currents over a generalized quadrilateral, a set of hierarchical mixed-order TVFEs for a triangular element has been developed [1, 2]. These TVFEs have passed a sanity check for eigenvalue computation and have been thoroughly tested for electromagnetic scattering computations involving two-dimensional cylinders of complicated shape and material composition. Because of the promising results when different order TVFEs are combined within a computational domain (as compared to cases where the same TVFE is used throughout the computational domain, more accurate results are obtained using less CPU time and less memory when different order TVFEs are combined within the computational domain) a set of hierarchical mixed-order TVFEs for a tetrahedral element has also been developed [3, 4].

This report describes the testing of the set of hierarchical mixed-order TVFEs for a tetrahedral element [3, 4] for eigenvalue analysis of three-dimensional cavities filled with complex materials. In section 2, E- and H-formulations are presented for FEM solution of three-dimensional eigenvalue problems in the case of inhomogeneous and anisotropic volumes enclosed by perfectly electrically conducting (PEC) surfaces. Issues related to efficient and robust numerical eigenvalue computation are discussed in section 3. Numerical results are given in section 4 to show the validity of the formulations and the computer code and to demonstrate that selective field expansion using hierarchical mixed-order TVFEs for tetrahedral elements is a promising approach for a certain class of eigenvalue problems.

2 Formulation

Consider a possibly inhomogeneous and anisotropic cavity V electromagnetically characterized by the permittivity tensor $\overline{\overline{\varepsilon}}$ and the permeability tensor $\overline{\overline{\mu}}$. The cavity V is assumed to be free of sources and the boundary S of V is assumed to be a PEC surface. The electric and magnetic field intensities $\mathbf{E}$ and $\mathbf{H}$, respectively, then fulfill Maxwell's equations [1]

$$\nabla \times \mathbf{E} = -j\omega \overline{\overline{\mu}} \cdot \mathbf{H} \tag{1}$$

$$\nabla \times \mathbf{H} = j\omega \overline{\overline{\varepsilon}} \cdot \mathbf{E} \tag{2}$$

Combination of Maxwell's equations (1) and (2) leads to the vector wave equations

$$\nabla \times (\overline{\overline{\mu}}^{-1} \cdot \nabla \times \mathbf{E}) - \omega^2 \overline{\overline{\varepsilon}} \cdot \mathbf{E} = 0 \tag{3}$$

[1] Throughout the report, a time factor $e^{j\omega t}$ is assumed and suppressed.

$$\nabla \times (\bar{\bar{\varepsilon}}^{-1} \cdot \nabla \times \mathbf{H}) - \omega^2 \bar{\bar{\mu}} \cdot \mathbf{H} = 0 \tag{4}$$

for $\mathbf{E}$ and $\mathbf{H}$. By applying Galerkin's method with the vector weighting function $\mathbf{T}$, we derive their weak forms

$$\int_V [(\nabla \times \mathbf{T}) \cdot (\bar{\bar{\mu}}^{-1} \cdot \nabla \times \mathbf{E}) - \omega^2 \mathbf{T} \cdot (\bar{\bar{\varepsilon}} \cdot \mathbf{E})]\, dV + \int_S \mathbf{T} \cdot (\hat{n} \times (\bar{\bar{\mu}}^{-1} \cdot \nabla \times \mathbf{E}))\, dS = 0 \tag{5}$$

$$\int_V [(\nabla \times \mathbf{T}) \cdot (\bar{\bar{\varepsilon}}^{-1} \cdot \nabla \times \mathbf{H}) - \omega^2 \mathbf{T} \cdot (\bar{\bar{\mu}} \cdot \mathbf{H})]\, dV + \int_S \mathbf{T} \cdot (\hat{n} \times (\bar{\bar{\varepsilon}}^{-1} \cdot \nabla \times \mathbf{H}))\, dS = 0 \tag{6}$$

where $\hat{n}$ denotes the outward directed unit normal vector to V. Since S is a PEC surface, the boundary integrals in (5) and (6) vanish and hence

$$\int_V [(\nabla \times \mathbf{T}) \cdot (\bar{\bar{\mu}}^{-1} \cdot \nabla \times \mathbf{E}) - \omega^2 \mathbf{T} \cdot (\bar{\bar{\varepsilon}} \cdot \mathbf{E})]\, dV = 0 \tag{7}$$

$$\int_V [(\nabla \times \mathbf{T}) \cdot (\bar{\bar{\varepsilon}}^{-1} \cdot \nabla \times \mathbf{H}) - \omega^2 \mathbf{T} \cdot (\bar{\bar{\mu}} \cdot \mathbf{H})]\, dV = 0 \tag{8}$$

We now discretize V via

$$V = \sum_{e=1}^{N_V} V^e \tag{9}$$

and enforce (7) and (8) in each element V^e, i.e.

$$\int_{V^e} [(\nabla \times \mathbf{T}) \cdot (\bar{\bar{\mu}}^{-1} \cdot \nabla \times \mathbf{E}) - \omega^2 \mathbf{T} \cdot (\bar{\bar{\varepsilon}} \cdot \mathbf{E})]\, dV = 0 \tag{10}$$

$$\int_{V^e} [(\nabla \times \mathbf{T}) \cdot (\bar{\bar{\varepsilon}}^{-1} \cdot \nabla \times \mathbf{H}) - \omega^2 \mathbf{T} \cdot (\bar{\bar{\mu}} \cdot \mathbf{H})]\, dV = 0 \tag{11}$$

Next, we expand $\mathbf{E}$ and $\mathbf{H}$ in V^e via

$$\mathbf{E}^e = \sum_{j=1}^{N} E_j^e \mathbf{W}_j^e \tag{12}$$

$$\mathbf{H}^e = \sum_{j=1}^{N} H_j^e \mathbf{W}_j^e \tag{13}$$

where E_j^e and H_j^e, $j = 1, \cdots, N$, are unknown expansion coefficients and $\mathbf{W}_j^e$ are vector basis functions for the eth element. Choosing the vector weighting functions $\mathbf{T}_i^e = \mathbf{W}_i^e$, $i = 1, \cdots, N$, then leads to

$$\sum_{j=1}^{N} \int_{V^e} (\nabla \times \mathbf{W}_i^e) \cdot (\bar{\bar{\mu}}^{-1} \cdot \nabla \times \mathbf{W}_j^e)\, dV\, E_j^e = \omega^2 \sum_{j=1}^{N} \int_{V^e} \mathbf{W}_i^e \cdot (\bar{\bar{\varepsilon}} \cdot \mathbf{W}_j^e)\, dV\, E_j^e \tag{14}$$

$$\sum_{j=1}^{N} \int_{V^e} (\nabla \times \mathbf{W}_i^e) \cdot (\bar{\bar{\varepsilon}}^{-1} \cdot \nabla \times \mathbf{W}_j^e)\, dV\, H_j^e = \omega^2 \sum_{j=1}^{N} \int_{V^e} \mathbf{W}_i^e \cdot (\bar{\bar{\mu}} \cdot \mathbf{W}_j^e)\, dV\, H_j^e \qquad (15)$$

for $i = 1, \cdots, N$. Introducing now the relative permittivity and permeability tensors $\bar{\bar{\varepsilon}}_r$ and $\bar{\bar{\mu}}_r$ by

$$\bar{\bar{\varepsilon}} = \bar{\bar{\varepsilon}}_r \varepsilon_0 \qquad (16)$$

$$\bar{\bar{\mu}} = \bar{\bar{\mu}}_r \mu_0 \qquad (17)$$

where ε_0 and μ_0 are the free space permittivity and permeability, respectively, we obtain

$$\sum_{j=1}^{N} \int_{V^e} (\nabla \times \mathbf{W}_i^e) \cdot (\bar{\bar{\mu}}_r^{-1} \cdot \nabla \times \mathbf{W}_j^e)\, dV\, E_j^e = k^2 \sum_{j=1}^{N} \int_{V^e} \mathbf{W}_i^e \cdot (\bar{\bar{\varepsilon}}_r \cdot \mathbf{W}_j^e)\, dV\, E_j^e \qquad (18)$$

$$\sum_{j=1}^{N} \int_{V^e} (\nabla \times \mathbf{W}_i^e) \cdot (\bar{\bar{\varepsilon}}_r^{-1} \cdot \nabla \times \mathbf{W}_j^e)\, dV\, H_j^e = k^2 \sum_{j=1}^{N} \int_{V^e} \mathbf{W}_i^e \cdot (\bar{\bar{\mu}}_r \cdot \mathbf{W}_j^e)\, dV\, H_j^e \qquad (19)$$

for $i = 1, \cdots, N$ with $k = \omega\sqrt{\varepsilon_0 \mu_0}$ being the wave number. These element equations can be formulated in the matrix form

$$A^e x = k^2 B^e x \qquad (20)$$

for both E- and H-formulation. Assembly of element equations and (for E-formulation) elimination of unknowns along S then leads to a global equation system of the form

$$Ax = k^2 Bx \qquad (21)$$

for both E- and H-formulation. Note that the system is smaller for E-formulation than for H-formulation due to the condensation of the equation system.

3 Numerical computation of eigenvalues

We seek the eigenvalues λ of the generalized eigenvalue problem

$$Ax = \lambda Bx \qquad (22)$$

where the matrices A and B are, in general, non-symmetric complex sparse matrices. The dimension of the eigenvalue problem can be large, the matrices A and B can be poorly conditioned and multiple eigenvalues can occur.

The nature of (22) imposes formidable requirements on the eigenvalue solver. After a thorough investigation of the available eigenvalue solvers and their underlying methods, the package ARPACK [5, 6] was opted for. ARPACK is based on a Krylov method called the

implicitly restarted Arnoldi method. The main advantage of ARPACK is matrix handling by means of a reverse communication loop in which the user supplies the action of a matrix on a vector. Via the reverse communication loop, the structure of the matrices A and B is hidden from ARPACK and the user is hereby free to use any desired storage format - potentially taking advantage of matrix sparsity.

For the application at hand, the generalized eigenvalue problem (22) is transformed into the standard eigenvalue problem

$$(A - \sigma B)^{-1} B x = \frac{1}{\lambda - \sigma} x = \theta x \tag{23}$$

The eigenvalues θ of (23) having the largest magnitude then correspond to the eigenvalues $\lambda = \sigma + 1/\theta$ of (22) being closest to σ. Hence, if the range of the sought eigenvalues λ of the generalized eigenvalue problem (22) is known, they can be found from the largest eigenvalues θ of (23) provided σ is chosen properly.

In the reverse communication loop, the solution of (23) with ARPACK requires the computation of

$$w = (A - \sigma B)^{-1} B v \tag{24}$$

for many given vectors v. A problem here is that the matrix $(A - \sigma B)^{-1} B$ is not known. However, the computation of w is equivalent to the solution of

$$(A - \sigma B) w = B v \tag{25}$$

for w for the given vectors v. Thus, we can compute Bv and solve the equation system (25). This can potentially be done taking full advantage of the sparsity of A and B. It is currently done by reordering the sparse matrices A and B to create banded matrices [2], computing $A - \sigma B$ (banded), LU factorizing $A - \sigma B$ (banded upper and lower triangular matrices) and then using substitution to solve (25). The LU factorization is based on a LAPACK routine for banded matrices that requires the storage of all entries (zeroes as well as non-zeroes) in the band. This is (although significantly more efficient than storing the full matrices) a complete waste of memory. The approach is simple and works well but is unattractive for very large equation systems. In such cases, one could perform a minimum degree permutation of A and B and carry out the LU factorization using a routine that only stores non-zero entries. Note, however, that this issue is independent of the functionality of ARPACK since matrix handling is decoupled from ARPACK via the reverse communication loop.

Fig. 1 and Fig. 2 illustrate the nature of $A - \sigma B$ before and after reordering for a matrix of dimension 784 and with 10593 non-zero entries (a black dot at a given position indicates that the corresponding matrix element of $A - \sigma B$ is non-zero - it is implicitly understood that

[2]The reordering is done using the TOMS 508 routine 'Reduce' [7, 8]. This routine implements the Gibbs-Poole-Stockmeyer algorithm [9].

the upper left corner corresponds to a row and a column number of 1 while the lower right corner corresponds to a row and a column number of 784). Prior to reordering, non-zeroes are observed far from the diagonal. Upon reordering, non-zeroes are only observed in and relatively close to the diagonal.

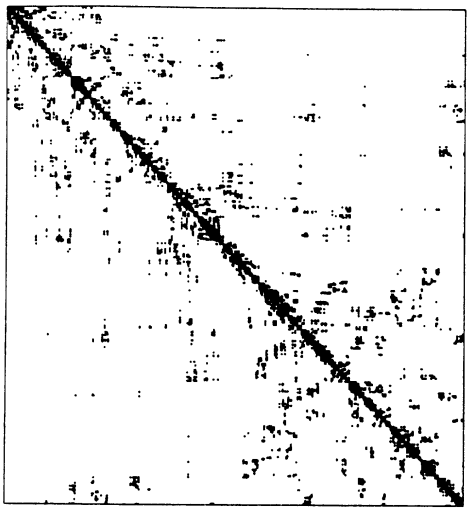

Figure 1: Distribution of non-zeroes of the matrix $A - \sigma B$ before reordering.

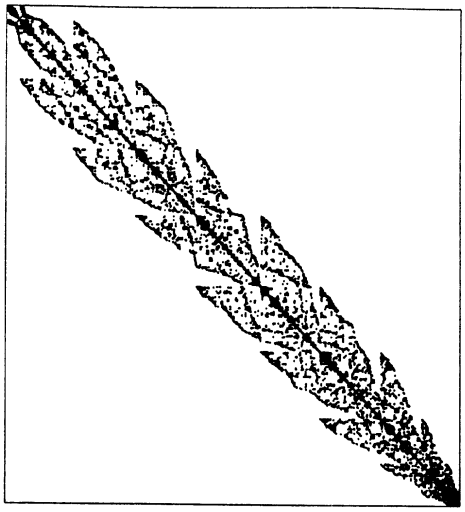

Figure 2: Distribution of non-zeroes of the matrix $A - \sigma B$ after reordering.

4 Numerical results

Throughout this section, a discretization of V into tetrahedral elements will be assumed.

4.1 TVFEs of order 0.5

In this subsection, we will expand $\mathbf{E}$ and $\mathbf{H}$ using a mixed-order TVFE of order 0.5 for a tetrahedral element. This TVFE was initially proposed by Whitney [10].

4.1.1 Homogeneous and isotropic rectangular cavity

We consider a rectangular cavity of dimensions $a \times b \times c$ filled with a homogeneous and isotropic material ($\overline{\overline{\varepsilon}}_r = \varepsilon_r \overline{\overline{\mathrm{I}}}$ and $\overline{\overline{\mu}}_r = \mu_r \overline{\overline{\mathrm{I}}}$ where $\overline{\overline{\mathrm{I}}}$ denotes a 3×3 unit dyad), see Fig. 3. The exact eigenvalues for this geometry are well-known and given analytically by [11]

$$k\sqrt{\varepsilon_r \mu_r} = \pi \sqrt{\left(\frac{m}{a}\right)^2 + \left(\frac{n}{b}\right)^2 + \left(\frac{p}{c}\right)^2} \tag{26}$$

or

$$kc\sqrt{\varepsilon_r \mu_r} = \pi \sqrt{\left(\frac{c}{a}\right)^2 m^2 + \left(\frac{c}{b}\right)^2 n^2 + p^2} \tag{27}$$

where m, n and p are non-negative integers fulfilling $(m \geq 1 \vee n \geq 1) \wedge p \geq 1$ for a TE_{mnp} (transverse electric) mode and $m \geq 1 \wedge n \geq 1 \wedge p \geq 0$ for a TM_{mnp} (transverse magnetic) mode. For $a/c = 0.75$ and $b/c = 0.5$, we find the analytical values in Tab. 1. Finite element method (FEM) results (317 tetrahedral elements) for E- and H-formulation (260 / 3118 and 506 / 6704 unknowns / non-zero matrix entries, respectively) are also shown and they are seen to agree well with the exact values. The results for H-formulation are seen to be more accurate than the results for E-formulation.

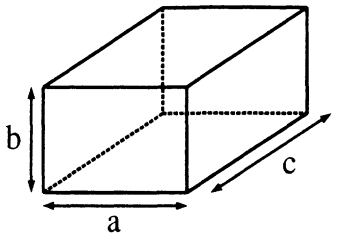

Figure 3: Homogeneous rectangular cavity.

Mode	Analytical	FEM-E	FEM-H
TE_{101}	5.2360	5.2183	5.2404
TE_{011}	7.0248	6.9171	6.9630
TM_{110}	7.5514	7.4347	7.5218
TE_{102}	7.5514	7.5219	7.5452
TX_{111}	8.1789	7.8921	8.1414

Table 1: Analytical and numerical (FEM) $kc\sqrt{\varepsilon_r \mu_r}$ values for homogeneous and isotropic rectangular cavity (Fig. 3). TVFE of order 0.5 applied.

4.1.2 Homogeneous and isotropic cylindrical cavity

We consider a cylindrical cavity of radius a and height L filled with a homogeneous and isotropic material of relative permittivity ε_r and relative permeability μ_r, see Fig. 4. The exact eigenvalues for this geometry are well-known and given analytically by [11]

$$ka\sqrt{\varepsilon_r \mu_r} = 2\pi \sqrt{\left(\frac{1}{2K_{mn}}\right)^2 + \left(\frac{a}{2L}\right)^2 p^2} \tag{28}$$

where K_{mn} is the n'th zero of the Bessel function J_m for a TM_{mnp} mode and the n'th zero of J'_m for a TE_{mnp} mode. For $a/L = 1$, numerical evaluation gives the analytical values in Tab. 2. FEM results (751 tetrahedral elements) for E- and H-formulation (688 / 9266 and 1083 / 15421 unknowns / non-zero matrix entries, respectively) are also shown and they are seen to agree well with the exact values. The results for E-formulation are seen to be slightly more accurate than the results for H-formulation.

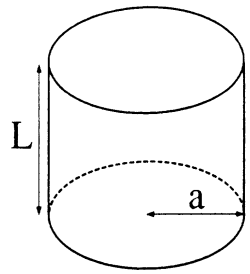

Figure 4: Homogeneous cylindrical cavity.

Mode	Analytical	FEM-E	FEM-H
TM_{010}	2.4055	2.3969	2.4473
TE_{111}	3.6415	3.6128	3.6462
TE_{111}	3.6415	3.6288	3.6485
TM_{110}	3.8312	3.7907	3.8925
TM_{110}	3.8312	3.8115	3.8989
TM_{011}	3.9568	3.9725	3.9795
TE_{211}	4.3807	4.3742	4.4010
TE_{211}	4.3807	4.3913	4.4125

Table 2: Analytical and numerical (FEM) $ka\sqrt{\varepsilon_r \mu_r}$ values for homogeneous and isotropic cylindrical cavity (Fig. 4). TVFE of order 0.5 applied.

4.1.3 Inhomogeneous and isotropic rectangular cavity

We consider a rectangular cavity of dimensions $a \times b \times c$. It is composed of a rectangular cavity of dimensions $a \times b \times d$ filled with a homogeneous and isotropic dielectric of relative permittivity ε_{r1} and a rectangular cavity of dimensions $a \times b \times (c-d)$ filled with a homogeneous and isotropic dielectric of relative permittivity ε_{r2}, see Fig. 5. For $d = 4$, $a/c = 0.75$, $b/c = 0.5$, $\varepsilon_{r1} = 10$ and $\varepsilon_{r2} = 1$, the exact analytical eigenvalues obtained via numerical solution of a transcendental equation, see for instance [11], are given in Tab. 3. FEM results (778 tetrahedral elements) for E- and H-formulation (695 / 9161 and 1151 / 16051 unknowns / non-zero matrix entries, respectively) are also shown and they are seen to agree well with the exact values. The results for E-formulation are seen to be more accurate than the results for H-formulation.

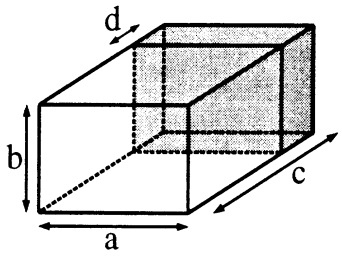

Figure 5: Inhomogeneous rectangular cavity.

Mode	Analytical	FEM-E	FEM-H
TE_{110}	2.8061	2.8130	2.7757
TM_{111}	3.0383	3.0349	3.0415
TE_{101}	3.3469	3.3549	3.3123
TE_{111}	3.6780	3.6787	3.6353
TM_{121}	3.8222	3.8207	3.8050
TE_{120}	3.8959	3.9412	3.8445

Table 3: Analytical and numerical (FEM) kc values for inhomogeneous and isotropic rectangular cavity (Fig. 5). TVFE of order 0.5 applied.

4.1.4 Homogeneous and anisotropic cylindrical cavity

We consider a cavity similar to the one in subsection 4.1.2, except that the relative permeability μ_r is replaced by the relative permeability tensor

$$\overline{\overline{\mu}}_r = \begin{bmatrix} \mu & j\kappa & 0 \\ -j\kappa & \mu & 0 \\ 0 & 0 & 1 \end{bmatrix} \tag{29}$$

The exact eigenvalues for this geometry are determined from the transcendental equation given by Kales [12]. Evaluation of $ka\sqrt{\varepsilon_r}$ for $a/L = 1$ and κ/μ-values between 0 and 1.4 was given by Krupka [13] in conjunction with the test of an approximate numerical method (based on mode expansion) for predicting the eigenvalues. The results are presented in Fig. 6 for modes where the value of $ka\sqrt{\varepsilon_r}$ for $\kappa = 0$ is less than 5 (solid lines). The curves are slightly jagged since the results were simply scanned from [13] and imported into a plotting program by approximate means. More accurate results can be found by solving the transcendental equation given by Kales [12] but this was deemed unnecessary. FEM results (751 tetrahedral elements) for H-formulation (1083 / 15421 unknowns / non-zero matrix entries) are also shown (dots) and they are seen to agree well with the exact values. Some of the FEM results do not seem to match an exact result but this is due to the fact that exact results for modes with $ka\sqrt{\varepsilon_r}$ larger than 5 for $\kappa = 0$ are not shown. FEM results for E-formulation have also been obtained but are not shown. They agree well with the results for H-formulation for $\kappa/\mu < 1$, cannot be evaluated for $\kappa/\mu = 1$ (E-formulation requires the inverse of $\overline{\overline{\mu}}_r$ which does not exist for $\kappa/\mu = 1$) and are wrong for $\kappa/\mu > 1$. The reason for this breakdown is not yet known.

4.1.5 Inhomogeneous and anisotropic rectangular cavity

We consider a cavity similar to the one in subsection 4.1.3, except that the dielectric of relative permittivity ε_{r1} is replaced by a magnetic material with a relative permeability tensor $\overline{\overline{\mu}}_{r1}$ given by (29). For $\mu = 1$ and $\kappa = 0.7$, FEM results (778 tetrahedral elements) are given in Tab. 4 for E- and H-formulation (695 / 9161 and 1151 / 16051 unknowns / non-zero matrix entries, respectively). The results for E- and H-formulation are seen to compare very well for the first five modes while the deviation is larger for the sixth mode. Exact analytical results for this geometry are not given.

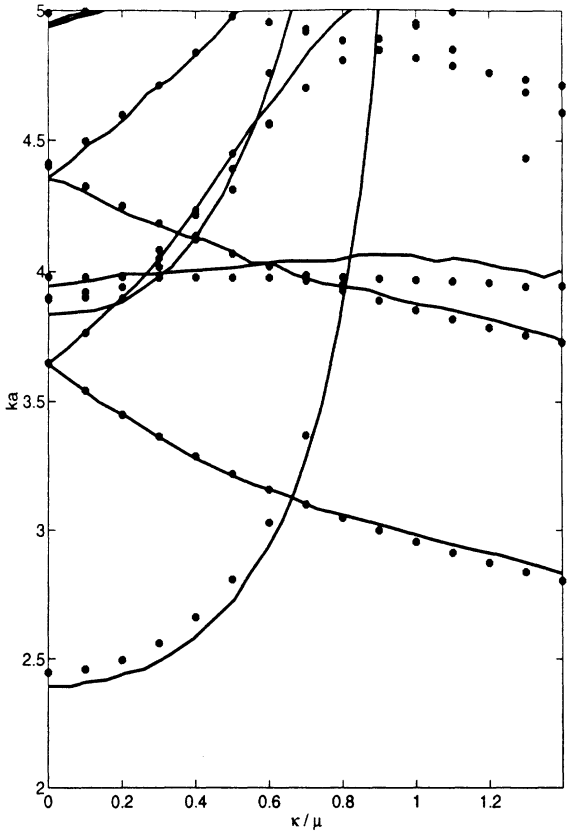

Figure 6: Analytical and numerical (FEM) $ka\sqrt{\varepsilon_r}$ values (solid lines and dots, respectively) for homogeneous and anisotropic cylindrical cavity (Fig. 4). TVFE of order 0.5 applied.

4.2 TVFEs of order 1.5

In this subsection, we will expand **E** and **H** using a mixed-order TVFE of order 1.5 for a tetrahedral element. This TVFE was proposed by Andersen and Volakis [3].

4.2.1 Homogeneous and isotropic rectangular cavity

We consider the same cavity as in subsection 4.1.1. Exact results as well as FEM results (80 tetrahedral elements) for E- and H-formulation (370 / 10370 and 670 / 23852 unknowns / non-zero matrix entries, respectively) are shown in Tab. 5. The results for E- and H-formulation are seen to agree well with the exact values. A comparison with the results in subsection 4.1.1 in general shows better agreement than for results obtained using the TVFE of order 0.5 over a finer mesh. This could be expected since the results in Tab. 5 are obtained using more unknowns and more non-zero matrix entries.

4.2.2 Inhomogeneous and isotropic rectangular cavity

We consider the same cavity as in subsection 4.1.3. Exact results as well as FEM results (130 tetrahedral elements) are given in Tab. 6 for E- and H-formulation (604 / 17876 and 1084 / 38080 unknowns / non-zero matrix entries, respectively). The results for E- and H-formulation are seen to agree well with the exact values. A comparison with the results

Mode	FEM-E	FEM-H
1	5.3566	5.3408
2	7.0111	7.0082
3	7.6941	7.6839
4	7.7983	7.7559
5	8.2321	8.2104
6	8.8001	8.6140

Table 4: Numerical (FEM) kc values for inhomogeneous and anisotropic rectangular cavity (Fig. 5). TVFE of order 0.5 applied.

Mode	Analytical	FEM-E	FEM-H
TE_{101}	5.2360	5.2404	5.2460
TE_{011}	7.0248	7.0440	7.0255
TM_{110}	7.5514	7.5739	7.5513
TE_{102}	7.5514	7.5832	7.6415
TX_{111}	8.1789	8.1738	8.2082

Table 5: Analytical and numerical (FEM) $kc\sqrt{\varepsilon_r \mu_r}$ values for homogeneous and isotropic rectangular cavity (Fig. 3). TVFE of order 1.5 applied.

in subsection 4.1.3 also shows reasonable agreement with results obtained using the TVFE of order 0.5 over a finer mesh.

Mode	Analytical	FEM-E	FEM-H
TE_{110}	2.8061	2.8044	2.8210
TM_{111}	3.0383	3.0596	3.0521
TE_{101}	3.3469	3.3569	3.3503
TE_{111}	3.6780	3.7324	3.6661
TM_{121}	3.8222	3.8492	3.9096
TE_{120}	3.8959	3.9779	3.9333

Table 6: Analytical and numerical (FEM) kc values for inhomogeneous and isotropic rectangular cavity (Fig. 5). TVFE of order 1.5 applied.

4.2.3 Inhomogeneous and anisotropic rectangular cavity

We consider the same cavity as in subsection 4.1.5. FEM results (130 tetrahedral elements) are given in Tab. 7 for E- and H-formulation (604 / 17896 and 1084 / 38226 unknowns / non-zero matrix entries, respectively). The results for E- and H-formulation are seen to compare very well. A comparison with the results in subsection 4.1.5 also shows reasonable agreement with results obtained using the TVFE of order 0.5 over a finer mesh. Exact analytical results for this geometry are not given.

Mode	FEM-E	FEM-H
1	5.3662	5.3591
2	7.0485	7.0449
3	7.7131	7.7203
4	7.8291	7.8108
5	8.2866	8.2596
6	8.8116	8.8029

Table 7: Numerical (FEM) kc values for inhomogeneous and anisotropic rectangular cavity (Fig. 5). TVFE of order 1.5 applied.

4.3 Convergence rate for TVFEs of order 0.5 and 1.5

We consider the same cavity as in subsection 4.1.1. A FEM solution (E-formulation) for the eigenvalues and the corresponding eigenvectors of the cavity is carried out for various tetrahedral meshes of different average edge length with TVFEs of order 0.5 and 1.5 used for field expansion.

The convergence rate for the two cases is illustrated in Fig. 7 where the average error of the first eight eigenvalues is plotted in percent as a function of the average edge length in the mesh (log-log plot). The approximate distribution around a straight line suggests that the average error decreases as x^n for a decreasing average edge length. For the TVFE of order 0.5, the exponent is 2.37 which is slightly larger than the expected value 2 [14]. This is due to the very low average error 0.56% for the average edge length 0.175. Similarly, for the TVFE of order 1.5, the exponent is 4.66 which is again larger than the expected value 4 [14] and the exponent 3.86 found in [14] for a different TVFE of order 1.5. This demonstrates that the TVFE of order 1.5 applied here has slightly better convergence properties than the one in [14] for this particular geometry and for the employed meshes. However, a relatively large uncertainty range can be expected for such numerically obtained exponents and thus no general statement can be made regarding the rigor of results based on the two different TVFEs of order 1.5.

4.4 TVFEs of order 0.5 and 1.5 mixed selectively

In this subsection, we will expand **E** and **H** using selective field expansion. The mixed-order TVFEs of order 0.5 and 1.5 for a tetrahedral element are mixed selectively within the computational domain for an effective expansion of the unknown field.

4.4.1 Inhomogeneous and isotropic rectangular cavity

We consider the same cavity as in subsection 4.1.3 and 4.2.2. Exact results as well as FEM results (130 tetrahedral elements as in subsection 4.2.2) are given in Tab. 8 for E- and H-formulation (354 / 9120 and 668 / 20060 unknowns /non-zero matrix entries, respectively). The dielectric material is modeled with the TVFE of order 1.5. In free space, the region close to the dielectric is a transition region where incomplete TVFEs (complete to order 0.5 but not to order 1.5) are applied while the region away from the dielectric is modeled with

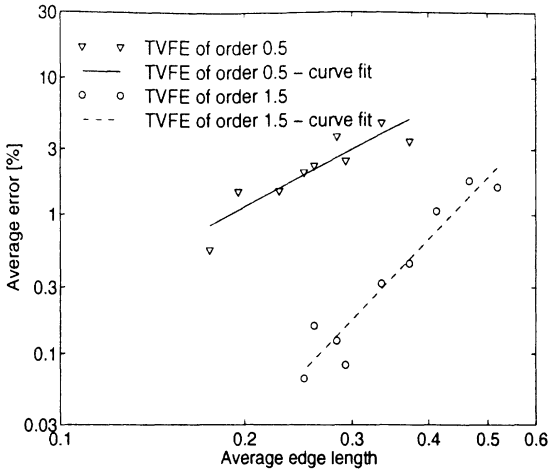

Figure 7: Convergence rate for expansion of field within homogeneous and isotropic rectangular cavity (Fig. 3) using TVFEs of order 0.5 and 1.5.

the TVFE of order 0.5. The results for E- and H-formulation are seen to agree well with the exact values. A comparison with the results in subsection 4.1.3 and 4.2.2 also shows reasonable agreement with results obtained using the TVFE of order 0.5 over a finer mesh and the TVFE of order 1.5 throughout the mesh.

Mode	Analytical	FEM-E	FEM-H
TE_{110}	2.8061	2.8144	2.8037
TM_{111}	3.0383	3.0565	3.0531
TE_{101}	3.3469	3.3657	3.3351
TE_{111}	3.6780	3.7377	3.6522
TM_{121}	3.8222	3.8470	3.9063
TE_{120}	3.8959	3.9886	3.9292

Table 8: Analytical and numerical (FEM) kc values for inhomogeneous and isotropic rectangular cavity (Fig. 5). TVFEs of order 0.5 and 1.5 applied selectively.

4.4.2 Inhomogeneous and anisotropic rectangular cavity

We consider the same cavity as in subsection 4.1.5 and 4.2.3. FEM results (130 tetrahedral elements as in subsection 4.2.3) are given in Tab. 9 for E- and H-formulation (354 / 9140 and 668 / 20206 unknowns / non-zero matrix entries, respectively). The magnetic material is modeled with the TVFE of order 1.5. In free space, the region close to the magnetic material is a transition region where incomplete TVFEs (complete to order 0.5 but not to order 1.5) are applied while the region away from the magnetic material is modeled with the TVFE of order 0.5. A comparison with the results in subsection 4.1.3 and 4.2.2 shows reasonable agreement with results obtained using the TVFE of order 0.5 over a finer mesh and the TVFE of order 1.5 throughout the mesh.

Mode	FEM-E	FEM-H
1	5.3527	5.3586
2	7.0303	6.9931
3	7.5569	7.6243
4	7.7378	7.7415
5	8.0194	8.2101
6	8.6920	8.6968

Table 9: Numerical (FEM) kc values for inhomogeneous and anisotropic rectangular cavity (Fig. 5). TVFEs of order 0.5 and 1.5 applied selectively.

4.5 Discussion

For a given (possibly inhomogeneous and anisotropic) cavity with a corresponding tetrahedral mesh, simulation of eigenvalues using the FEM with TVFEs of order 0.5 used for field expansion gives the resonant wavenumbers and the corresponding resonant modes with a certain accuracy. For improving the accuracy of the results, the TVFE of order 0.5 can be used over a finer tetrahedral mesh or a TVFE of order 1.5 can be used (partly or fully, depending upon the configuration) over the same mesh.

When aiming to find the appropriate method for a given problem, a variety of factors must be considered :

- The number of unknowns. This affects the CPU time for the eigenvalue solver and the memory demand.
- The number of non-zero matrix entries in the global matrices. This also affects the CPU time for the eigenvalue solver and the memory demand.
- The accuracy of the computed resonant wavenumbers. Certain problems may require very accurate values, others only rough estimates.
- The accuracy of the corresponding resonant modes. Higher order field expansions tend to result in smoother fields than lower order expansions.
- Ease of mesh generation. It is in general easier to grow a coarse mesh than a fine mesh. However, certain complex geometrical details may not lend themselves to coarse mesh generation.
- Matrix condition numbers. These affect the CPU time for iterative solvers. Large matrix condition numbers generally lead to a large number of iterations before convergence is achieved.

This, typically, will not uniquely lead to an optimal (least number of unknowns, least number of non-zero matrix entries, most accurate eigenvalues, most accurate eigenmodes, easiest mesh generation, best matrix conditioning and least total solution time) approach and various trade offs must be considered. Thus, we cannot expect to conclude decisively once and

for all what the best approach will be. It will inevitably depend upon the problem and the specific requirements for its solution. Further discussion is given in [15].

The ambiguity described above can be easily demonstrated via an example. For simplicity, let us consider the inhomogeneous and isotropic rectangular cavity from subsection 4.1.3, 4.2.2 and 4.4.1 (Fig. 5). Exact analytical as well as approximate numerical kc-values are given in Tab. 3, Tab. 6 and Tab. 8. Based on these values, we calculate the error in percent of the first six modes for the three different TVFE options (TVFE of order 0.5 with a fine mesh is denoted 'Case # 1', TVFE of order 1.5 with a coarse mesh is denoted 'Case # 2' and TVFEs of order 0.5 and 1.5 mixed selectively with a coarse mesh is denoted 'Case # 3') for E- and H-formulation, see Fig. 8 and Fig. 9.

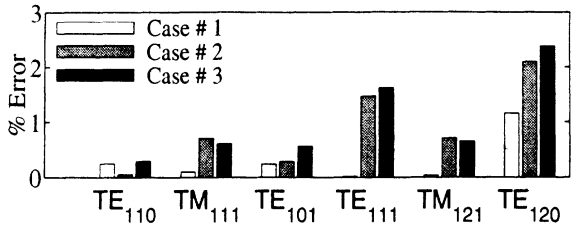

Figure 8: Eigenvalue error (E-formulation) for inhomogeneous and isotropic rectangular cavity (Fig. 5).

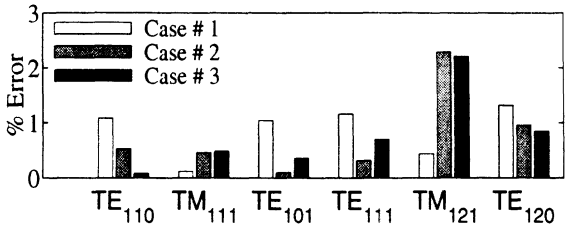

Figure 9: Eigenvalue error (H-formulation) for inhomogeneous and isotropic rectangular cavity (Fig. 5).

Comparing Case # 2 and Case # 3, we see that the average error is approximately the same. This is the case for both E- and H-formulation. Thus, we do not compromise accuracy by modeling only part of the cavity with the TVFE of order 1.5 and part of the cavity with the TVFE of order 0.5 as compared to using the TVFE of order 1.5 throughout the cavity. However, the storage and CPU-time requirements drop making selective field expansion an attractive option.

Comparing Case # 1 and Case # 3, we see that Case # 1 is best for E-formulation while Case # 3 is best for H-formulation. This demonstrates that the choice of TVFE(s) is not necessarily unambiguous. This unambiguity can be further demonstrated by considering the eigenmode corresponding to a given eigenvalue. As noted above, Case # 3 is generally better than Case # 1 for H-formulation. However, for the TM_{111} mode, Case # 1 gives a more accurate eigenvalue than Case # 3. The tangential magnetic field on the back PEC wall is plotted for Case # 1 and Case # 3 in Fig. 10 and Fig. 11, respectively. Clearly, transitions are much smoother for Case # 3 than for Case # 1 and significantly more accurate fields at edges can be observed for Case # 3 as compared to Case # 1 (for Case # 1 the magnetic field possesses normal components at edges and these do not exist for Case # 3). Thus, for a mode where Case # 1 gives a more accurate eigenvalue than Case # 3, Case # 3 gives a more accurate eigenmode than Case # 1.

The results presented in previous sections clearly show that selective field expansion using hierarchical mixed-order TVFEs of order 0.5 and 1.5 for tetrahedral meshes is a promising

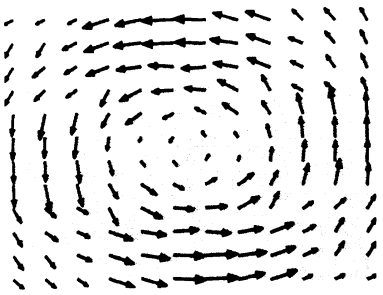

Figure 10: Magnetic field on the back PEC wall for TM_{111} mode of inhomogeneous and isotropic rectangular cavity (Fig. 5) with TVFE of order 0.5 applied (Case # 1).

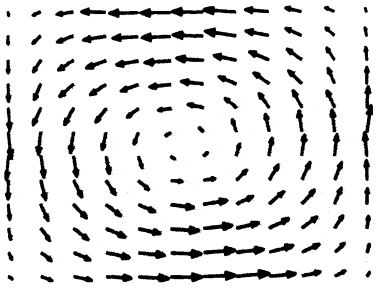

Figure 11: Magnetic field on the back PEC wall for TM_{111} mode of inhomogeneous and isotropic rectangular cavity (Fig. 5) with TVFEs of order 0.5 and 1.5 applied (Case # 3).

approach for a certain class of problems and hereby encourage further studies of the approach for more challenging problems.

5 Summary and conclusions

In this report, electric and magnetic field formulations were presented for FEM solution of three-dimensional eigenvalue problems in the case of inhomogeneous and anisotropic volumes enclosed by perfectly electrically conducting surfaces. Issues related to efficient and robust numerical eigenvalue computation were discussed and numerical results were included to show the validity of the formulations and the computer code. From the numerical results, field expansion combining lowest and higher order hierarchical mixed-order TVFEs selectively in a computational domain is seen to be a promising alternative to field expansion using lowest or higher order mixed-order TVFEs throughout the computational domain. Further studies must show if this is also the case for more challenging problems such as antenna radiation problems and scattering problems.

References

[1] L.S. Andersen and J.L. Volakis, 'A novel class of hierarchical higher order tangential vector finite elements for electromagnetics', *Proceedings of the IEEE Antennas and Propagation Society International Symposium 1997*, Montréal, Québec, Canada, vol. 2, pp. 648-651, July 1997.

[2] L.S. Andersen and J.L. Volakis, 'Development and application of a novel class of hierarchical tangential vector finite elements for electromagnetics', Submitted to *IEEE Trans. Antennas Propagat.*, September 1997.

[3] L.S. Andersen and J.L. Volakis, 'Hierarchical tangential vector finite elements for tetrahedra', *IEEE Microwave and Guided Wave Letters*, vol. 8, pp. 127-129, March 1998.

[4] L.S. Andersen and J.L. Volakis, 'Hierarchical tangential vector finite elements for tetrahedra', *Proceedings of the IEEE Antennas and Propagation Society International Symposium 1998*, Atlanta, Georgia, USA, vol. 1, pp. 240-243, June 1998.

[5] ftp://ftp.caam.rice.edu/pub/software/ARPACK/

[6] R.B. Lehoucq, D.C. Sorensen and C. Yang, 'ARPACK users guide : Solution of large scale eigenvalue problems by implicitly restarted Arnoldi methods', Draft, July 1996.

[7] H.L. Crane, N.E. Gibbs, W.G. Poole and P.K Stockmeyer, 'Algorithm 508 - Matrix bandwidth and profile reduction', *ACM Trans. Math. Software*, vol. 2, pp. 375-377, December 1976.

[8] http://www.netlib.org/toms/508

[9] N.E. Gibbs, W.G. Poole and P.K Stockmeyer, 'An algorithm for reducing the bandwidth and profile of a sparse matrix', *SIAM J. Num. Anal.*, vol. 13, pp.235-251, April 1976.

[10] H. Whitney, *Geometric integration theory*, Princeton University Press, 1957.

[11] R.F. Harrington, *Time harmonic electromagnetic fields*, McGraw-Hill Book Company, USA, 1961.

[12] M.L. Kales, 'Modes in wave guides containing ferrites', *J. Appl. Phys.*, vol. 24, pp. 604-608, May 1953.

[13] J. Krupka, 'Resonant modes in shielded cylindrical ferrite and single-crystal dielectric resonators', *IEEE Trans. Microwave Theory Tech.*, vol. MTT-37, pp. 691-697, April 1989.

[14] J.S. Savage and A.F. Peterson, 'Higher-order vector finite elements for tetrahedral cells', *IEEE Trans. Microwave Theory Tech.*, vol. MTT-44, pp. 874-879, June 1996.

[15] J.S. Savage, 'Comparing high order vector basis functions', *Proc. of the 14th Annual Review of Progress in Applied Computational Electromagnetics*, Monterey, CA, USA, vol. 2, pp. 742-749, March 1998.

Review of Microstrip Patch Antennas on Ferrite Substrates

by Zhifang Li, May 1998.

1. Outline

I have copies of all the following papers (about 30) reviewed. Papers which were carefully read are reviewed in detail, and the rest of papers come with a short summary. In the next section, the papers are listed alphabetically by the last name of the most 'significant' (or 'recognizable') author.

2. Review of Ferrite Papers

[Balanis 97] A.C. Polycarpou, C.A. Balanis, et.al., "Radiation and scattering from ferrite-tuned cavity-backed slot: theory and experiment"
IEEE AP manuscript received 10/97.

(For a shorter and published version, see also A.C. Polycarpou and C.A. Balanis, "Analysis of ferrite loaded cavity backed slot antennas using a hybrid FEM/MoM approach", IEEE Antennas and Propagation Society, AP-S International Symposium (Digest), v. 2, 1997, pp.652-655.

Computation method: 3D FEM-MoM hybrid, FEM with linear tetra elements for inside cavity and spectral domain MoM for exterior region. Exponential behavior of the governing Green's function is numerically asympototiclly extracted to speed up the MoM using spatial domain integration.
Antenna(s) studied: ferrite-tuned cavity-backed rectangular slot antennas (i.e. ferrite cavities), with cavity partially filled with magnetized ferrite layers and mounted on infinite ground plance coated with dielectric/magnetic overlay. UHF band. Cavity is square, cylindrical probe feed parallel to ground plane (for the radiating ferrite cavity), dc magnetic field applied in the direction of the probe, i.e. *y-direction.*
Theory presented: Formulation of MoM, FEM, Magnetized ferrite, Demagnetization effects.
Parameters computed: RCS, input impedance, return loss, gain and efficiency, compared with experimental data.
Parameters varied: bias field, linewidth, saturation magnetization.
As a *scatterer*: tuning *y-biased* **RCS** by varying H0 (phenomenon explained by normalized propagation constant of low-f, res--f, and high-f regions), $4\pi M_s$ (explained by increasing effective permeability in low-f region), and linewidth delta H. When H0 increases, resonant frequency increases; when $4\pi M_s$ increases, resonant frequency decreases; when varying linewidth delta H, the resonant frequency remains unaffected.
As a *radiator*: internal field computed by external field and demagnetizing factor first. Computation of **input impedance** with one/two pairs of magnets and compared with measurements. When H0 increases (from one pair to two pairs of magnets), the resonant frequency increases (explained by the relationship between H0 and effective permeability). Tuning percentage 45%. Also, return loss improves for higher resonant frequency. Gain is also calculated (with or without mismatch).
Comparison made: scattering cavity with Kokotoff's and radiating cavity with experimental data.

Antenna manufactured: analyzed using HP8510 network analyzer.
What's unique from other paper: in the UHF band instead of microwave band. Author declared this is the first paper to present comparisons between measurements and computations of ferrite-tunable antennas.
Other notions: demagnetizing factor: 0/1 for patch antenna if the bias field is parallel/normal to the endfaces of the substrate. For the author's antenna, it is estimated between 0 and 1 based on magnetostatic model by Joseph.

[Buris, Funk and Silverstein 93] N.E. Buris, T.B. Funk, and R.S. Silverstein, "Dipole arrays printed on ferrite substrates"
IEEE Trans. Antennas Propagat., vol. AP-41, pp. 165-176, Feb. 1993.

Study infinite dipole arrays printed on ferrite substrates; Both in-plane and normal bias are studied; Emphasis on scan performance (by varying the bias field and scan angle) and input impedance calculations; Using full-wave analysis.

[Das 82] N. Das and S.K. Chowdhury, "Rectangular microstrip antennas on a ferrite substrate"
IEEE Trans., AP-30, pp. 499-502, 1982.

Resonant length of printed antenna can be reduced when using ferrite substrates, which is very useful in low UHF frequencies. The bandwidth seems also improved. Author declared first to do the above.

[Das 83] S.N. Das, S.K. Chowdhury, and J.S. Chatterjee, "Circular microstrip antenna on ferrimagnetic substrate"
IEEE Transaction on Antennas and Propagation, vol. AP-31, no. 1, pp. 188-190, Jan. 1983.

Computation method:
Antenna(s) studied: circular microstrip antenna on a ferromagnetic substrate, operated in lower range of UHF, back-fed by a TEM line.
Theory presented: explanation of realizable circular antenna at lower freq due to higher effective permeability, and broad-band nature from large variation of effective permeability with a small variation of relative permeability.
Parameters computed: resonant radius, bandwidth, return loss, radiation pattern.
Parameters varied:
Comparison made: compared with purely dielectric substrates and measured data.
Antenna manufactured: two circular patch antennas of radii 1cm and 1.6 cm.
Significance: reduced resonant radii and improved bandwidth on ferrite substrate. Calculated effective permeability agree well with measured-then-calculated data. But the efficiency is low.
What's unique from other paper: first of circular ms antenna to be studied at lower UHF band.
Other notions: In all Das' papers, ferrites were not biased (pointed by [Pozar and Sanchez 88]

[Das 93] R.K. Mishra, S.S. Pattnaik, and N. Das, "Tuning of microstrip antenna on ferrite substrate"
IEEE Transactions on Antennas and Propagation, vol. 41, no. 2, pp.230-233, Feb. 1993.

Computation method: arithmetic and a little bit of calculus.
Antenna(s) studied: rectangular microstrip antennas on a ferrimagnetic substrate, operated in lower range of UHF.
Theory presented: traditional formula for resonant freq in TM01 mode and the effective permittivity in UHF range for rectangular antennas is listed, also the limitation of Pucel and Masse's formula for effective permeability with magnetization is pointed out (max relative substrate permeability is limited to unity), this paper derives a different formula to calculate the absolute relative permeability by exploiting the Maxwell equations.
Parameters computed: relationship between effective permeability and freq/length, effective permeability and bias field,/freq are plotted.
Parameters varied: find the relationship of H and freq for a fixed rectangular patch via computed graphs.
Comparison made: values computed from theory are compared with measured data.
Antenna manufactured: one rectangular patch antenna.
Significance: theoretical, tuning the freq. Tuning process: freq + antenna length -> effective permeability -> dc bias field.
What's unique from other paper:
Other notions:

[Lee and Harackiewicz 96] B.Lee and F.J. Harackiewicz, "The RCS of a microstrip antenna on an in-plane biased ferrite substrate"
IEEE Trans. Antennas Propagat., vol. AP-44, pp. 208-211, Feb. 1996.

Computation method: Moment method with exact spectral-domain Green's function. Probe feed model.
Antenna(s) studied: rectangular microstrip patch on an in-plane biased ferrite substrate; also a loaded rectangular patch on biased ferrite substrate.
Theory presented: see 'significance' below.
Parameters computed: monostatic RCS with various incident angles; and all four elements of the cross section matrix are examined; patterns are also plotted.
Parameters varied: In-plane biased field; different incident angles; with load or no load; different probe feed locations.
Comparison made: with [Yang et.a. 93] and [Newman and Forrai 87] (of dielectric case).
Antenna manufactured: None.
Significance: RCS peaks of ⊥ modes can be moved to higher freq by increasing the magnetic bias field, but the magnitude is almost unchanged; however, RCS peaks of \\ modes are almost unchanged by the bias field. For unmagnetized ferrite, the cross-polarized RCS components are zero; and for the magnetized ferrite, they are as significant as the co-polarized RCS components. Also, resonant RCS can be significantly reduced with a loaded patch. Also, if the feed is located on the axis perpendicular to the bias, it would not affect the peak RCS of ⊥ modes.
What's unique from other paper: studying full RCS matrix of patch on ferrite substrates (not the first! [Pozar 92] already has it!)
Other notions: Harackiewicz was Pozar's student.

[Henderson 88] A. Henderson, J.R. James, and A. Fray, "Magnetised microstrip antenna with pattern control"
Electronics Letters, vol. 24, no. 1, pp. 45-47, Jan.1988.

Computation method:
Antenna(s) studied: circular microstrip antenna, back-fed, sandwiched between an upper thick ferrite layer (superstrate/overlay) and a lower alumina (aluminum oxide) substrate layer, magnetized by a permanent magnet.
Theory presented: theory explaining how the beam will occur and the relationship between beam scan symmetry and the positions of the magnets.
Parameters computed: Pattern of both unmag- and magnetized antennas of different ferrite thicknesses are measured and plotted.
Parameters varied: ferrite thickness of the circular antenna superstrate.
Comparison made: magnetized compared with unmagnetized
Antenna manufactured: see 'Antenna(s) studied' above
Significance: low-profile ferrite antenna for beam steering capability. H-pattern shows a 30 degrees beam scan for magnetized antenna. Gain increase is also observed, claimed to be consistent with the dissipative behavior of ferrite material. Narrow bandwidth and significant insertion loss seems always to be the characteristics.
What's unique from other paper:
Other notions:

[How et.al. 92] H. How, et.al., "Radiation frequencies of ferrite patch antennas"
Electronics Letters, vol. 28, no. 15, pp. 1405-1406, 16th July 1992.

Computation method: arithmetic
Antenna(s) studied: rectangular microstrip antenna (claimed to be identical as [Pozar and Sanchez 88], but actually a little different in geometric and electric parameters); use of electromagnet to bias; fed by coaxial line
Theory presented: Two different radiation modes whose frequencies behaved differently with bias field: radiation freq increased with increasing bias field under transverse mode (magnetisation perpendicular to propagation direction), while decreased with increasing bias field under longitudinal mode (magnetisation parallel to propagation direction). A theoretical model was proposed based on the two modes, and using the model, the formulas of the permeability $\mu_{\perp}$ and $\mu_{\parallel}$ are given by averaging over multi-domains, thus the formula for the radiation frequencies for the TM_{100} and TM_{010} are obtained from the permeability.
Parameters computed: permeability, radiation frequency.
Parameters varied: bias field
Comparison made: measured and theoretical data of radiation frequencies.
Antenna manufactured: see 'Antenna(s) studied' above
Significance: rather theoretical. see 'theory presented' above.
What's unique from other paper:
Other notions: there is no adjustable parameters in the calculation of the theoretical curves.

[How et.al. 94] H.How, et.al., "Magnetic Steerable Ferrite Patch Antenna Array"

IEEE Transactions on Magnetics, vol. 30, no. 6, pp. 4551-4553, Nov. 1994.

Computation method: arithmetic
Antenna(s) studied: 1. single isolated circular ferrite patch antenna, fed by a microstrip line, magnetized normally (*z-bias*). 2. 2x4 ferrite circular patch array, fed by microstrip lines, magnetized by permanent magnet, *x-/y- bias.*

Theory presented: For the single circular patch, formulas of $\frac{\mu}{\mu_0}$, $\frac{\kappa}{\mu_0}$, internal field, effective permeability, demagnetizing factor. (where were they from?)
Parameters computed: For single circular patch: Radiation frequencies vs. normally biased magnetic field.
Parameters varied:.magnitude (for the single patch) and direction (for the array) of biased magnetic field.
Comparison made: theory and experiments.
Antenna manufactured: see 'Antenna(s) studied' above.
Significance: 1. For single circular patch: Radiation frequencies vs. normally biased magnetic field are plotted. Frequencies are distinguished in three regions. CP modes are discussed. 2. For the ferrite array, radiation pattern of unmagnetized, x-bias, and y-bias are (only) measured and plotted, showing that beam can be steered by varying the magnitude and direction of the applied biasing field.
What's unique from other paper:
Other notions:

[How et.al. 94] Hoton How, Ta-Ming Fang, and Carmine Vittoria, "Intrinsic modes of Radiation in ferrite patch antennas"
IEEE Transactions on Microwave Theory and Techniques, vol. 42, no. 6, pp. 988-994, June 1994.

[How and Vittoria 94] Hoton How and Carmine Vittoria, "Radiation Modes in Circular Patch Antennas"
IEEE Transactions on Microwave Theory and Techniques, vol. 42, no. 10, pp. 1939-1944, October 1994.

[How et.al. 97] Hoton How, et.al. "Antenna array of circular patches on ferrite substrate"

IEEE Transactions on Magnetics, vol. 33, no. 1, pp. 735-738, Jan. 1997.

[Sun, How, et.al.] L. Sun, H. How, C. Vittoria, and M.H. Champion, "Steerable linear dipole antenna using ferrite phase shifters"
Manuscript (source unknown)

[Kokotoff 95] D. Kokotoff, "Full-wave analysis of a ferrite-tuned cavity-backed slot antenna"
Ph.D. thesis, 249 pages, Arizona State University, 1995. (Balanis' student)

[Tsang and Langley 94] K.K. Tsang and R.J. Langley, "Annular ring microstrip antennas on biased ferrite substrates"

Electronics Letters, vol. 30, pp. 1257-1258, 1994.

Annular ring ms antennas studied with *normal bias*; Circular polarization is generated using a single electromagnetically coupled feed for both fundamental and higher-order modes; Resonant frequency can be tuned over 15% range; Axial ratio seems insensitive to the bias field strength; Author declared this paper was the first to study ferrite patches operating at higher order modes.

[Tsang and Langley] K.K. Tsang and R.J. Langley, "Microstrip antennas on ferrite substrates"
source not available

Computation method: None, purely experimental.
Antenna(s) studied: annular ring microstrip antenna on biased square ferrite substrates.Two rings for the two modes? fed by single em coupled microstrip line.
Theory presented: TM11 and higher TM21 modes are described.
Parameters computed: Radiation freq and CP patterns measured.
Parameters varied: Bias field.
Comparison made: None.
Antenna manufactured: see 'Antenna(s)' above
Significance: circular polarization generated using a single em coupled feed for both TM11 and TM21 modes. Both LHCP and RHCP are generated. Initially, resonant freq for RHCP increased and for LHCP decreased with the increase of bias field until the saturation magnetisation reached; then both resonant freq for RHCP and LHCP increased as plotted in the figure (but the author claimed that both decreased with RHCP decreasing more rapidly?). The resonant freq can be tuned over a 15% range for normal bias (*z-bias*). And the beam direction of the fundamental mode can be steered by +/-40 degrees using a *transversely* biased ferrite *superstrate* and the power also increased with increase of bias field. In detail, the resonant freq declined for superstrate than that without superstrate.
What's unique from other paper:
Other notions: Axial ratio (AR) of the patterns insensitive to the bias field strength. Efficiency and gain are good. This paper is similar in content to the last one [Tsang and Langley 94].

[Batchelor and Langley 95] J.C. Batchelor and R.J. Langley, "Microstrip ring antennas operating at higher order modes for mobile communications"
IEE Proc.-Microw. Antennas Propag. vol. 142, no. 2, pp. 151-155, April 1995.

Beam steering for vehicles traveling up and down hills or changing latitude within a continent is achieved by dual mode concentric rings. Various feeding techniques have been investigated for exciting these modes. Such mode switched antennas are a cheap and viable alternative to an expensive phased array antenna.

[Batchelor and Langley 97] J.C. Batchelor and R.J. Langley, "Beam scanning using microstrip line on biased ferrite"
Electronics Letters, vol. 33, no. 8, pp. 645-646, 10th April 1997.

Computation method: None, purely experimental.

Antenna(s) studied: 2-element circular array on biased square ferrite substrates. Fed by a microstrip line. Normally biased with a permanent magnet. A 4-element array is also designed.
Theory presented: Biasing the ferrite causes a shift in the phase length of the ms line feed, hence varying the beam angle.
Parameters computed: Radiation patterns plotted.
Parameters varied: Normal bias field.
Comparison made: Measurements vs. simulation (use HP MDS software); and 2-element compared with 4-element array.
Antenna manufactured: see 'Antenna(s)' above.
Significance: If the substrate is dielectric, applying the dc bias field will not change the resonant freq of the circular patches. But with a ferrite substrate, the beam can be scanned by up to 40 degrees. At this point, the scan loss is about 2dB, mainly due to the ferrite becoming lossy as it approaches absorption resonance. Also, if 4-element, then beam width in one plane is narrower, but less magnetic bias is needed to produce the same shift in beam direction, and better sidelobe levels (4-element array is still under construction).
What's unique from other paper:
Other notions: Sidelobes appeared as the scan angle increased as expected in a simple array.

[Tsang and Langley 98] K.K. Tsang and R.J. Langley, "Design of circular patch antennas on ferrite substrates"
IEE Proceedings - Microwaves, Antennas and Propagation, vol. 145, no. 1, pp. 49-55, Feb. 1998.

The cavity model is extended to include multilayer ferrite-dielectric substrates with em feedline coupling to the patch. (Need further reading!)

[Schuster and Luebbers 96a] J.W. Schuster and R.J. Luebbers, "Finite difference time domain analysis of arbitrarily biased magnetized ferrites"
Radio Science, v. 31, no. 4, pp. 923-929, Jul-Aug 1996.

This paper could be seen as a longer version of the following one [Schuster and Luebbers 96b].

[Schuster and Luebbers 96b] J. Schuster and R. Luebbers, "FDTD for three-dimensional propagation in a magnetized ferrite"
Proc. AP-S International Symposium & URSI Radio Science Meeting, v. 3, pp. 1648-1651, 1996.

Computation method: FDTD.
Antenna(s) studied: None.
Theory presented: Recursive convolution method is applied to modify the standard Yee FDTD algorithm to deal with dispersive media. Arbitrary direction for the biasing field is allowed and a maximum of three complex numbers per cell storage is required. Update equations for both total and scattered field forms have been derived.
Parameters computed: permeability vs. freq plotted; co- and cross-polarized backscatter RCS from a ferrite sphere also plotted.
Parameters varied: Frequency.
Comparison made: None.
Antenna manufactured: None.

Significance: Theoretical.
What's unique from other paper:
Other notions: This paper is a condensed version of the previous one [Schuster and Luebbers 96a].

[Okamoto and Ikeda 79] N. Okamoto and S. Ikeda, "An experimental study of electronic scanning by an antenna loaded with a circular array of ferrite rods"
IEEE Trans. Antenna Propagat., vol. AP-27, 426 (1979).

The experimental data has been obtained for an antenna consisting of a circular array of 12 anisotropic ferrite rods, a truncated biconical horn, and a core wire of a coaxial cable at the center of the horn. The main lobe can not be rotated continuously, but at intervals of about 30 degrees by gradually changing the applied magnetic fields. Reciprocity does not hold. Input impedance also exhibited.

[Pozar and Sanchez 88] D.M. Pozar and V. Sanchez, "Magnetic tuning of a microstrip antenna on a ferrite substrate"
Electronics Letters, vol.24, no.12, pp. 729-731, 9th June 1988.

Computation method: none, pure experiment.
Antenna(s) studied: rectangular microstrip antenna, on a ferrite substrate layer, magnetized by a permanent magnet along one of its three principal axes.
Theory presented: Several resonant dips appeared, due to higher-order patch modes with poor patterns, or surface or volume mode resonances of the substrate. Back lobe in patterns claimed to be caused by the small ground plane of the substrate.
Parameters computed: Resonant frequencies observed, co- and cross-polarized principal plane patterns measured.
Parameters varied: Bias orientations.
Comparison made: None.
Antenna manufactured: Yes, as below, and coaxial probe fed near the edge of the longer dimension. Permanent magnet was used instead of preferred electromagnet.
Significance: operating freq of a ms antenna on a ferrite substrate can be tuned by varying the dc magnetic bias field to obtain a narrow band but tunable antenna. 40% tuning range gained along y-bias, with usable patterns and return loss. Co-polarization is OK, but cross-polarization is high. Conclusion: tuning range: for x- and z- bias, 16%, and resonant freq increased with bias strength; for y-bias, 39%, resonant freq decreased with bias strength.
What's unique from other paper:
Other notions: internal bias field not known. No analytical model realized yet.
Discussions on other possibilities: more tuning range; reduce the magnetic loss by using a small ferrite bar or disc embedded in a dielectric substrate below the patch, but this might reduce the tuning range; or sandwich a thin ferrite substrate with one or more dielectric layers; polarization purity: reduce the high crosspolarisation levels by generating circular polarization with a rectangular patch with x or y bias field; impedance match: by adjusting the feed point or using a matching transformer; consider the effects of bias fringing fields, demagnetization factors, and other effects.

[Pozar 89] D.M. Pozar, "Radar cross-section of a microstrip antenna on normally biased ferrite substrate"
Electron. Lett., vol. 25, no. 16, pp. 1079-80. Aug. 1989.

Computation method: Full-wave moment method, probe feed model.
Antenna(s) studied: Microstrip antenna on normally biased ferrite substrate.
Theory presented: None.
Parameters computed: Resonant freq of RCS peak.
Parameters varied: Biased field.
Comparison made: Unbiased vs. 'latched' (i.e. bias removed after magnetization) vs. magnetized.
Antenna manufactured: None.
Significance: RCS peaks wrt the frequency can be moved by changing the bias field. Latching the ferrite causes the RCS peaks to shift up in frequency with a reduction in RCS magnitude. Biasing the substrate causes the resonant frequency to shift up more, and the RCS reduce more. Also, load has the effect of reducing RCS peaks.
What's unique from other paper:
Other notions:

[Pozar 92 & 94] D.M. Pozar, "Radiation and scattering characteristics of microstrip antennas on normally biased ferrite substrates"
and "Correction to radiation and scattering characteristics of microstrip antennas on normally biased ferrite substrates" (with H.Y. Yang)
IEEE Trans. Antennas Propagat., vol. AP-40, pp. 1084-92, Sep. 1992.
IEEE Trans. Antennas. Propagat. vol. AP-42, pp. 122-123, Jan. 1994.

Computation method: Full-wave spectral domain moment method, probe feed model. Computation complexity and factors for consuming more time are discussed.
Antenna(s) studied: Isolated patch antenna and infinite antenna arrays on normally biased ferrite substrate.
Theory presented: ferrite Green's function and far-field expressions required for the MoM analysis are presented at the Appendix, other MoM solutions for probe-fed patch and arrays and RCS were in earlier 80's papers of Pozar (see the references of this paper). Also, a simple cavity model solution for a circular patch on a normally biased ferrite substrates for RHCP and LHCP behaviors are provided to have some prediction and insight into the operations.
Parameters computed: Resonant freq, axial ratio, gain (including losses), efficiency; reflection coefficient magnitude (for impedance matching) for infinite arrays; monostatic RCS.
Parameters varied: Biased field.
Comparison made: Unbiased vs. 'latched' (i.e. bias removed after magnetization) vs. magnetized.
Antenna manufactured: None.
Significance: 1. obtain circular polarization from a square patch with two feed points, or with a single feed probe, switchable between LHCP and RHCP, and tunable versus frequency by adjusting the bias field; Also, impedance bandwidth is narrow, but axial ration bandwidth is large; 2. provide wide-angle impedance matching for a phased array of ms patches by dynamically adjusting the bias field with scan angle; No scan blindness happens in LHCP case, but happens in RHCP case; 3. switch the antenna 'on' or 'off', where RCS can by reduced by 20-40 dB in 'off' state [see the next paper Pozar 92 too].

What's unique from other paper: AP paper of the year; first time of showing the above significance.
Other notions: In 94 paper the correction was made that the RCS reduction didn't occur and the curve was wrong. The reduction only occurs for CP waves. A case of RCS reduction for linearly polarized scattering was also reported there with a '77 reference.

[Pozar 92] D.M. Pozar, "RCS reduction for a microstrip antenna using a normally biased ferrite substrate"
IEEE Microwave and Guided Wave Letters, vol.2, no.5, pp. 196-198, 1992

Computation method: full-wave moment method.
Antenna(s) studied: square ms antenna on normally biased ferrite substrate, probe-fed.
Theory presented: Some theory of the cutoff region (where $\mu_{eff} < 0$) has been explained and formula is given, more details in Pozar's Microwave Engineering book.
Parameters computed: monostatic RCS, all 4 components examined; Input impedance.
Parameters varied: Biased vs. unbiased field.
Comparison made: Biased vs. unbiased.
Antenna manufactured: None.
Significance: RCS of a rectangular patch antenna on properly *normally* biased ferrite substrate can be reduced by 20-40 dB over a broad frequency range.
What's unique from other paper:
Other notions: Load also affects RCS: open circuited highest and resistive load reduces the peak; (see [Lee and Harakiewicz 96])

[Roy et.al. 92] J.S. Roy, P. Vaudon, A. Reineix, F. Jecko, and B. Jecko, "Circularly polarized far fields of an axially magnetized circular ferrite microstrip antenna"
Microwave and Optical Technology Letters, vol. 15, no. 5, pp. 228-230, May 1992.

The capability of circularly polarized far-field radiation of a circular microstrip ferrite antenna with only one probe feed excitation is theoretically shown. Theory is confirmed by the measurement.
Explanation: In ferrite, the applied bias magnetic field can separate n=+1 and n=-1 circular modes sufficiently to generate circular polarization in a ferrite antenna with single feeding.
(I need to read this paper again!)

[Ruppin 87] R. Ruppin: Electromagnetic modes of a ferromagnetic slab
J. Appl. Phys. 62(1). July 1987 pp.11-15

Main idea: Study the dispersion relation of long-wavelength retarded magnetic modes of a ferromagnetic slab. Theory is applied to a calculation of the ferromagnetic resonance lines of a yttrium iron garnet film.
Significance: Modified the low-k part of the Damon-Eshbach dispersion curves where approximation is not valid; modes in general direction of propagation instead of modes propagating in the direction perpendicular to the magnetic field;
(This paper is more theoretical; needs further reading.)

[Stern et.al. 87] R.A. Stern, R.W. Babbit, and J. Borowick, "A mm-wave homogeneous ferrite scan antenna'
Microwave J., pp. 101-108, April 1987.

To develop a ferrite-type dielectric waveguide antenna for phase scanning in the mm-wave region. Such an antenna is fabricated by cutting periodic grooves into the side wall of an optimized ferrite waveguide, thereby forming a series of radiating elements. No discrete components to be assembled, better than previous conventional inertialess beam scan antennas, but it's still bulky (i.e. high-profile).

[Yang et.al. 93] H.-Y. Yang, et.al., "The RCS of a microstrip patch on an arbitrary biased ferrite substrate"
IEEE Trans. Antennas. Propagat., vol. 41, pp. 1610-14, Dec. 1993.

Computation method: Full-wave moment method.
Antenna(s) studied: Rectangular ms antenna on biased ferrite substrate. Formulation on arbitrarily biased, but computation on *y-biased, x-biased and z-biased.*
Theory presented: In the analysis the direction of the bias field is not prescribed (arbitrarily biased), and magnetic loss is included. Moment method formulation also discussed. Computation results explained.
Parameters computed: the $\theta\theta$ component of RCS. Resonant freq vs. bias field.
Parameters varied: Biased field.
Comparison made: Biased vs. unbiased.
Antenna manufactured: None.
Significance: The resonant freq is significantly varied with the change of the bias field *except* those resonant modes with a dominant magnetic-field component in the direction of the bias field. This phenomenon is explained with a waveguide cavity model. Compared with unbiased substrate, the first resonant freq decreases for z-bias and increases for x-bias if dc bias field is applied. The first resonant freq for both x- and z-bias increases with the bias field, and for y-bias the first resonant freq is almost independent of the bias field strength (only for the antenna that the author studied, I think).
What's unique from other paper:
Other notions: Magnetic loss reduces RCS at resonance significantly, but has little effect on the resonant frequencies.

[Yang 96] H.-Y. Yang, "Characteristics of switchable ferrite microstrip antennas"
IEEE Trans. Antennas. Propagat., vol. AP-44, no. 8, pp. 1127-32, Aug. 1996.

Using of in-plance biased ferrite superstrates to significantly reduce RCS for the design of switchable antennas.
(Need further reading)

3. Summary

The material properties of ferrites are controlled by the direction and strength of an externally applied magnetic field, thus enabling control of various radiation and scattering characteristics of the antenna.

Properties of ferrites antenna: low loss ferrite substrates, high permittivity, anisotropic permeability which can be described by a tensor. In-plane bias easier to achieve than a normal bias because an in-plane bias allows two pole pieces of the magnet to be in close contact with the substrate [Pozar and Sanchez 88]. Also, the in-plane external bias is equal to the internal bias for the case of an infinite substrate [Lee and Harackiewicz 96].

Ferrite applications: Microwave integrated circuits; antennas for tunability, polarization diversity, beam steering, RCS control, surface wave reduction, gain enhancement, patch size reduction, etc.

Values being affected: resonant frequency, input impedance, RCS, main beam, antenna efficiency, axial ratio, etc.

Resonant frequency tuning: vary the DC bias field with usable pattern and return loss [Pozar];
RCS control: Bias field strongly affects the resonant frequency of all modes with dominant electric field in the direction of magnetization [Pozar 92 -- *RCS reduction*] [Some other papers in section 2 explore this problem significantly]. Use of ferrite cover layer to reduce RCS significantly [Yang 96].

Gain improvement: can be achieved at the cost of bandwidth; however, bandwidth is not a major issue for tunable antennas. Can be achieved by placing a dielectric and/or magnetic overlay (superstrate?) on top of the infinite ground plance. (See Balanis 97's reference [20][21].)

Beam steering: scan the main beam by changing the bias on the ferrite material [Stern 87] [Batchelor and Langley 97]. Similarly, use ferrites in phase-shifters for phased arrays. [How et.al. 94]. Also, a microstrip line printed on a ferrite changes its phase significantly when a normal directed bias is applied. This can also be used to steer the beam of a travelling wave fed array. [Batchelor and Langley 1997]
(Traditional beam steering techniques: 1. Use of periodic structures consisting of scatterers in the form of metallic gratings, diodes, or varactors. Disadvantage: mechanical rotations limit the steering rate. 2. Electronic steering with use of delay lines/ phase shifters. Disadvantage: more intricate and expensive with the increase in array elements.)

Pattern control: use of biased ferrite superstrate to control pattern [Henderson 88] [Tsang and Langley >=94]

Generation of circular polarization: [Tsang and Langley 94] [Pozar 92]

Patch size reduction: use high permittivity of the ferrite to reduce the size of the patch element at low frequencies [Das, Chowdhury, et.al.]

4. Appendix I: Papers needed but not available from me:

[Yang et.al. 90] I. Hsia, H.-Y. Yang, and N.G. Alexopoules, "Microstrip antenna on ferrite substrates"
1990 IEEE Antennas Propagat. Symp. Dig., pp. 370-373, Dallas, TX.

A biased ferrite substrate can be used to reduce surface wave excitation for a printed dipole antenna.

[Mahalik 97] N.P. Mahalik, "Tuning procedure in microstrip antennas on ferrite substrate"
IEE Proc. of 1997 10th International Conference on Antennas and Propagation, pp. 1.294-297.

[Langley et.al. 97] J.C. Batchelor, G. Classen, and R.J. Langley, "Microstrip antennas on ferrites"
IEE Proc. of 1997 10th International Conference on Antennas and Propagation, pp. 1.30-33.

5. Appendix II. My Observations

1. No FEM was used except [Balanis 97] manuscript where FEM/MoM hybrid was used; Most of the papers used MoM, such as Pozar's and Yang's. Note: Arik's paper (not included in this review) uses FE-BI method ["Patch antennas on ferromagnetic substrates", whose published shorter version can be found in 1997 AP symposium digest].

2. No multilayer result exhibited except [Balanis 97] manuscript and in [Kokotoff 95]'s Ph.D. thesis. The use of ferrites and dielectrics in a multilayer configuration should allow better bandwidth, and may permit easier integration of such antennas into MIC systems [said in Pozar 92 & 94].

3. Nobody has ever used optimization techniques to deal with ferrite antenna design.